



UNIVERSITÀ
DEGLI STUDI
FIRENZE

XXXI

Dottorato Regionale in Scienze della Terra

Cordinator:
Prof.ssa Lorella Francalanci

μ -LIBS-Scan for Cultural Heritage Geomaterials

PhD Candidate:
Stefano Pagnotta

Tutor:
Prof. Marco Lezzerini

Co-Tutor:
Dr. Stefano Legnaioli

2015-2018



UNIVERSITÀ
DEGLI STUDI
FIRENZE

DOTTORATO DI RICERCA IN
Scienze della Terra

CICLO XXXI

COORDINATORE Prof. Lorella Francalanci

μ -LIBS-Scan for Cultural Heritage
Geomaterials

Settore Scientifico Disciplinare GEO/09

Dottorando

Dott. Stefano Pagnotta
Matr. DT.18070

Tutore

Prof. Marco Lezzerini

Co-tutore

Dr. Stefano Legnaioli

Coordinatore

Prof. Lorella Francalanci

Anni 2015/2018

μ -LIBS-Scan for Cultural Heritage Geomaterials

Keywords: micro-LIBS-Scan, Laser-Induced Breakdown Spectroscopy, Archaeometry, Cultural Heritage, analysis of natural materials.

Summary

Introduction	1
1. State of art	3
1.1 The Laser-Induced Breakdown Spectroscopy (LIBS) technique	3
1.2 LIBS in Earth Sciences	5
2. Instrument	15
2.1 Mobile Dual Pulse Instrument (Modi)	15
2.2 LIBS depth profiling	18
2.3 Micro-Laser-Induced Breakdown Spectroscopy-Scanner (μ-LIBS-Scan)	20
2.4 Control Software	23
2.5 Energy of the laser and measurement spot	25
2.6 Mapping and analysis softwares	28
3. Case Studies	33
3.1 Inhomogeneous materials	33
3.1.1 Pottery	33
3.1.1.1 Clustering of archaeological pottery by means of LIBS and statistical methods	34
Materials and methods	34
3.1.2.1 Micro-chemical evaluation of ancient potsherds by μ-LIBS scanning on thin section negatives	39
Materials and methods	39
3.1.3 Mortar analysis	46
Materials and methods	46
3.2 Other geomaterials	51
3.2.1 μ-LIBS analysis of geostandard	52
Materials and methods	52
3.2.2 μ-LIBS analysis of weathered limestone	57
Materials and methods	57
3.2.3 Layered rocks	59
Materials and methods	59
Conclusions and Future works	63
References	65
Technical appendix	75
MATLAB[®] scripts	75

Data sheets	82
Other schemes and data	86
Abbreviations	87
Figure Captions	89
Table captions	91

Introduction

At the beginning, my research project had to be something that was strictly related to pottery analysis, archaeometry and the applications of geology to Cultural Heritage. During these three years, I realized that my starting idea was something already seen, already proposed, even if with other types of materials and in others contexts. I began to use the available LIBS instrumentation, with its limits and its defects, but undoubtedly with so much potential for geological applications, trying to improve it, in collaboration with the company that manufactures the instrument (Marwan Technology-Pisa). The main improvements I contributed regard the use of a microscope with at least a 10X objective and a software-operated sample holder. In particular, I developed the control software and, a specific routine for the data processing. I started working with MATLAB®, trying to develop and optimize the LIBS technique for Cultural Heritage geomaterials. In particular, I focused the work on the analysis of highly inhomogeneous materials such as mortars and archaeological pottery with the aim of overcoming the measurement uncertainties in those materials where the matrices considerably varied. The followed strategy was to realize the elementary maps of representative portions of materials. Moreover, the use of different statistical methods for the data processing allowed to overcome the intrinsic drawbacks. The main results of my project are the capability to obtain virtual elemental cross-section of the analyzed samples and the possibility to carry out in a fast way quantitative information with proper precision and accuracy. At the end of my project, there are still several aspects to be improved and carried out. For instance, a possible improvement could be the realization of a more compact and lightweight instrument, with a tunable laser and a 20X objective. Finally, I would like to compile the analysis code in a multiplatform software able to work on IOs, Android and Windows devices.

Three chapters, a conclusion paragraph, and technical appendix compose my PhD thesis. The first chapter briefly summarizes the state of art about the LIBS technique, strictly related to the applications in the field of Earth Sciences and Cultural Heritage. The second chapter deals with the technical description of the instrument used, both the hardware and the control software. Chapter three sets out the main cases study on which I tested the LIBS technique. The last paragraph contain short conclusions and a possible future development of the instrument I set up. A technical appendix is also included with all things that, due to

space and the organization of writing, could not be set in the thesis: the MATLAB® routines for 1) load the spectra and place them in a matrix made by linear vector; 2) extracting the elemental map; 3) create specific elemental intensity ratio maps; 4) reload the map and place it in a new linear vector; 5) create a mixed vector on which perform the PCA analysis and segmentation; 6) performing a normalization (if necessary); 7) extracting a mean spectrum for each segment that can be analyzed by calibration-free method for quantitative analysis. I have also insert the dataset for the geostandards (quantitative value calculated by Artificial Neural Network), a list of Hand Held-Laser Induced Breakdown Spectroscopy (HH-LIBS) instruments and a List of Micro-LIBS system.

1. State of art

1.1 The Laser-Induced Breakdown Spectroscopy (LIBS) technique

The Laser-Induced Breakdown Spectroscopy (LIBS) is a laser based spectroscopic technique that has, as well as all the atomic emission spectroscopy (AES) methodologies, advantage and dis-advantage [1]. The main advantages with respect to the conventional optical emission techniques are: no sample preparation, very fast measurements (few seconds), high spatial resolution (in the order of μm), no limitations on light elements detection and the generation of plasma is made by a laser (there is no need of plasma torch).

Moreover, thanks to the recent technological evolutions, the devices can be miniaturized up to be able to perform in situ measurements. In the past, the LIBS has been already used for in situ analyses, for instance for studying extraterrestrial geological materials.

The basic idea of the LIBS technique is very simple: a high energy pulsed laser is focused on the sample's surface, transforming some micrograms of the material into a plasma. The signal emitted during the consequent cooling, due to electrons recombination and atoms desexcitation, is collected and sent to a spectrometer through an optical fiber (Fig. 1). The study of the spectra allows qualitative and quantitative analysis referring, for identification of elemental peaks, to the NIST databases. In particular, for the quantitative analysis, several strategies has been proposed. If it is possible to assume the local thermodynamic equilibrium (LTE) condition [2], the concentration of the atomic species can be obtained, without the need for a standard [3]. This is particularly suitable for all those applications where it is often difficult if not impossible to have proper reference standards [4].

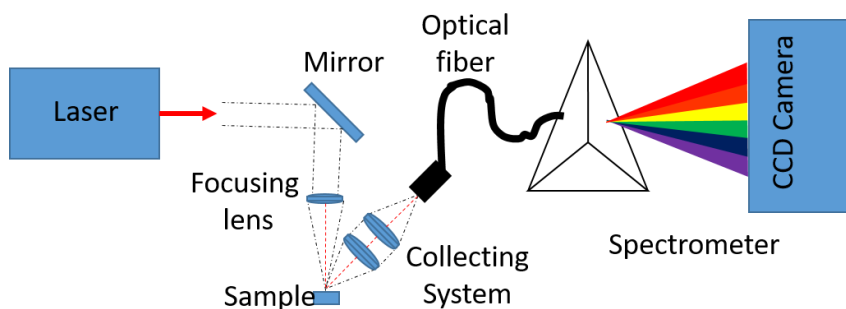


Fig. 1 A simple scheme of the Laser Induced Breakdown Spectroscopy (LIBS) apparatus.

To improve the performances of the technique, different solutions and instrumental configurations have been exploited during the years, one of the most effective approach is the Double Pulse method (DB-LIBS) [5–7].

The DP-LIBS consists in the excitation of the plasma with two temporally separated laser pulses, with a reciprocal delay in the range of microseconds or tens of microseconds, instead of a single laser pulse: the first pulse creates a sort of low vacuum in the area to be analyzed, the second pulse generates the plasma plume (Fig. 2).

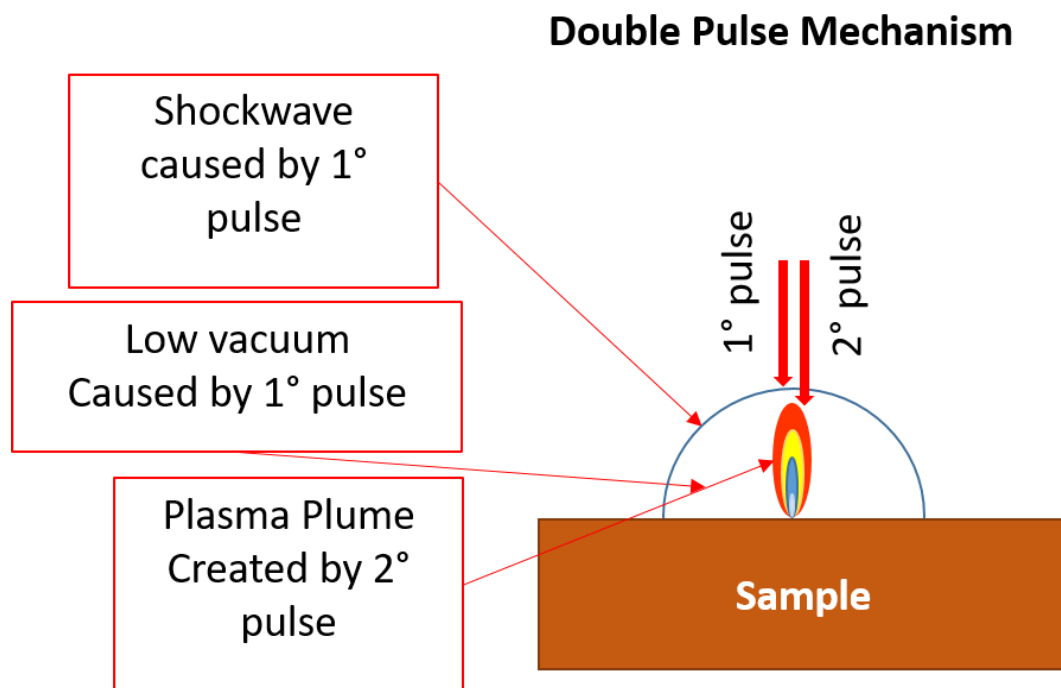


Fig. 2 A scheme to resume the mechanism of double pulse.

It is possible to realize it using different configuration: collinear, parallel, orthogonal and slightly off-center (Fig. 3).

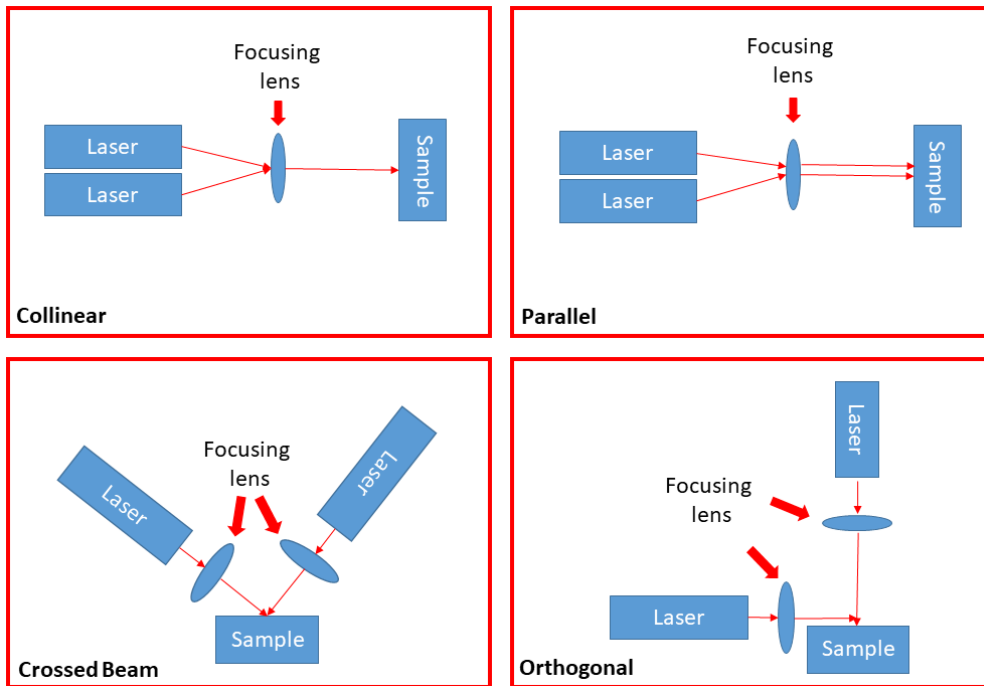


Fig. 3 The main configurations used for Double Pulse LIBS.

The shock wave created by the first impulse generates a sort of a rarefied gas bubble in front of the sample surface, the ablation due to the second pulse occurs inside the bubble. The peculiar environment characterized by a low atmospheric pressure causes an enhancement in the ablated mass and consequently an enhancement in the LIBS signal. The advantages of this method have been demonstrated in many papers (an almost actual review is in [8], Cap. 5): the increasing of the s/n ratio of the peaks intensity of the atomic species is of different orders of magnitude with respect to a single pulse, improving the limit of detection for trace elements.

1.2 LIBS in Earth Sciences

Why using LIBS in the Earth Sciences? Although several analytical techniques are dedicated to the specific Earth Sciences applications, most of these are difficult to bring to the field. The analytical instrumentation trend is increasingly pushing towards hand-held or transportable instruments in order to perform even complex analyses directly *in situ*. As previously reported, a very attractive feature of the LIBS is that it can be implemented in different situation: laboratory, industrial facility, or *in situ* for close-in or stand-off

analysis. In Table 1 a comparison between LIBS and other standard techniques used in geochemical analysis for major and minor elements [8,9], is reported.

Table 1 The LIBS techniques compared with other classical methods for geochemical analysis (adapted from Musazzi & Perini [8] p. 314 and from Naes et al. [9]). EMP=Electro Magnetic Pulse Analysis; pXRF= X-Ray Fluorescence; INAA=Instrumental Neutron Activation Analysis; LA-ICP-MS=Laser Ablation-Ion Coupled Plasma with Mass Spectrometry; RSD= Relative Standard Deviation; TPA= Time used Per Analysis.

Parameter	EMP	pXRF	INAA	LA-ICP-MS	LIBS
accuracy	Semi-Quantitative	Semi-Quantitative	Quantitative	Quantitative	Semi-Quantitative
Precision RSD	Good (5-10%)	Good (5-10%)	Good-excellent (5%)	Excellent (<5%)	Fair-Good (5-20%)
Sensitivity	100's ppm	100's ppm	Ppb	<1ppm	10's ppm
Discrimination	Very good-excellent	Very good-excellent	Very good	Excellent	Very good-excellent
Complexity	Easy to use	Easy to use	Fairly difficult to use	Difficult to use	Easy to use
Sample	Non-destructive	Non-destructive	Non-destructive	Minimally Destructive	Minimally Destructive
TPA	Minutes	Minutes	Hours	Minutes	Seconds
Cost	~\$700K	\$75-150K	~\$100K	~\$250	\$75-150K

LIBS technique offers precision (in terms of RSD) and accuracy similar to XRF but a better sensitivity and the best TPA among the techniques. The analysis of geological materials can be carried more accurately with chemical methods, but this requires the use of expensive, time consuming and often (usually) destructive methodologies.

The possibility to have compact LIBS instruments, together with the ability to perform standoff measurements (Fig. 4), made the technique a perfect tool to carry on in situ geological studies. An interesting example is the MARS ROVER mission [10–13]. The Mars Science Laboratory (MSL) mission in 2012 [14–18] sent a LIBS tool called ChemCam to Mars [19]. The ChemCam prototype collected thousands of spectra now available to anyone who wants to analyze them¹ [20–25]. In an environment such as an extraterrestrial planet, where miniaturization, robustness, simplicity and the ability to carry out remote analysis are fundamental issues, the LIBS technique has immediately received a widespread interest. The first idea of bringing a LIBS instrument on another planet is a consequence of some photo taken by Venera 13 on the Venus surface in 1982 [26], where the atmosphere in the photo let hypothesize the use of a standoff instrument for analysis of the surface [27–31].

¹ <https://msl-scicorner.jpl.nasa.gov/Instruments/ChemCam/>

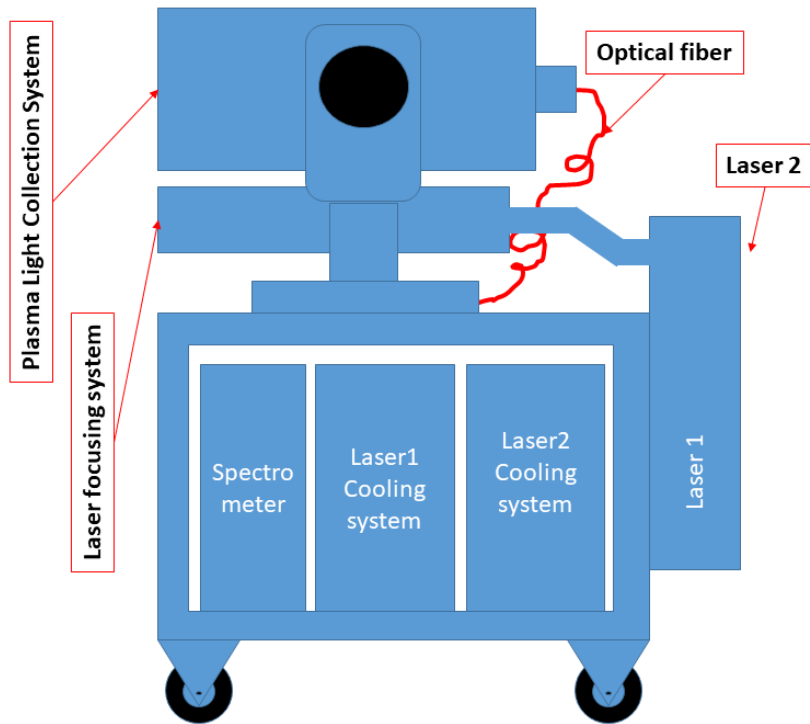


Fig. 4 Double pulse stand-off system scheme (based on the model developed by U.S. Army Research Laboratory [32]). In this scheme laser 1 hides the laser 2. In this system, there are two laser in order to realize the double pulse technique.

The relevant aspect of the pioneering choice representing by Chemcam is the possibility to offer remote rock identification, quantitative analysis, detection of hydrated minerals and water ice, depth profiling and laser cleaning of rocks.

The literature about LIBS geological application has grown year after year; most of the manuscripts refers to the analysis and provenance of geo-materials [33–44], but there was an explosion with the realization of hand-held devices (HH-LIBS) (Table 2).

Table 2 List of commercial Hand Held LIBS on the market.

	Brand	Model
1	Bruker	EOS 500
2	BwTek	NanoLIBS-Q
3	Hitachi	Vulcan Smart
4	Oxford Instruments	mPulse
5	Rigaku	KT-100S
6	SciAps	Z200
7	SciAps	Z200 C+
8	SciAps	Z300
9	SciAps	Z50
10	SciAps	Z500
11	TSI	CHEMLITE™

Even if these devices have some limitations with respect to laboratory instrumentation, they can carry out thousands of measurements in situ directly on the rocks, or others materials, without sample preparation. The implications of this advantage are many. The main field of application is for quality analysis of the materials and for sorting in the industry. However, HH-LIBS instruments have been used also in Cultural Heritage [45], to detect heavy metals present in soils [46,47], in the analysis of speleothems [48], for the study of rare earths in uranium ores [49] and to characterize meteorite analogue terrestrial weathered stones [50,51]. In the paper published in 2016 by Connors et al. [19], the use of the z-500 SciAps device is shown. Different geological samples were analyzed and mapped through with this handheld tool, reporting all the potential and capabilities for qualitative and quantitative analysis on heterogeneous materials. In this case, a slab of rock from a gold mine was mapped and analyzed showing the distribution of mineral elements important for the individuation of the potential of the mineral extraction: in particular, the distribution of iron, cobalt, copper and gold in pyrite was mapped with the instrument².

Among the possible LIBS applications, one of the most assessed is the quick and precise identification of the rock composition using chemo-metric methods [52,53]. Assuming that the geological process behind the formation of rocks, mineral, etc. leaves a chemical trace in the materials, we can recognize in our analysis a sort of fingerprint useful to classify the samples. The basic concepts of geochemical fingerprinting are very robust [54] and based on well-established and well-known law and processes [55–59].

In order to classify and to characterize the geomaterials (qualitatively and in the correct way) analyzing the LIBS spectra, the first drawback to overcome is the abundance of elemental peaks in the spectra. Obviously, due to the complexity of the analyzed material, it is impossible to be able to discriminate through the analysis of a few atomic elements. It is necessary to use a method that takes into account several atomic elements at the same time: dimensional reduction algorithms such as Principal Component Analysis (PCA) can help, but, dealing with complex materials, not always there is a linear relationships, so in these cases it is possible to recur to the use of Neural Network (NN) [40,60]. NN not only can manage with the high dimensionality of the LIBS spectra, but also can separate, classify and identify materials on the bases of well-known training

² They calibration curve is realized using a series of standards (pellet made from homogenized powder) provided by Ore Research and Exploration of Australia (OREAS), Japan Oil Gas and Metals National Corporation (JOGMEC) and National Institute of Standards and Technology (NIST).

sets. Up to date, the number of works on the qualitative identification of geomaterials has grown considerably, often with very satisfactory results: the review by Quiao et al. [61] (

Table 3) showed that the choice of the suitable statistical method depends on the complexity of the matrix that we want to analyze. Complex matrices with many elements requires complex classification algorithms. In different cases, LIBS coupled with statistical methods (mainly multivariate approaches) have obtained up to 100% matching in some cases (both on rocks and minerals), such as carbonates, quartzites, shales, slates, cherts, pyroxenes, pyroxenoids, amphiboles, phyllosilicates, feldspars, fluorites (as reported by Quiao et al. [61]). In the work of Sheng et al. [62] about the classification of iron ores, the authors reported the use of LIBS coupled with a Random Forest (RF) algorithm [63]. Results were compared with those obtained with a Support Vector Machines (SVM) algorithm [64,65]. Both the results are acceptable, even if the authors claim that the RF are significantly better than SVM results.

As previously reported, LIBS is able, with its limits and uncertainties, to realize good quantitative data [66]. As others chemical methods, it is possible to use appropriate standards for build calibration curves. Unfortunately, it requires an *a-priori* knowledge of the sample's matrix, but, particularly in the study of geomaterials, this is not always possible. In these cases, it has been developed a Calibration Free method (CF-LIBS) [67] that, taking into account a condition of local thermodynamic equilibrium (LTE) and that the plasma is optically thin, allows to obtain quantitative measurements without need of standards or calibration curves. In the literature, an evaluation of different methods is reported: in some articles the precision range [68–70] and the accuracy [71] is considered, in other papers the correlation factor and/or the relative mean square error (RMSE) is reported. Generally, there is no agreement on the parameter to be considered for the error estimation. The review by Quiao et al. shows that the precision ranges in the iron ore materials goes from 2 to 25 relative wt% for Ca, Si, Mg, Al, Ti (using the Fe as internal standard). Instead, if we consider standardless methods (CF-LIBS) performed on volcanic materials (dacite, rhyolite, andesite and basalt) and sedimentary rocks (sandstones), the accuracy is better than 20 wt% on the major elements (excluding calcium) and better than 60 wt% for minor elements [61]. In the Table 4, I reported the main results of the survey published by Quiao et al [61].

One of the main problem that afflict the LIBS measurements, especially on heterogeneous samples as the rock samples, is the self-absorption. This phenomenon is verified when the plasma produced has a very high density and it is optically thick: it increases the line width and decreases the line height [72]. There are several approaches for correcting self-absorption in CF-LIBS [73,74]. Recently Grifoni et al., published a brief comparison between the classical methods, One Point Calibration (OPC), a sort of calibration free assessed with only one similar matrix reference sample, the CF-LIBS and the most recent calibration Sigma (C-Sigma), reaching the conclusions that the only method which is robust against self-absorption and matrix effect is the One-Point-Calibration technique [75].

Table 3 Survey of works dealing with LIBS classification of geological materials as reported by Quiao et al [61] (p.10 Table 2).MV-MC=Maximum variance modification to Maximum Correlation; PCA=Principal Component Analysis; PLS-DA=Partial Least Square-Discriminant Analysis; SIMCA=Soft Independent Modeling by Class Analogy; ANN=Artificial Neural Network; SVM=Support Vector Machines; SPLS= Sparse Partial Least Square; LS-SVM= Least Square-Support Vector Machines; TFe= Total Iron.

Test Samples ³	Methods	Correct identification rates	reference
Sulfide minerals in sulfur-bearing drill cores	A linear fitting procedure	6-8% Misclassified	[68]
Carbonate, pyroxenes, wollastonite, amphiboles, phyllosilicates, feldspar	Correlation coefficient	100%	[41]
Pyroxenes	MV-MC	98.2%	[38]
Feldspars	MV-MC	86.4%	
Carbonates	MV-MC	99.3%	
Beryls	MV-MC	58.8%	
Beryls	Linear correlation analysis	94.6% (35of 37 correct id.)	[76]
Beryls	PCA	Cluster analysis	[77]
Carbonates	PLS-DA	100% correct classification and 0.07% misclassification	[37]
Fluorites	PLS-DA	100%	
Shales, slates	PLS-DA	100% correct classification and 0.7% misclassification	
Quartzites, cherts, glassy volcanics	PLS-DA	100% correct classification and 2.4% misclassification	
Ugrandite, pyralspite	PLS-DA	98%	[53]
Limestone beds	Matching algorithm (series of binary PLS-1 models)	100%	[78]
Igneous rocks	SIMCA	88.1%	[60]
Iron rock, grey soil, obsidian rock, ultrabasic rocks, wollastonite	ANN	100%	[79]
Hematite, graphite, sulfide mixture, olivine, dolomite, kaolinite, andesite, gabbro, basalt, obsidian, shale, molybdenite, fluorite.	ANN	100%	[40]
Sedimentary rocks	SVM/PLS-DA	>90%	[36]

³ All the terms refers to Oxford Dictionary of Earth Sciences [193].

Motto-Ros et al. in 2008 [80] proposed the use of NN to study rocks coming from a meteoritic impact crater, the authors quantified Fe, Mg, Si, Mn, Al, Ca and Ti concentration with a standard deviation of 15 wt% better than the values measured by X-ray fluorescence⁴. In a very recent work, Guo et al. proposed a hybrid method of Sparse Partial Least Square (SPLS) and Least Square-Support Vector Machines (LS-SVM) reporting values of root mean square error of prediction (RMSEP) very encouraging in analysis of iron ore samples [81].

Table 4 Works dealing with LIBS quantitative analysis as reported in Quiao et al [61] (p.11 Table 3 modified by adding recent works and correcting some results). ANN=Artificial Neural Network; PLS= Partial Least Square; CF-LIBS= Calibration Free Laser-Induced Breakdown Spectroscopy.

Test Samples	Methods	Elements	Results	Reference
Iron ore	Calibration curve with Fe internal standard	Ca, Si, Mg, Al, Ti	Precision range ≈ 2 to ≈ 25 wt%	[69]
Ore samples	Calibration curve with Ar internal standard	Fe, Ca, Mg	Precision: 3wt%	[70]
Mineral drill core	Calibration curve with a normalization approach	Cu, Mn, Ni, Fe, Cr	R ² : 0.92-0.99	[82]
Igneous rocks	PLS	Si, Al, Fe, Mg, Mn, Ca, Na, K.	Calibration model	[60]
Igneous rock powder	PLS with Optimizzation	Si, Al, Ti, Fe, Mg, Mn, Ca, Na, P, K.	Errors: 0.02-1.6 wt%	[83]
Certified laboratory samples and rocks from meteorites impact sites	ANN	Fe, Mg, Si, Mn, Al, Ca, Ti	MD <15wt%	[80]
Silicate samples	PLS2	Si, Al, Ti, Fe, Mg, Ca, Na, K.	RMSE: 0.08-3.07 wt%	[84]
Igneous and highly metamorphosed rocks	Lasso	Si, Al, Ti, Fe, Mg, Mn, Ca, K, Na, P.	RMSE:0.19-3.37 wt%	[85]
Volcanic rocks	CF-LIBS	Fe, Si, Mg, Ca, Ti, Mn, Al, Na, K, Cu, Ba.	Accuracy: better than 20% on Major elements (escluding Ca) and better than 60 wt% on Minor elements	[71]
Basalt rocks	CF-LIBS	O, Si, Fe, Al, Ca, Mg, Na, Ti, K, Sr, Ba.	Accuracy:93-99 wt% (Mg, Sr, Ba);1-49 wt% (others)	[86]
Iron Ore Samples	SPLS+LS-SVM	TFe, SiO ₂ , Al ₂ O ₃ , CaO, MgO	RMSEP: TFe=0.62 wt% SiO ₂ =0.36 wt% Al ₂ O ₃ =0.04 wt% CaO= 0.09 wt% MgO= 0.21 wt%	[81]

The possibility to carry out stand-off measurements, without the need of reference standards is very appealing and some research groups have tried to test this approach in scenarios imagining the exploration of the Martian soil [87–90]. The literature dedicated to the LIBS application for extra-planetary exploration

⁴ No reference for the used instrument but they refers to Bulk XRF analysis.

shows that the technique is suitable for all those applications that cannot be managed directly by an operator and that require remote control [91,92]. Some research groups are already hypothesizing and testing new systems for planetary exploration of Venus and Europa, a Jupiter satellite moon [93,94].

A portable instrument for elementary analysis, which has almost no limitations on identifiable elements, is preferable when it is necessary to analyze thousands of points on an outcrop. The capability of carry out the analysis in real time, determining the elemental composition, allows to explore the potential of specific geological formation, to identify its boundary (if reachable without having to dig). In principle, it would be possible monitoring in real time the change in eruptive casting composition, always taking advantage of a standoff system⁵. One of the most common field of LIBS application is the study of the efficiency of the mining industry and the analysis of toxic contaminant metals [95–97]. Harmon et al. [98] and Hark et al. [99] tried to use LIBS to determine the origin of some coltan⁶ [100,101] samples, a mixture of columbite (Fe,Mn)Nb₂O₆ and tantalite (Fe,Mn)Ta₂O₆, which are of great interest for high-tech applications, but at the same time involve critical ethic concerns, due to the fact that the extraction of this mineral is done mainly in the Democratic Republic of the Congo, so there are several internal conflicts for the control of coltan mines [102].

Considering that LIBS allows for a good spatial resolution and the possibility of carrying out analyzes in depth, it has been used for the analysis of speleothems, geological formation generating from the re-deposition of rainwater. Studying their growth, it is possible to create a sort of paleo-climatic archive able to provide information on the climatic evolution of terrestrial environments at micro and macroscale. Laserna (Univ. of Malaga) and its group were among the first to use LIBS to carry out studies on the formations present in the Nerja Cave (Malaga, Spain). They reported the trends of Mg and Sr in agreement with the paleo-climatic indicators of the region that is rich of dolomite with high Mg content and aragonite including Sr in its structure. They investigated also samples with different degrees of superficial alteration. The results showed that the speleothems are essentially formed by two zones, in the first one, the outer part, they found Fe, Si and Al (alteration layer), while in the second one these elements were absent [48,103,104]. Other groups dedicated specific studies on stalagmites that can be sampled more easily, causing less damage to the

⁵ At the time of writing this doctoral thesis, there are still no applications in this field, but, only, several applications dedicated to the analysis of high temperature casting alloys directly in the casting.

⁶ Coltan is the common name for columbite-tantalite minerals.

environment. Ma et al. [105] performed a two-dimensional mapping of some stalagmite slices from the Soreq Cave (Israel), identifying the main mineralogical elements and phases. Galbács et al. [106] analysed three samples (taken along the horizontal axis of the stalagmites) coming from the Baradla Cave (Aggtelek, Hungary) to carry out a qualitative study to identify the majority and minority elements (Ca, Mg, C, O and Al, Si, Fe, Mn). Finally, Fortes et al. [107] analyzed the spatial distribution of paleo-climatic indicators in the stalagmites slabs. The LIBS data on the Mg / Ca and Sr / Ca ratios showed a good agreement with the results obtained by ICP-AES, but exclusively in samples with a high content of Sr.

A part of my PhD project deals with the analysis of archaeological ceramics. For the characterization of this kind of materials, a well-established analytical procedure has to follow. It includes the measurement of chemical and mineralogical characteristics by microscopy (stereo-microscope and thin sections), X-ray diffraction and geochemical analysis. Recently, μ -Raman spectroscopy (to characterize pigments) and mass spectrometry (trace element analysis) have been added to this analysis package [108–133]. LIBS at the beginning has always been configured as a fast technique that in the field of ceramics can be used for preliminary screening and samples clustering and for the analysis of depth profiles when particular coatings are present, moreover it can be transported directly *in situ*.

One of the first LIBS applications concerns the analysis of glazes. Yoon et al. [134] built a calibration curve of different glass beads to obtain a quantitative analysis of glazes of ceramics. In another work, Colao et al. [135] determined both the glaze and the decorative layer composition and consequently classified ancient pottery samples using LIBS. Following this line, several authors worked on the analysis of archaeological materials in a qualitative way, performing classification experiments [136–140]. Genc Oztoprak et al. [141] proposed LIBS as a methodology for the analysis of glazes, pigments and whole ceramic body, evaluating the possible sample's damage with respect to other well-established, but destructive, methodologies. To demonstrate the effectiveness of LIBS, they analyzed some clay deposits, coming from nearby sites, and classified the spectra by PCA and PLS-DA algorithms, obtaining archaeologically interesting results. There is, in the glaze, a group of elements that are the same for Islamic and Byzantine periods: Ca, Al, Si, Mg, K, V and Na; while Sr is present only in the Islamic period. The use of Zn is verified for brown-glazed pottery. The presence of vanadium is verified, but this element, at that time, was used also for heat shield and tools coatings. Previously, in 2008, Erdem et al. [142] analyzed the clays and the slip of some potsherds belonging

to the Turkish Iron Age and using a PCA on the LIBS spectra they determined the origin of the ceramic fragments. Melessanaki et al. [143] proposed the LIBS screening of different types of archaeological materials including ceramics. One of the strengths of this technique is certainly the ability to perform a depth profile of the analyzed material, in order to follow qualitatively and quantitatively the composition of the sample shot after shot layer by layer. López et al. [144] compared the LIBS data with those obtained by micro-analysis X (SEM / EDX), finding a good agreements between the LIBS and EDX results: Si, Al, K, Ca and Fe are detected, but Mg and Ti (present in LIBS spectra of slips of two samples) are not present in the EDX analysis. Khedr et al. [140] presented LIBS as a valid *in situ* analytical tool for chemical analysis and rapid depth profiling. LIBS technique permits the possibility to detect also rare earth elements (REE). In the work of Wang et al. [145], they analyzed a glass-ceramic sample containing crystals of CaMoO_4 . The used setup was composed by an Nd:YAG laser (at 3rd harmonics, $\lambda=266\text{nm}$), a 40X magnification objective (UV dedicated) and a spectrometer with an iCCD camera. They mapped the distribution of some REE elements (La, Nd, Pr, and Eu), together with Mo, Ca, Sr, Al, Fe Zr in the analyzed area. As demonstrated by Rai et al. [146], LIBS increasingly appears to be an advantageous tool for *in situ* analysis of archaeological materials by providing indirect analysis on the source of raw materials, or better, indicating hypotheses about possible sources of supply. Lasheras et al. [147] showed that the use of calibration curves built on different standards for each detected element increases the reliability and the confidence of the method obtaining results very close to those obtained with Atomic Absorption.

2. Instrument

In this chapter, all aspects strictly related to the instrument μ -LIBS-Scan manufactured by Marwan Technology (Pisa) and ALS-Lab-CNR-ICCOM (Pisa) will be discussed, both the hardware and the software. The set-up is briefly explained with particular attention to the coupling with the microscope and the relationship between analysis spots and laser fluency; finally, the software for the control and management of the instrument together with the routines for the LIBS spectra processing are presented.

2.1 Mobile Dual Pulse Instrument (MODi)

As previously reported, one of the greatest advantages of LIBS technique is the possibility to realize *in situ* measurements with a transportable instrument. The idea behind the Mobile Dual Pulse Instrument (MODi⁷), manufactured by Marwan Technology, is to take advantage of a dual pulse laser [148] coupled with standard-less methods for elemental quantification (CF-LIBS method) [3,4,73,149–151]. The system is equipped with a CCD spectrometer that covers a range from 200 to 900 nm with a resolution of 0.1 nm in the UV region (190-420 nm) and 0.3 nm in the VIS-IR region (410-900 nm). The single components of the instrument are relatively small (main body; W=0.50 m x L=1 m x H=0.70 m and with microscope H=1.30 m) offering the possibility to compact the instrument in a small volume. The instrument includes an analysis chamber (Fig. 5), where an inert gas can be flushed through an insert nozzle (Fig. 6), and an external arm with to perform analysis directly on the object (Fig. 7).

⁷ MODi is the starting instrument from which μ -LIBS-Scan has been developed.



Fig. 5 The internal analytical chamber. The sealing door, placed for security reasons, is useful for retain the atmosphere when the chamber is flushed with inert gas.

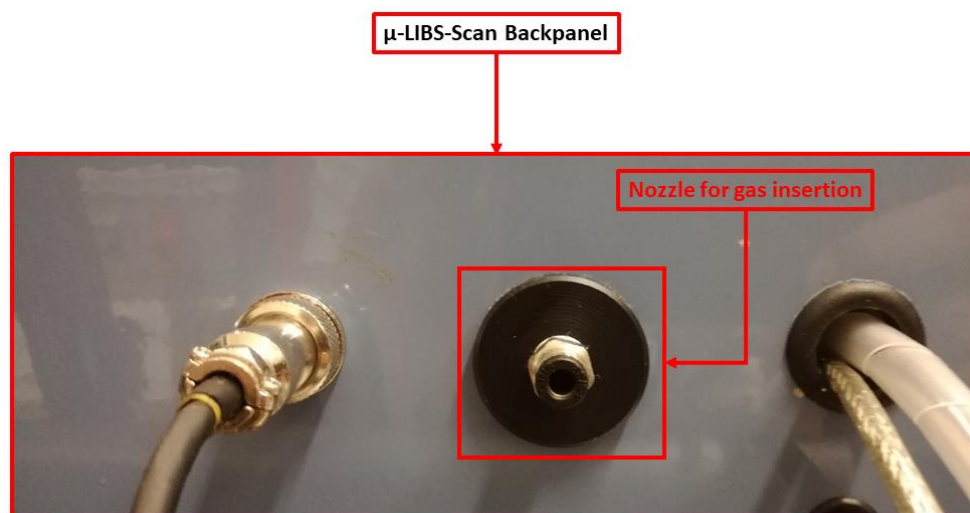


Fig. 6 The insert gas nozzle in the Backpanel of Modi



Fig. 7 External arm of the Modi system. A complex mirroring system with five junctions guides the laser outside the instrument. An optical fiber placed at 45° respect of the surface of the sample collects the plasma light.

The internal chamber is equipped with a micro-cam for sample viewing and laser focusing (Fig. 5), and can be integrated with a motorized sample holder in the X, Y and Z directions. To make the instrument and modular, the chosen geometry for the case is a sort of parallelepiped, where the control systems are placed in the bottom, while the laser head and the optical systems are all placed in the upper half.

2.2 LIBS depth profiling

The capability of acquiring different spectra shot by shot going deeper into the sample makes the instrument suitable for those analyzes that require micro drilling and depth profiling. The amount of ablated material depends on the laser settings and the nature of the analyzed material. In order to have an estimation of the system's analysis performances, some tests have been performed, setting the laser beam energy at the minimum (30 mJ per pulse). The chosen samples were small blocks of gypsum, a soft material with hardness 2 (Mohs scale) and density of 2.3 g / cm^3 . Following the method presented by Borisov et al. [152] two pieces of gypsum with flat surfaces have been coupled, with a tape and the analysis performed on the junction. After the measurements, the two pieces have been separated showing the profile of the LIBS craters. The Fig. 8 shows the craters after 25, 50 and 100 shots.

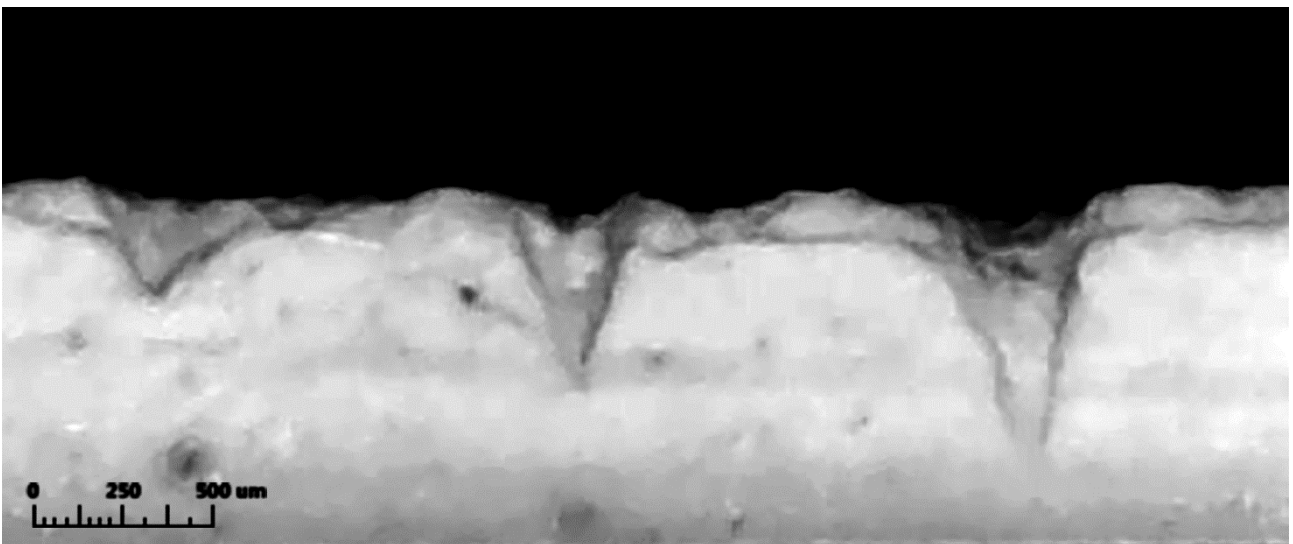


Fig. 8 Craters made by laser in the analytical chamber. From left to right: after 25, 50 and 100 laser shots

Plotting the approximate depth measured on the micro-photo versus the number of the laser pulses, we can notice that the ablation rate fit approximately an exponential curve (Fig. 9).

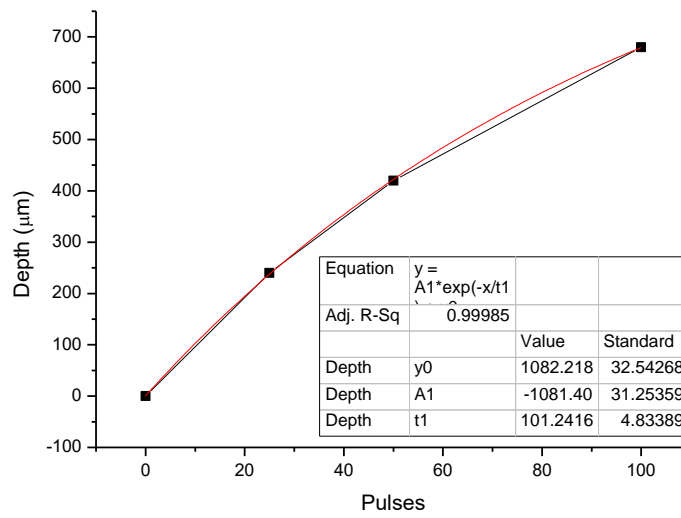


Fig. 9 Depth of craters (μm) versus number of laser pulses. We can estimate that the depth of craters follow approximately an exponential curve.

2.3 Micro-Laser-Induced Breakdown Spectroscopy-Scanner (μ -LIBS-Scan)

Up to date, the LIBS mapping has been used with remarkable results in the biological and medical field [153], for the analysis of metallic coatings and for the analysis of minerals [154].

The μ -LIBS system is based on the Modì system (by Marwan Technology, Pisa), coupled with a microscope Zeiss Axioplan Scope A1 (Fig. 10) equipped with a 10X objective produced by Thorlabs (LMH-10X-1064) in order to focus the laser beam on to sample. A specific ball lens focuses (Fused Silica Ball lens 8 mm \varnothing by Edmund Scientific) into an optical fiber (core 200 μ m) the plasma light. The ball lens is placed at 45° respect to the laser beam. The use of the ball increases the amount of the collectable plasma light⁸.



Fig. 10 Photo of the microscope mounted on the micro-LIBS system.

Two compact motorized translation stages by Thorlabs (MTS25- ZB) with 25 mm travel range, 0.05 μ m incremental movement and 1.6 μ m of bidirectional repeatability assure the movement of the sample holder. The stages are mounted in an X-Y configuration and allow the scansion of an area of about 6.25 cm² (Fig. 11).

⁸ The value for numerical aperture of the free optical fiber is 0.22, the use of a ball lens cause the gain of 2-2.5x in respect of the free fiber. For an optimal adjustment of the ball lens, the optical fiber must be positioned at the back focal distance of 3.78 mm.

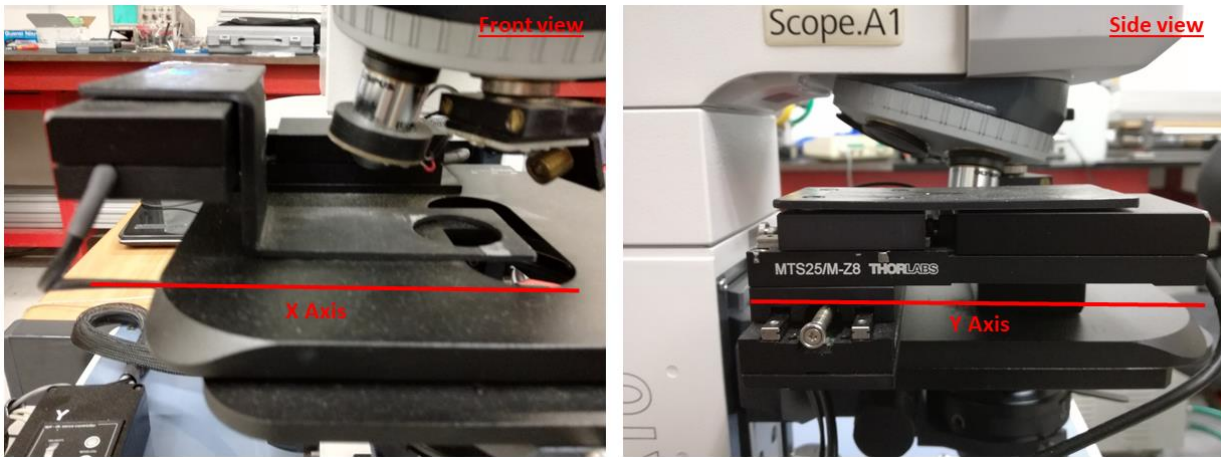


Fig. 11 A front and side view of the motorized stage.

Digital images of the analyzed zone can be acquired with a Dinolite™ cam (5 MP) mounted on the tri-ocular microscope's head (Fig. 12). The sample can be observed in transmitted and reflected light with a dedicated 10X objective, produced by Olympus (PLN-10X/0.25), for selecting the point of analysis or the starting point for realizing a mapping.



Fig. 12 The Dinolite™ Cam mounted in the tri-ocular eyepieces.

The maximum height of an object, in order to be easily placed under the microscope, must be 5 cm high due the structural configuration of microscope. The table below resumes the system characteristics (Table 5).

Table 5 System characteristics of the Micro-Scan

	Specifics
Maximum travel range (x axis)	2.5 cm
Maximum travel range (y axis)	2.5 cm
Maximum scanned area (XY)	6.25 cm ²
Minimum increment movement	0.05 μm
Maximum height of the object under microscope	5 cm
Maximum number of layers without refocusing	10

The maximum number of layers that can be analyzed in depth profiling may depend on the nature of the material and on the condition of the plasma: in soft materials, the laser goes deeper and it causes the defocusing after few laser shots, instead, in hardest materials the defocusing is slower. The depth of field (DOF), that is the system's ability to maintain focus for different sample positions, is a sort of cylinder, whose high depends on several parameters: the laser beam characteristics and the lens specifics (Fig. 13).

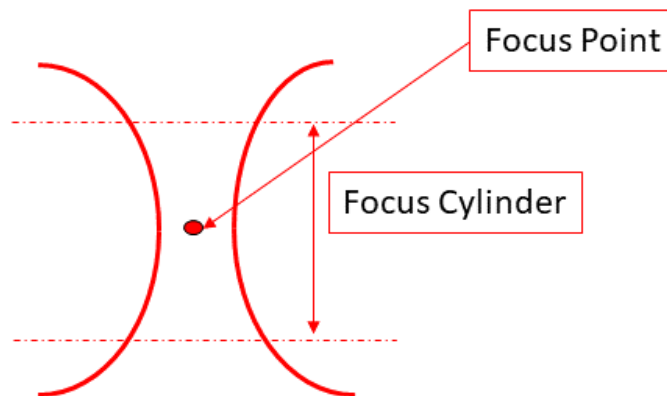


Fig. 13 Scheme of the focal point.

For the micro-LIBS system with a 10X objective (0.25 numerical aperture), the DOF can be estimated in 8.5 μm [155].

2.4 Control Software

The recent technological development offers several options, in order to control and synchronize the different components of the LIBS apparatus, such as full digital or hybrid analog / digital options. For the Modì system, the full-digital option has been selected using control libraries, compatible with Visual Basic and C++, supplied by the manufacturers of the different components. The control and synchronization software of the micro-LIBS-scanner has been realized with LabView 8.5. The user interface (UI) of the control software is quite simple and permits to control the dimension of the maps and the synchronization between the motorized stages, the laser shots and, consequently, the acquisition of the spectrometer (Fig. 14). The motors are put in standby, together with the laser, waiting for the settings by the user. When the virtual button that starts the analysis is pushed the laser starts to shot, and the spectrometer starts to acquire spectra, following the movement of the motors.

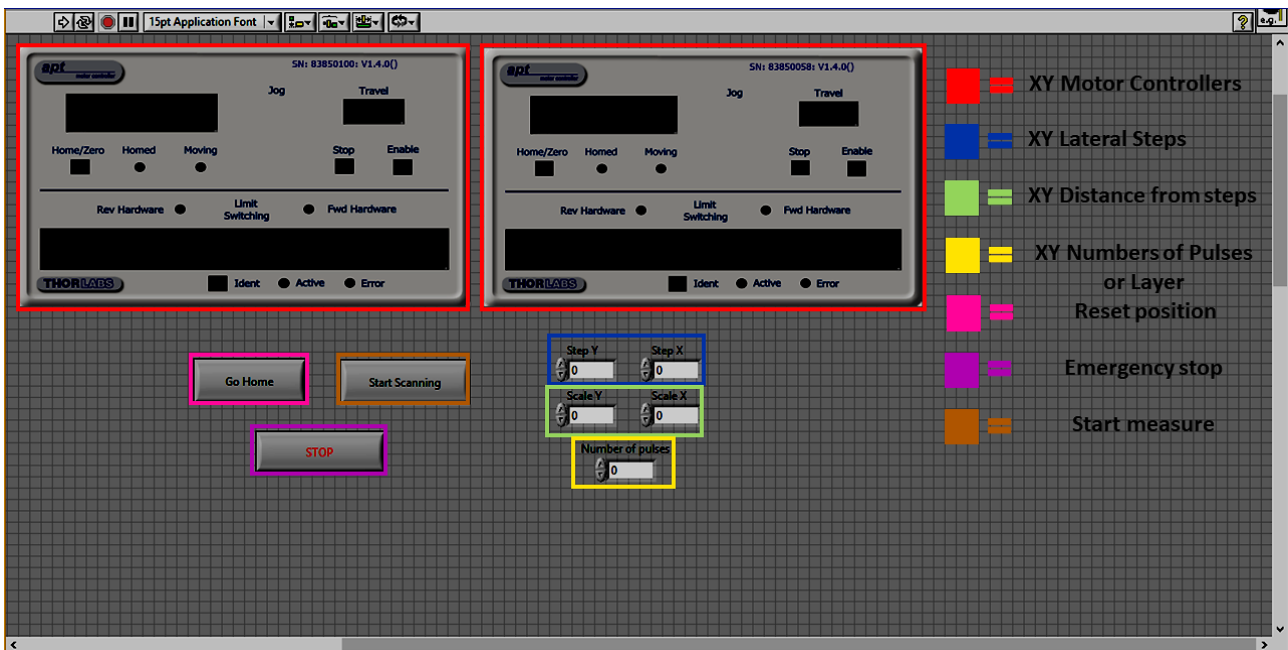


Fig. 14 User Interface (UI) of the micro-libs-scanner.

In the following diagram (Fig. 15) the chain of operations to be done to generate a single layer or multilayer map is shown.

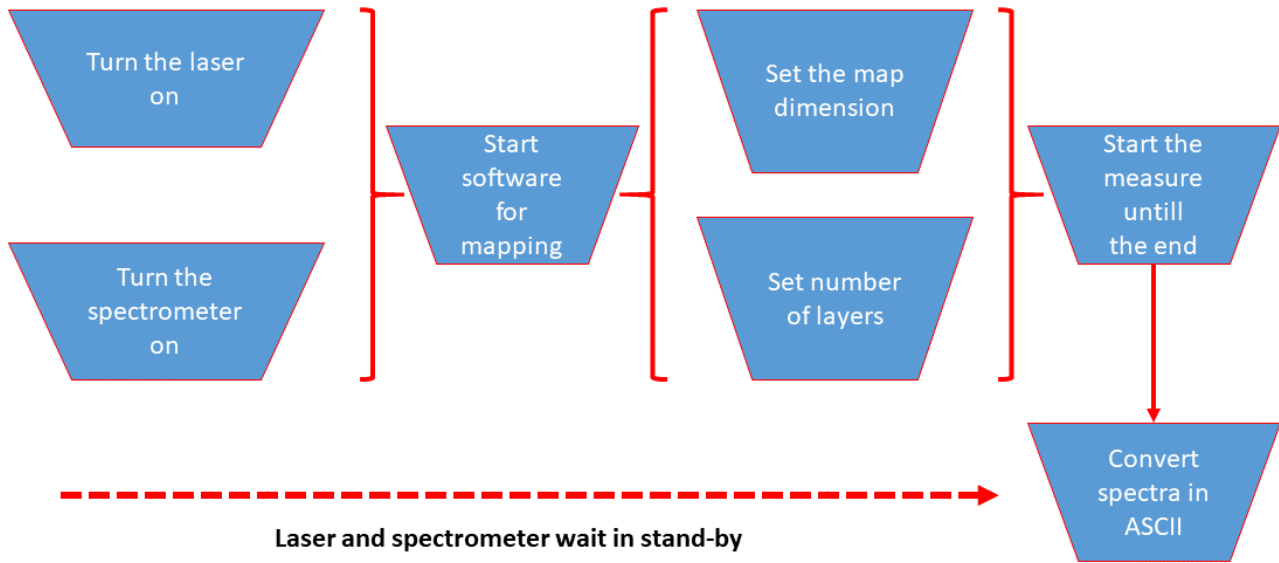


Fig. 15 Diagram of operation for control system.

The system is semi-automated: The operators must anyway activate the laser and spectrometer separately with the proprietary software (Fig. 16).

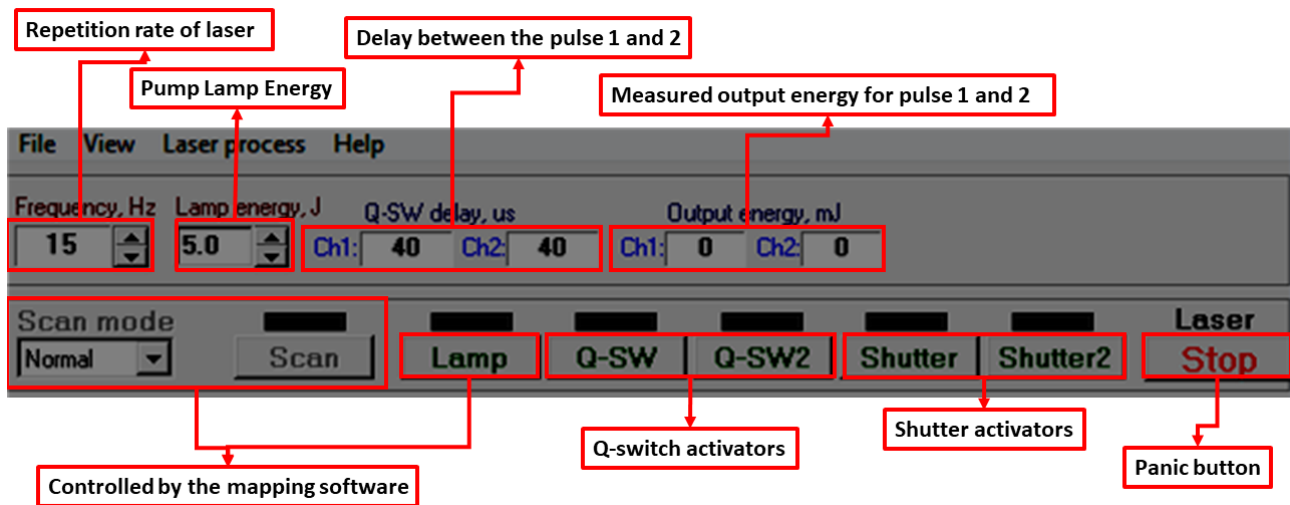


Fig. 16 UI of the laser control software

2.5 Energy of the laser and measurement spot

To realize the breakdown condition, that is, the portion of the specimen hit by the laser can vaporize and turn into plasma, the laser irradiance must be high. The plasma temperatures reach typically several thousand degrees (more or less 10000 K). For laser pulses between 10 and 100 mJ, with focal lenses between 5 and 20 cm, the irradiance is in the range of 10^9 to 10^{11} W/cm² [66]. To vary the energy of the two pulses, it is necessary to change the pump lamp energy value. The double laser, inside the instrument, in fact, is made by one flash lamp and two rods of Nd:YAG, the gain medium. In this way, it is possible to simultaneously vary the output pulse energy. Unfortunately, the two beams are quite different in term of energy, the first one is lower than the second one, but this is not a problem for LIBS measurements [156] (Table 6).

Table 6 Table of the energies measured for the Modì laser. First pulse (F1), second pulse (F2) and F1+F2. Notice that the F1+F2 value is not the sum of the F1 and F2, but a completely independent measure performed directly on the double pulse.

Pump Lamp Energy (J)	F1 (mJ)	F2 (mJ)	F1+2 (mJ)
13	0.83±0.2	4±0.2	4.6±0.2
14	1.73±0.4	4.8±0.4	7±0.4
15	2.4±0.1	6.4±0.1	8.7±0.1
16	3.8±0.2	7.6±0.2	11.2±0.2
17	4.9±0.2	8.6±0.2	13.3±0.2

The dimension of the spot cannot be changed in the MODì instrument, because the optical system (both for focusing and collecting) is fixed, but the diameter of the crater changes depending on which type of analysis do you want to perform. The possibility to use the double pulse approach allows to improve signal-to-noise ratio with the same total laser energy, but the dimension of the crater irreparably increases [157]. The Fig. 17 shows the spectrum of a 2+2 mJ double pulse and the relative crater: the obtained spectrum results even more intense with respect to a single pulse spectrum with 10 mJ of total energy. In the 2+2 mJ double pulse spectrum, the main peak (calcium around 525 nm) reach about 12600 counts (u.a.), while in the Fig. 18 we can see that the spectrum (with 10 mJ energy) in a single pulse mode has a spectrum with much lower intensity where the calcium peak at 525 nm has a maximum of about 2600 counts (u.a.). The two different modes and energies show the same crater size of about 50 µm. The double impulse proves to be advantageous because with the same size of crater it has a more readable spectrum.

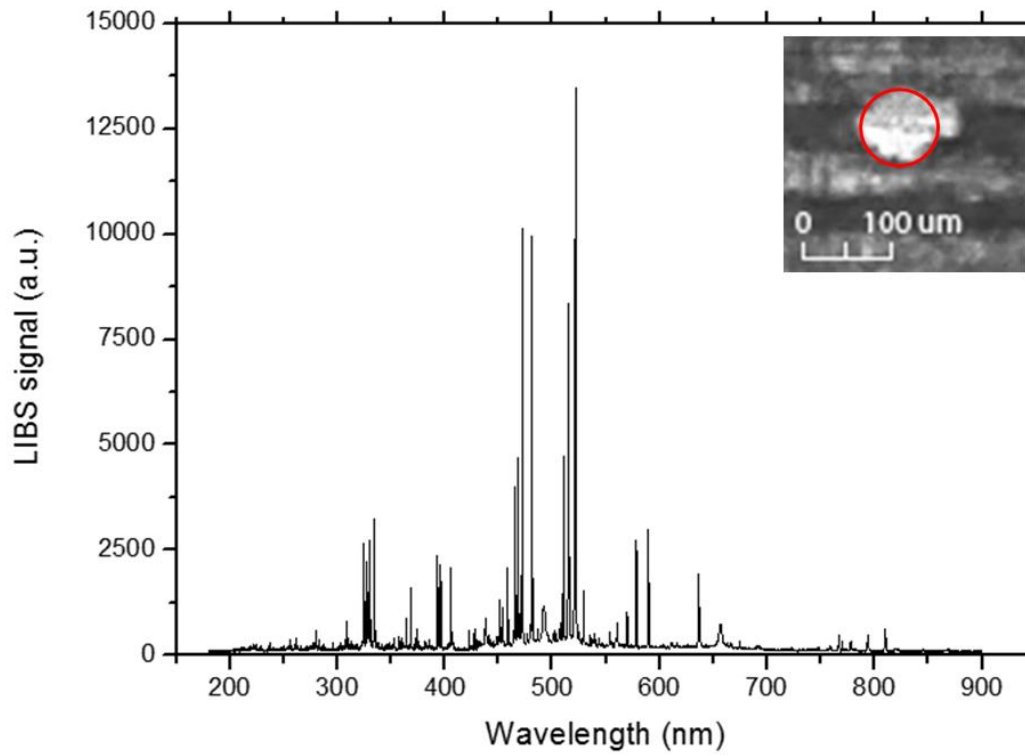


Fig. 17 Double Pulse LIBS spectrum of a brass sample (2 mJ per pulse, 1 μ s between pulses). The crater is not circular due a little divergence of the two beams. Figure is taken from Grassi et al. [157] and re-elaborated.

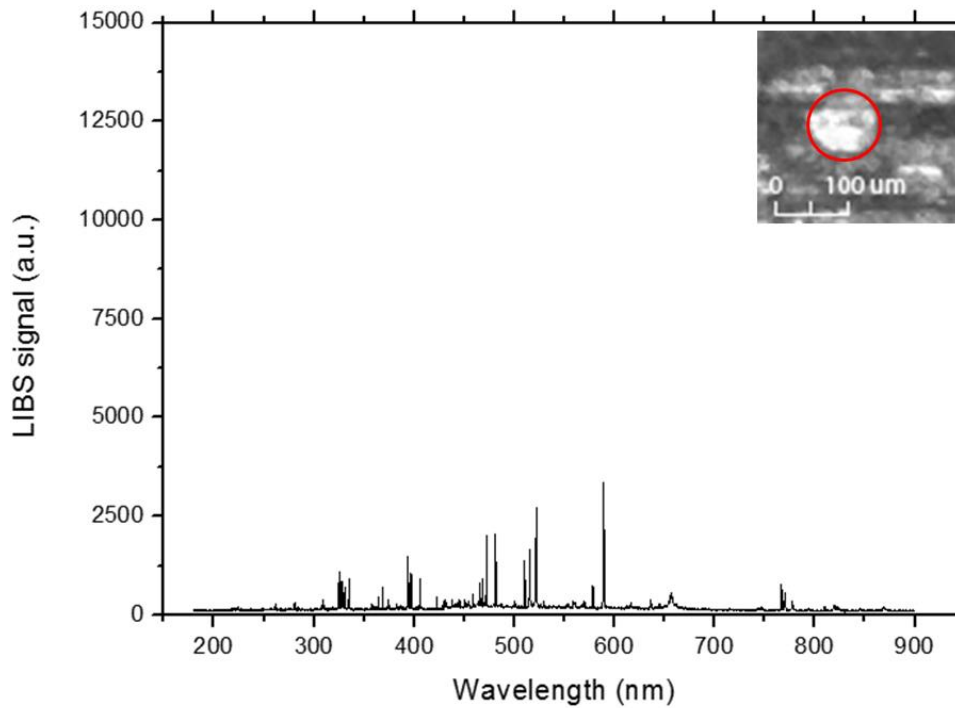


Fig. 18 Single Pulse LIBS spectrum of a brass sample (10 mJ pulse). We can see a very low intensity of the entire spectrum. On the main peak (around 525 nm) the intensity is lower of about 3000 counts. Figure is taken from Grassi et al. [157] and re-elaborated.

Another advantage of the use of the double pulse technique is that the influence of environmental gases is reduced (as previous explained in Cap. 1).

2.6 Mapping and analysis softwares

The qualitative and quantitative analysis of the LIBS spectra (identification of the elementary peaks, their fitting) as well as the spectra manipulation (sum and averaging) is done with a software written in C++ by the ICCOM CNR-ALS Lab group (LIBS++) (Fig. 19).

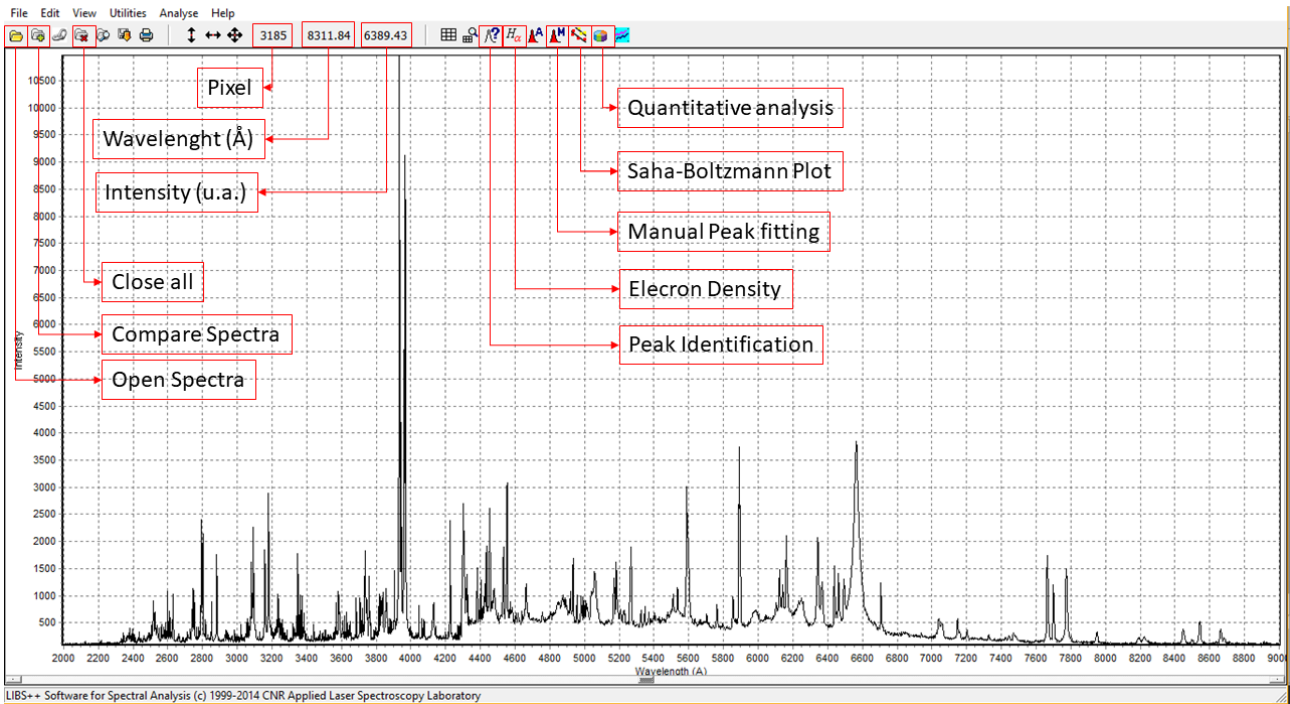


Fig. 19 Principal UI of LIBS++ Software

A second routine, dedicated to elementary mappings and to the statistical analysis, is written in MATLAB®. It is possible selecting, in MATLAB® script, the pixel number associated to the center of the peak of interest to create the corresponding map. The map can represent the intensity of the peak, or, if you consider a short range around the peak, the sum of the intensity values, or the integrated intensity of the peak. Furthermore, through the software it is possible to normalize to the total intensity of the spectrum (Fig. 20).

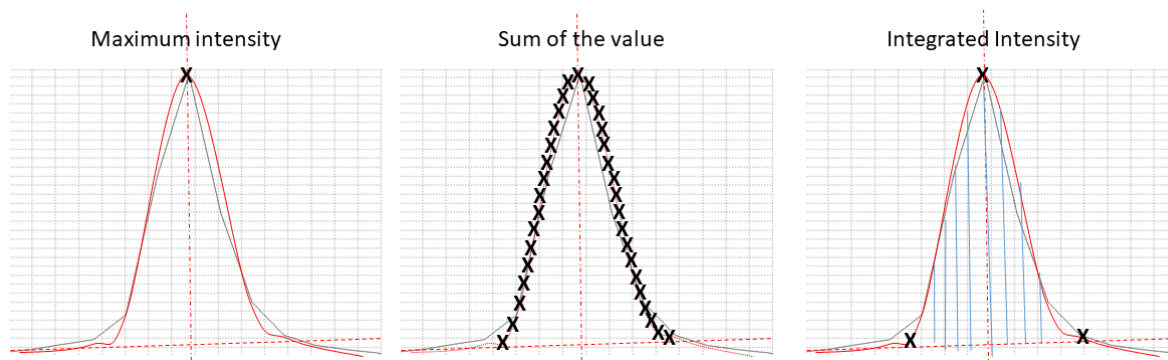


Fig. 20 Different approaches to elaborate data to create the maps

For the integration, a Gaussian profile is selected. The script, described in detail in the Appendix of this work, follows several steps to obtain the elemental maps that can contain different information as previous explained. To better visualize the information shown in the single elementary maps, it is possible to combine them to build a sort of false color map. In Fig 17 the single map of silicon, aluminum and calcium (from an archeological potsherd) are combined in a false color map.

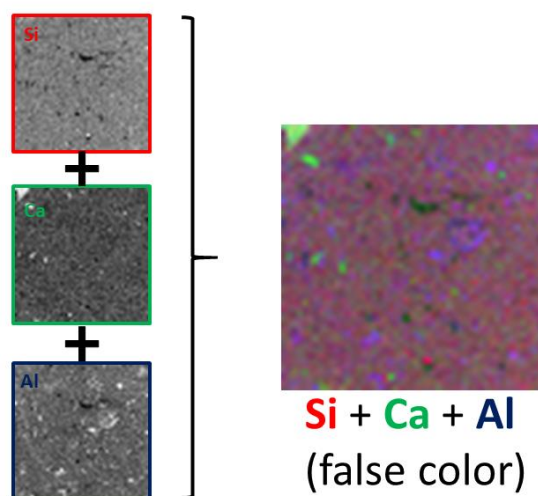


Fig. 21 A scheme of the realization of false color maps, useful for identifying the distribution of the main elements.

The workflow for the generation of individual elementary maps is divided in six steps. First, all the spectra related to a single analysis area are loaded. The spectra are stored in a linear vector. Then, you can select the peak center, or a range around the peak. The generated data are arranged in a new linear vector. This choice allows to have a complete and unprocessed copy of the spectra that can be subsequently processed. The linear vector undergoes a new process that models it to take the shape of the set scan area. The script

generates a three-dimensional matrix: x-axis and y-axis are the relative positions of the analyzed point and z-axis contains the information on the elementary peaks or portions of the spectrum. From this matrix, we can extract the values of z-axis corresponding to a given peak or to an area of the spectrum obtaining the distribution maps (Fig. 22).

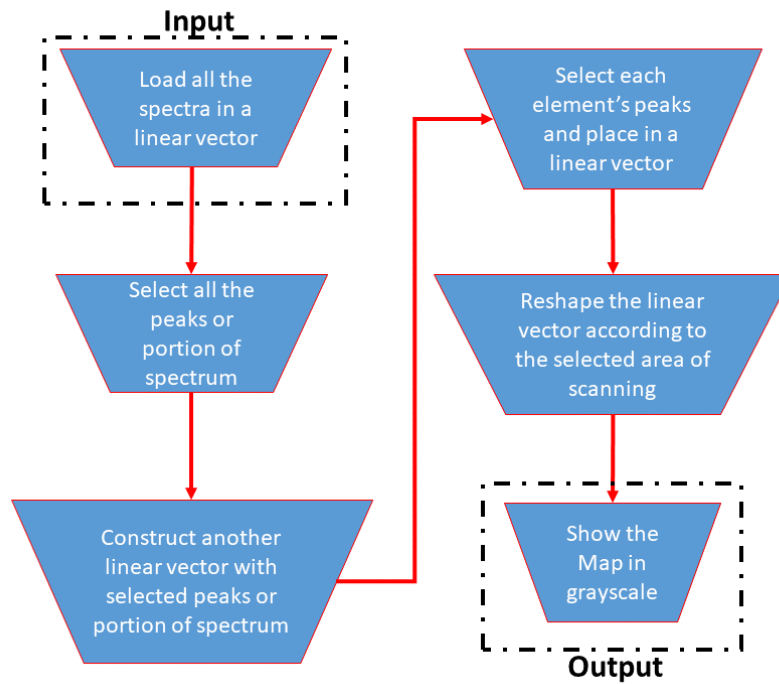


Fig. 22 Workflow for generating the elemental maps.

The distribution maps of the single elements of interest can be used with other analysis tools, such as the Principal Component Analysis (PCA). This method allows reducing the dimensional space and it is particularly useful when the elements to be displayed are more than three. The algorithm, with a proper linearization creates new spatial coordinates, called principal components, which are able to explain a statistically significant variation within the set of original maps [158–166]. The new maps obtained represents a dimensional reduction ($R^{n1} \rightarrow R^{n2}$, where $n2 < n1$) that can easily visualized in a false RGB color space (Fig. 23).

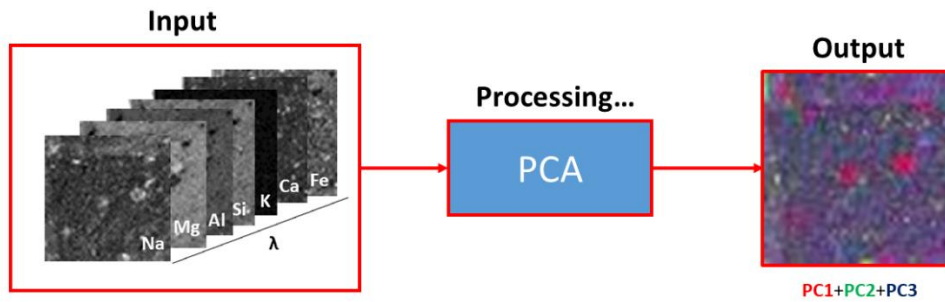


Fig. 23 Data flow and processing for obtain a false color PCA map.

Sometimes, a non linear approach can be preferable in order to cluster the spectra referring to the minerals species instead of the concentration of the single element. A specific script is dedicated to the data segmentation with self-organized neural networks (SOM). Kohonen self-organized maps belong to the unsupervised ANN algorithms. The process does not use error-minimization functions (i.e. back-forward propagation or last mean square), but competitive-type (so called vector quantization) algorithms. The maps merging is not automatically realized, a preliminary test of the individual segments is performed with the extraction of the weights of each component in the single segment/map. In this way, it is possible to quantify the area in the map occupied by the single segment (Fig. 24). The extraction of this type of information allows us, once we have identified the nature of the segment we are observing, to quantify its distribution within the mapped area. For example, if we could identify a segment composed of iron oxides in a matrix of barium, we could establish, within the investigated area, the ratio between matrix and inclusion of iron oxides.

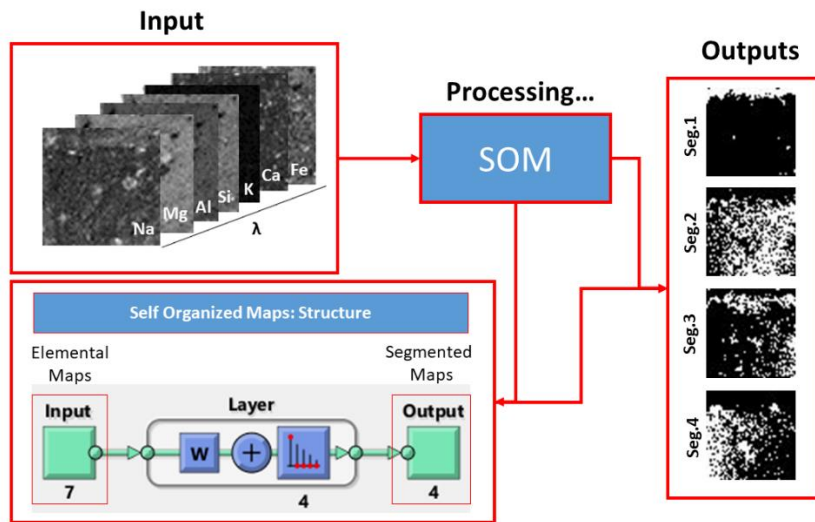


Fig. 24 Data flow and processing through SOM algorithm for obtaining segmentation of elemental maps.

3. Case Studies

In this chapter, the main applications, some of them already published as preliminary results during the three years of PhD [157,167–171], are reported.

3.1 Inhomogeneous materials

The inhomogeneous materials are the class of objects, natural or artificial, whose microscopic structure is not organized according to fixed modules of constant composition, but whose matrix varies completely in a punctual and random way. There are several examples of these materials: starting from some types of natural rocks up to artificial materials such as mortars and ceramics to which clasts of different compositions are added to improve their mechanical and thermal properties.

3.1.1 Pottery

There are several established procedures for the analysis and characterization of ancient and modern ceramics. What they have in common is their cost-effectiveness in economic terms and the need to take samples to make thin sections or destructive analysis. The use of the LIBS allows carrying out measurements directly on the sample, without any preparation. The measurements can be performed on a single spot on the entire scanned surface, on the single layer (mean value of single segment value), in depth or multilayer.

3.1.1.1 Clustering of archaeological pottery by means of LIBS and statistical methods

The real novelty of the μ -LIBS scan is the possibility of making elementary mappings on surfaces that can reach 2.5 cm on each side. The elementary mapping allows the identification of the qualitative distribution of specific elements and, through specific data processing commonly used in the imaging analysis, the identification of the relationships existing among them. To do that, however, it is necessary to test methods that extracted information on clusters from raw spectra by means of statistical methods such as a PCA that reduce the dimensionality of the inputs giving new components based on the correlation between the initial inputs.

Materials and methods

The analyzed materials come from an archeological site in Abruzzo, investigated until the mid-1990s: the Settefonti a Prata d'Ansidonia (AQ-Italy). The Department of Civilizations and Forms of Knowledge of the University of Pisa made the samples available (11 selected, as representative, over 17000 studied potsherds). They all belong to an advanced stage of the Final Neolithic and fall into what the academics call Ripoli culture (Fig. 25). From the site, investigated only partially for an area of about 100 m², came more of 17000 potsherds that have been previously studied in a systematic way and from which a series of significant fragments have been selected to be submitted to archaeometric surveys.



Fig. 25 The analyzed samples from Settefonti a Prata d'Ansidonia archaeological site (AQ-Italy). The sample 7FFig.2 is not in the table.

Archaeologists divided these fragments into four classes with different characteristics to each other, which probably also correspond to different uses (Table 7).

Table 7 Clusterization of potsherds based on archaeological classification.

Class.	Id. Samples
Figulina ware	7FFig.1, 7FFig.2, 7FFig.3, 7FFig.8
Black gloss surface ware	7FFN.7, 7FFN.35, 7FFN.36
Red surface ware	7FFR.1, 7FFR.22, 7FFR.25
Coarse ware	7FGr.17

The analysis of the fragments in thin section confirmed the distinction made by archaeologists on a technological basis, highlighting that the bulk material of black glossy surfaces contains fragments of shredded ceramic (Fig. 26).

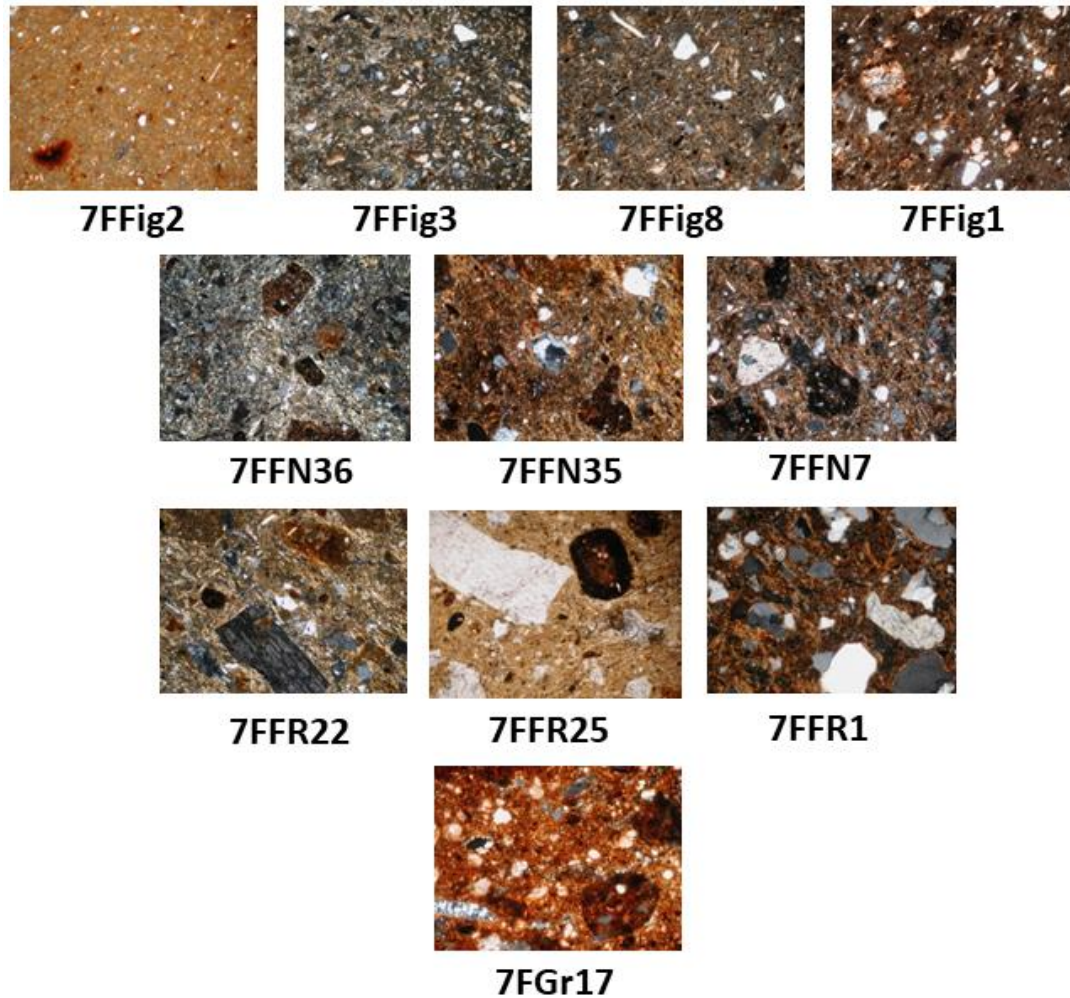


Fig. 26 Thin section of the samples analyzed. First row, from left to right: 7FFig2, 7FFig3, 7FFig8, 7FFig1. Second row, from left to right: 7FFN36, 7FFN35, 7FFN7. Third row, from left to right: 7FFR22, 7FFR25, 7FFR1. The last pic is 7FGr17.

The analysis of the thin sections allowed to create a new subdivision of the material in four classes, based on the granulometry and its main rock and crystal contents (Table 8).

Table 8 Thin section analysis of samples. Q=Quartz; K=K-Feldspar; Pl=Plagioclase; Ph=Phyllosilicate; C=Carbonate; Cal= Calcite; Gg=Grog*; Fs= Fossils. *Grog is a technical term that indicates the use of shredded ceramics in the raw materials.

	Q	K	Pl	Ph	C	Cal	Gg	Fs
7FFig2	X	X		X		X		
7FFig3	X	X		X	X	X		
7FFig8	X	X		X	X			X
7FFig1	X	X		X	X			
7FFN36	X	X		X	X		X	X
7FFN35	X	X		X	X	X	X	
7FFN7	X	X	X	X	X		X	
7FFR22	X	X	X	X	X	X		
7FFR25	X	X	X	X	X			
7FFR1	X		X	X	X			
7FGr17	X		X	X	X			X

All samples were analyzed by means of LIBS spectroscopy, with lamp energy set at 17.5 joule. Five consecutive laser shots were made at 5 different points of the sample fracture avoiding striking the visible inclusions. The spectra of the first shots were discarded and the remaining 20 spectra were averaged. To process the LIBS spectra the graph theory algorithm has been used [172]: the whole spectrum, without any qualification or preventive identification is used to implement this algorithm that is able to separate the spectra of different samples based on intrinsic characteristics of the individual spectra, without any supervision by the operator. Applying this method [172–175] to the measured LIBS spectra, the samples can be divided in 4 clusters, listed in the Table 9 and shown in the Fig. 27.

Table 9 Modularity class applied to the graph of the samples.

Id. Sample	Modularity class
7FFIG1	0
7FFIG2	0
7FFIG3	0
FFFIG8	0
7FFN7	1
7FFN35	3
7FFN36	1
7FFR1	2
7FFR22	2
7FFR25	2
7FGr17	3

7FFIG1
7FFIG2
7FFIG3
FFFIG8

7FFR1
7FFR22
7FFR25

7FFN17
7FFN35

7FFN7
7FFN36

Fig. 27 Graph showing the clusters obtained applying a modularity class algorithm.

Comparing the results of the fast clustering of the samples with LIBS and graph theory with the ones obtained from the thin section analysis, the only sample that is wrongly classified is 7FNN35 probably due to the presence of high contents of calcite that saturate the calcium-related peaks. In fact, the only difference found in the corresponding thin section is the presence of calcite and the absence of plagioclase. However, the error is still acceptable from the perspective in which we use the technique as preliminary screening.

3.1.2.1 Micro-chemical evaluation of ancient potsherds by μ -LIBS scanning on thin section negatives

The main idea behind this work was to try if it is possible to exploit the negatives of thin sections created for the analysis of ceramic fragments to carry out elementary mappings and subsequent considerations on the features identified through them. Part of the work was published recently on the Mediterranean Archeology and Archaeometry following the presentation in the Cultural Heritage session at the SGI Congress held in Pisa in September 2017.

Materials and methods

In this study, four fragments from Fucino (Abruzzo, Italy) (Fig. 28) have been analyzed thanks to the permission of *Soprintendenza Unica Archeologia, Belle Arti e Paesaggio per la Città dell'Aquila e i Comuni del Cratere*. The samples belong to an advanced stage of the final Neolithic and are quite similar in their aspect: the surface presents a very intense glossy black finish with an almost metallic appearance.

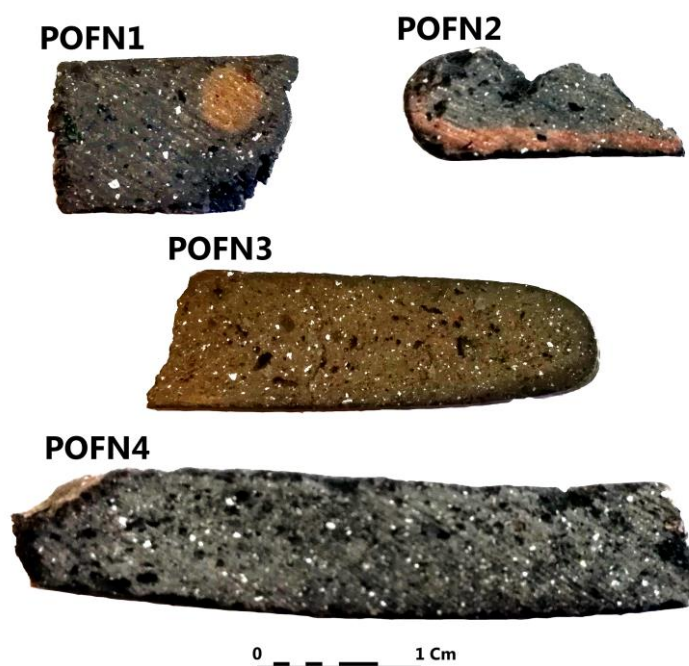


Fig. 28 The analysed samples.

The choice of the samples was based on the statistical representativeness of this specific ceramic class, its characteristics and the availability of the samples themselves. Table 10 summarizes the selected samples. The class of body shape of the pottery vessels is the same as well as the bulk granulometry. The data were acquired using a μ -LIBS-Scan in raster of 50x50 shots at a lateral resolution of 100 μ m for 25 mm².

Collected spectra were processed by the developed routine on MATLAB® (described in Cap. 3), able to select the intensity lines of interest for each detected element (Na, Mg, Al, Si, K, Ca, Fe) in the square matrix associated to the scanned surface (Table 11).

Table 10 Summary table of analyzed samples.

Sample	Provenance	Shape	paste	Finishing
POFN1	Paterno (Abruzzo)	Tronco-conical vessel	Semi-depurated	Black-gloss
POFN2	Paterno (Abruzzo)	Tronco-conical vessel	Semi-depurated	Black-gloss
POFN3	Paterno (Abruzzo)	Tronco-conical vessel	Semi-depurated	Black-gloss
POFN4	Paterno (Abruzzo)	Tronco-conical vessel	Semi-depurated	Black-gloss

Table 11 Wavelength of the characteristic elements studied.

Element	Wavelength (nm)
Na	819.48
Mg	279.55
Al	309.24
Si	288.16
K	766.50
Ca	422.68
Fe	259.88

At the same time, the software performs a normalization procedure point-by-point based on the total intensity of the LIBS spectrum, to minimize effects caused by changes in the focusing of the laser beam (Fig. 29).

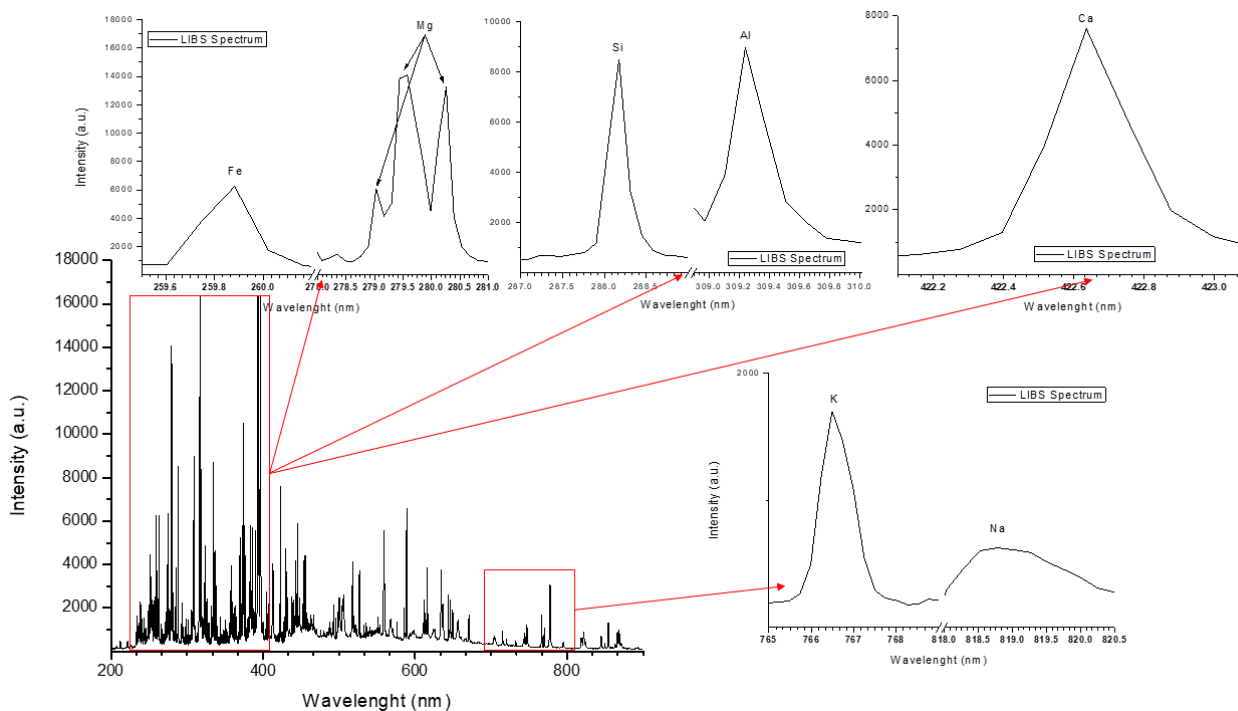


Fig. 29 LIBS spectrum of a potsherd.

Once the intensity has been obtained for each row of each element on the whole scanned surface, a greyscale map is built, where 0 is the minimum intensity value (corresponding to black) and 255 is the maximum value of intensity (corresponding to white). The maps were placed in a hyperspectral “cube”, where the X and Y coordinates (common to all the maps) identify the point in the two-dimensional Cartesian space and Z (different for each map of each element) is the intensity related to the single identified element (Fig. 30).

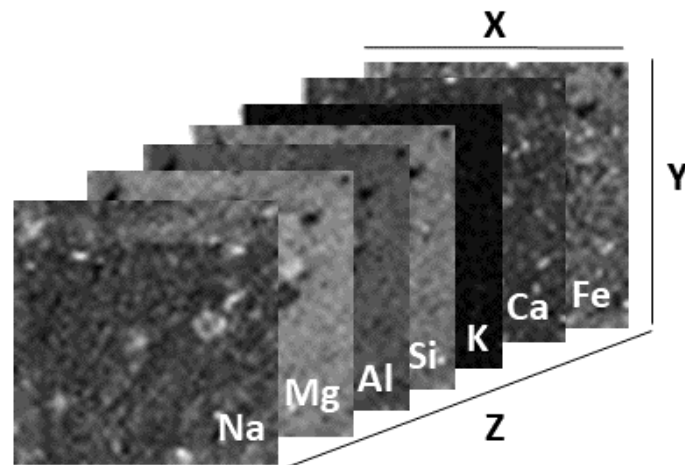


Fig. 30 A representation of a Hyperspectral cube.

After creating the hyperspectral cube, using a method that derives from the multispectral image analysis, the main characteristics of the samples have been identified and the elemental distribution determined in the analyzed surfaces. In addition, three elementary maps (Si, Ca, Al) have been combined in order to observe the relative distribution of three main elements constituting the archaeological ceramics (Fig. 31). Through this method, it is possible to observe the relative distribution of all the elements of interest, their association, highlighting, as in this case, clasts of particular composition. Clasts containing mainly calcium (in green) are separated from the silico-aluminate matrix of ceramics (purple). Inside them, variations, even minimal, of composition, not visible in the pictures of the scanned surfaces, are defined with different shades of purple in the maps (Fig. 31).

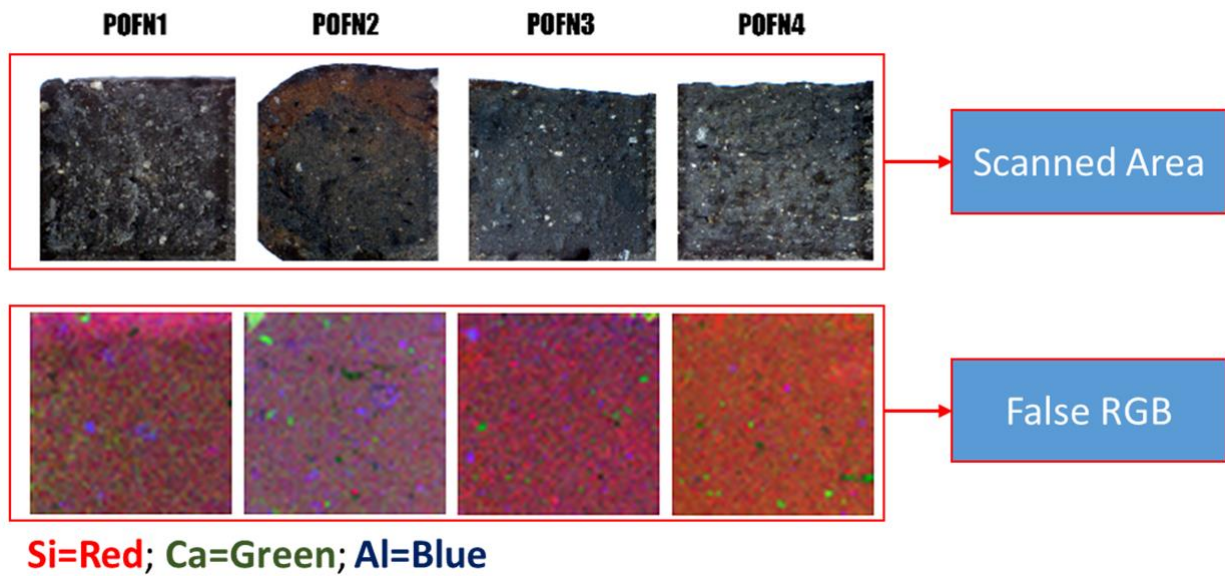


Fig. 31 False-RGB using elemental maps of Si, Al and Ca compared to real photo of scanned surfaces.

To quantify the composition of the different areas, a segmentation of the scanned surfaces has been realized using the SOM network, as reported in Chapter 2 (Fig. 32). It was built a network for each analyzed sample and each one was trained separately⁹, for this reason, it is not possible a direct comparison between the samples. However, four different segments were identified for each sample together with the percentage of occupied space in the scanned area (Table 12).

⁹ This procedure was necessary because for the training of several samples at the same time a more performing machine (personal computer) is required and able to perform calculations in parallel with other machines and / or to exploit the graphic processor unit (GPU) of the video card.

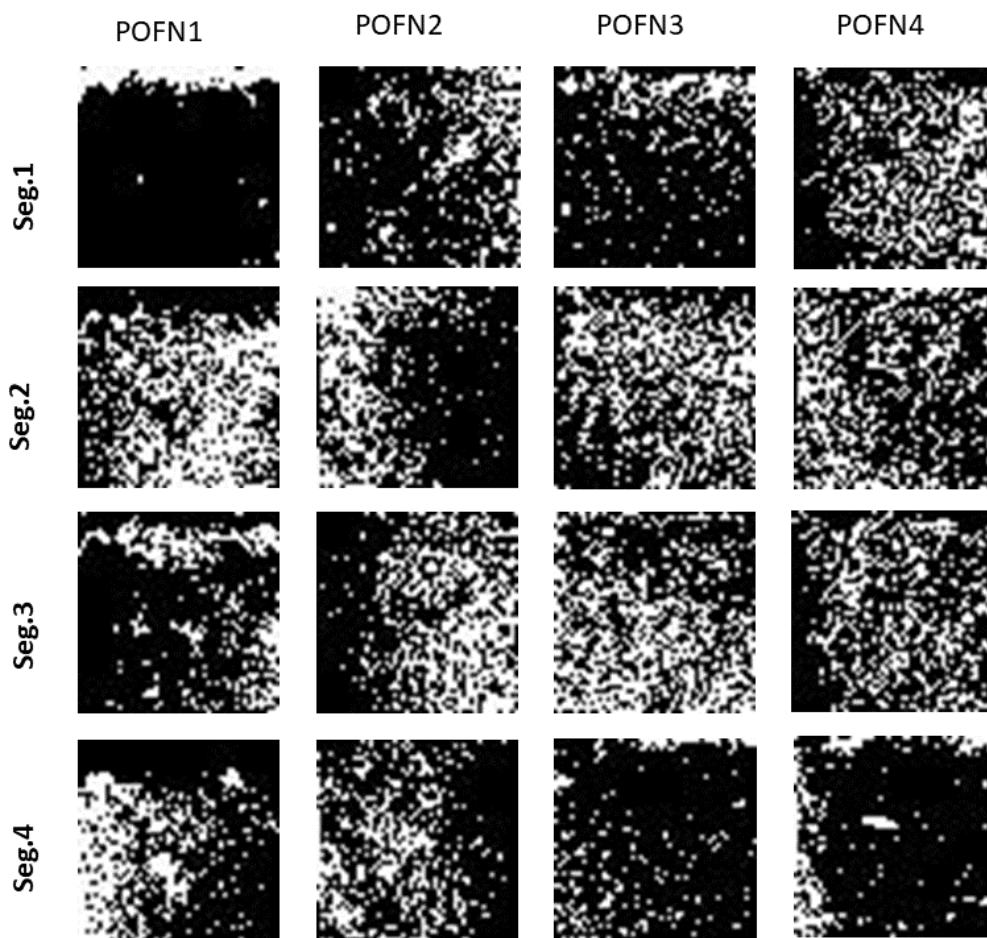


Fig. 32 Segmentation of the analyzed areas on samples using Self Organized Maps.

Table 12 Percentage of the scanned area occupied by each segment.

	POFN1	POFN2	POFN3	POFN4
Seg.1	10.04%	18.64%	13.8%	30.16%
Seg.2	43.96%	25.12%	36%	30.68%
Seg.3	18.2%	32.64%	40.44%	26.56%
Seg.4	27.3%	23.60%	9.76%	12.6%

The spectra belonging to the same segment have been averaged with a proper MATLAB code and the result analyzed using the Calibration-Free LIBS (CF-LIBS) method. The results are shown in Fig. 33, Fig. 34, Fig. 35 and Fig. 36).

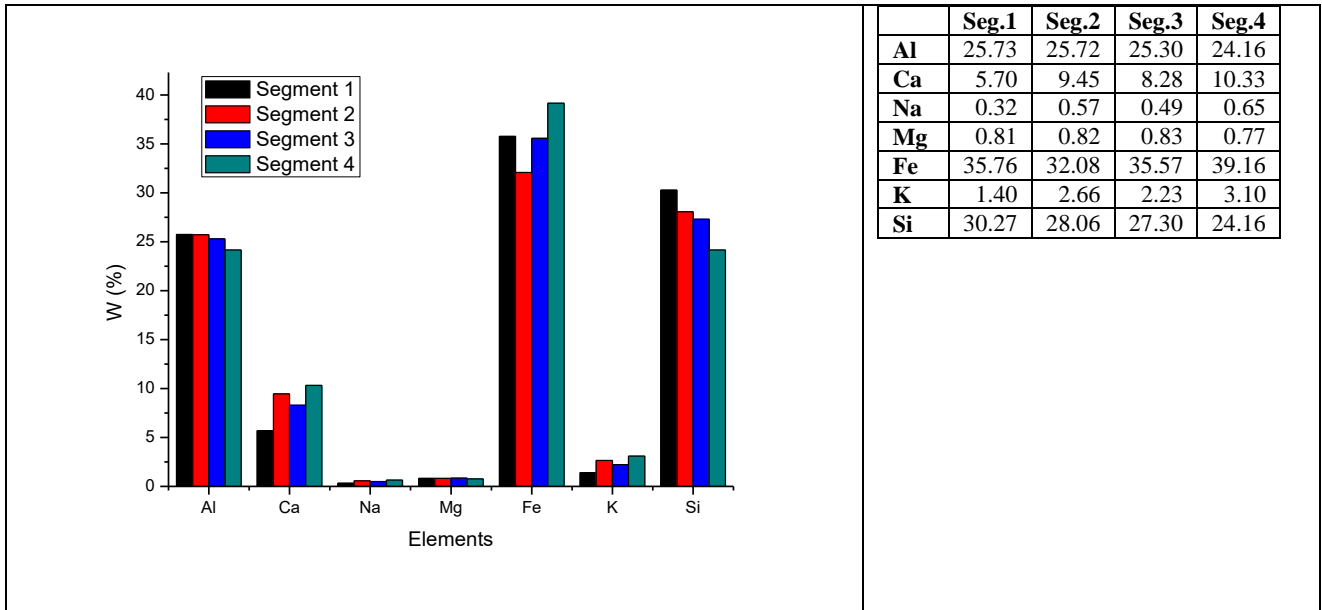


Fig. 33 POFN1 Quantitative analysis on segmented elemental map.

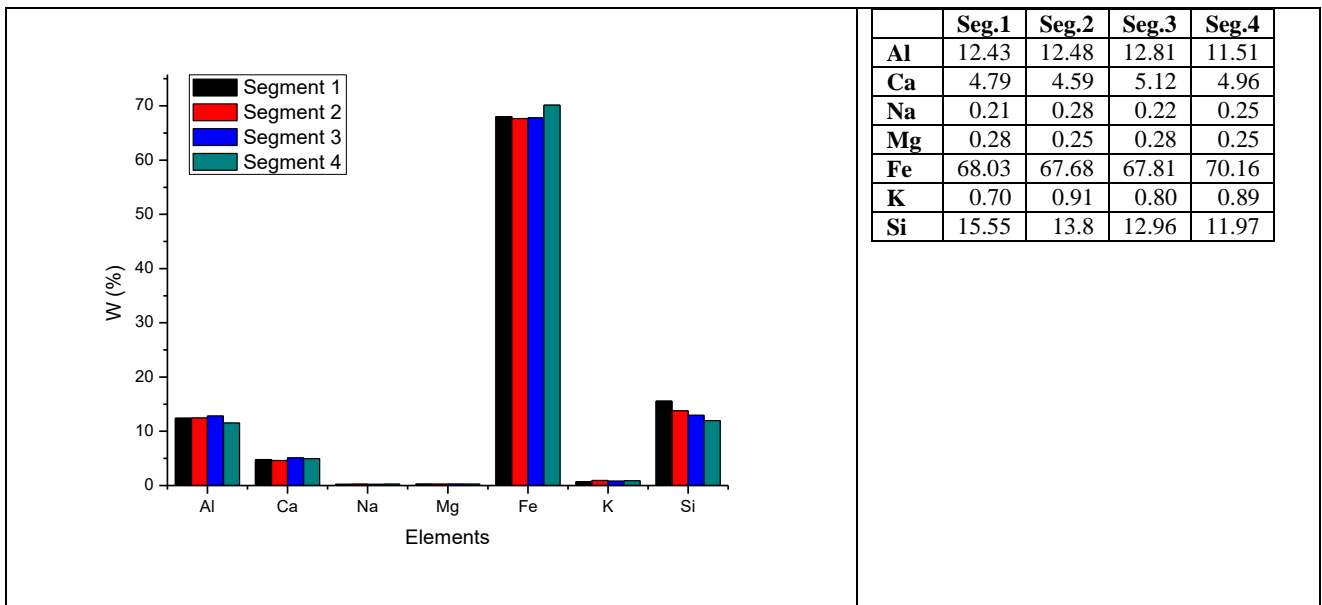


Fig. 34 POFN2 Quantitative analysis on segmented elemental map.

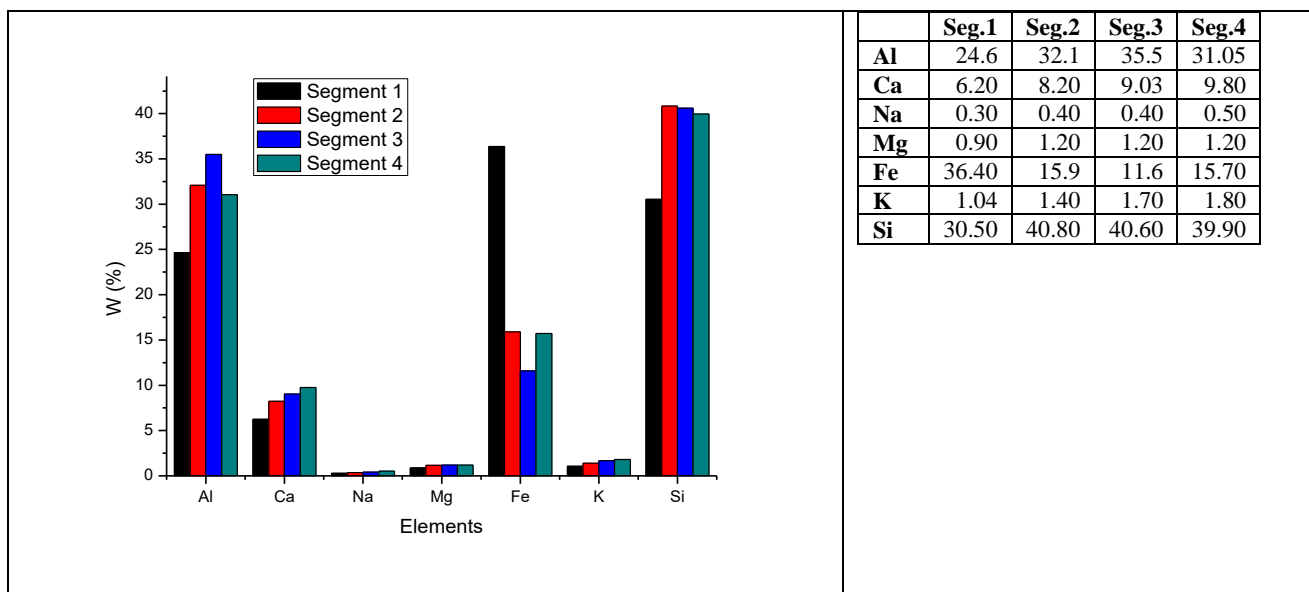


Fig. 35 POFN3 Quantitative analysis on segmented elemental map.

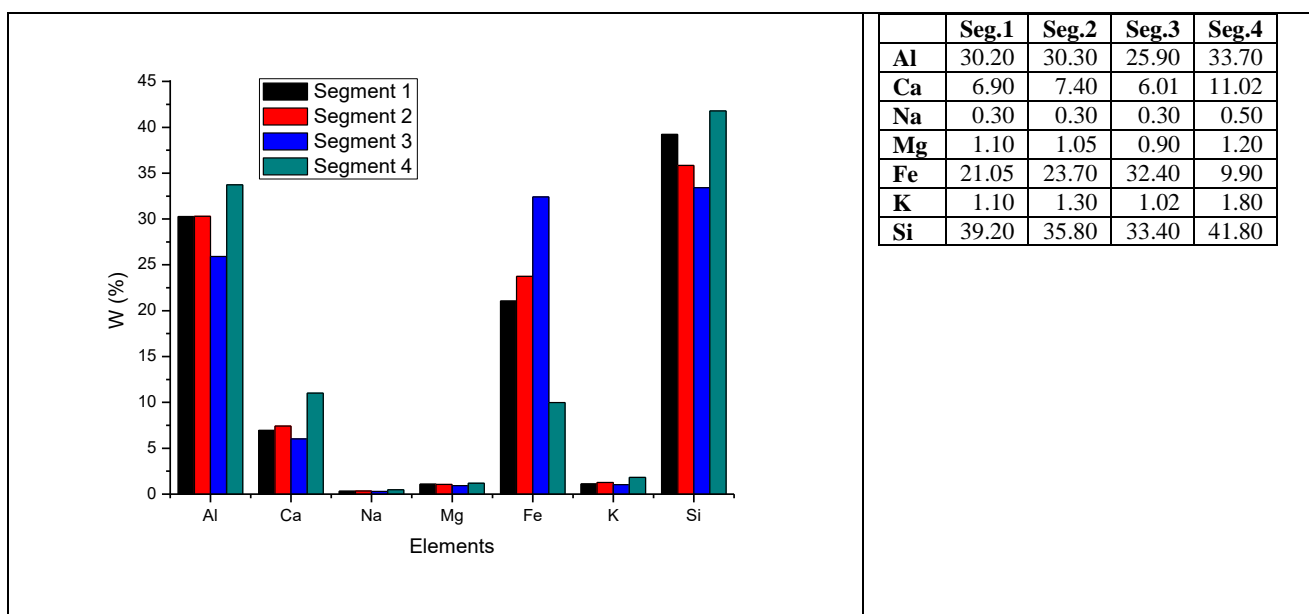


Fig. 36 POFN4 Quantitative analysis on segmented elemental map.

The analysis by means of elementary mapping of ceramic fragments has shown that, although they belong to a stylistically homogeneous vessel class, they technologically present small, but significant differences in the elemental composition of the ceramic body. The most evident inhomogeneity is shown in the POFN2 fragment, which seems to be very different from the other fragments for the total iron content, which is very high compared to the other fragments. Obviously, with few samples, it is difficult to try to formulate hypotheses; the difference could be intentional, due to the use of different raw materials or to the addition of iron oxides as contaminant.

3.1.3 Mortar analysis

As for ceramics also for ancient and modern mortars, there are several well-established analytical procedures, but, at the same time, the mortars are suitable samples to be analyzed by μ -LIBS mapping, because of their heterogeneity due to the different composition of binders and aggregates. The mixture of the components used for the realization of the mortar reacts with the environment transforming partially or completely the matrix. These differences can be highlighted, qualitatively, through the compositional imaging that with different shades of color. Once these areas (binder, aggregate and reaction zones) have been identified, it is possible to estimate quantitatively their elementary composition.

Materials and methods

Two fragments of mortars from the Castle of Adrano (Sicily) have been studied, thanks to the permission of the *Soprintendenza per i Beni culturali e Ambientali di Catania*. The two samples (classified with the inventory numbers N2-2 and S2-3) consist of polished thin sections consolidated by epoxy resin. Their main characteristic is a heterogeneous binder with the presence of aggregates (volcanic ash) with a large variation in grain size (Fig. 37).

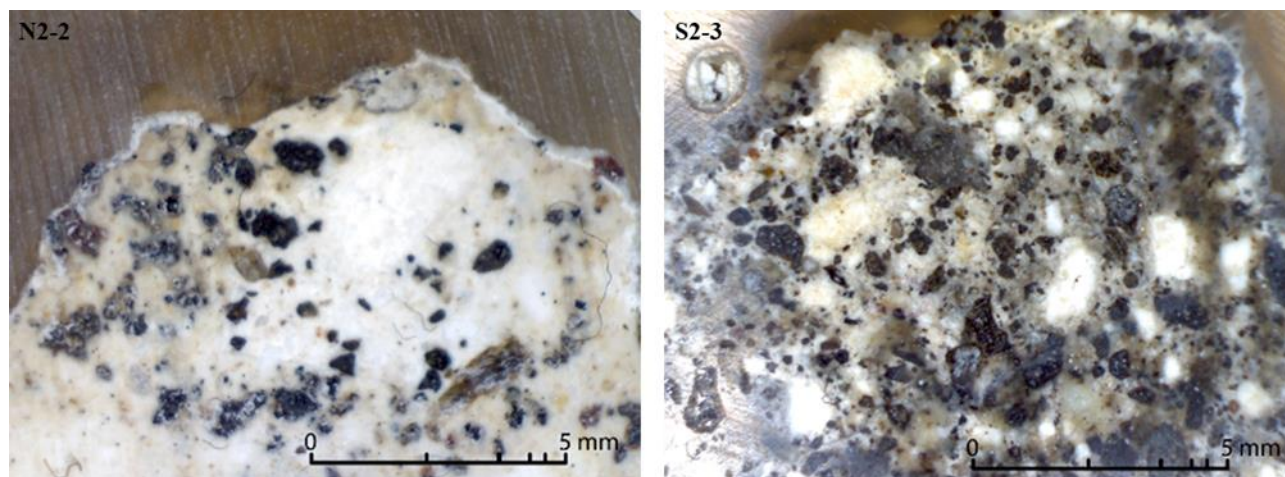


Fig. 37 Micro-photos of the two analyzed samples (Taken from Pagnotta et al. [167]).

The two micro-photos in Fig. 37 show the types of analyzed mortars. The color of the background paste appears the same, but the grain size and the distribution of the aggregates are very different from each other. For this analysis, the element maps were acquired on a 50x50 matrix (2500 LIBS spectra) with a lateral resolution of 100 μ m, for a total scanned area of 25 mm², with the laser operating at 1 Hz repetition rate. The diameter of the laser crater at the sample surface was about 20 μ m. In the following Table 13, the central lines of the analyzed elementary peaks are reported.

Table 13 Selected elements and central wavelength (Taken from Pagnotta et al. [167]).

Element	Ion.	λ (nm)
C	I	247.8
Na	I	589.0
Mg	II	279.4
Al	I	309.3
Si	I	288.2
Fe	I	372.0
Ca	I	445.2

First of all, the distribution maps of the intensity of the selected elements were built (Fig. 38).

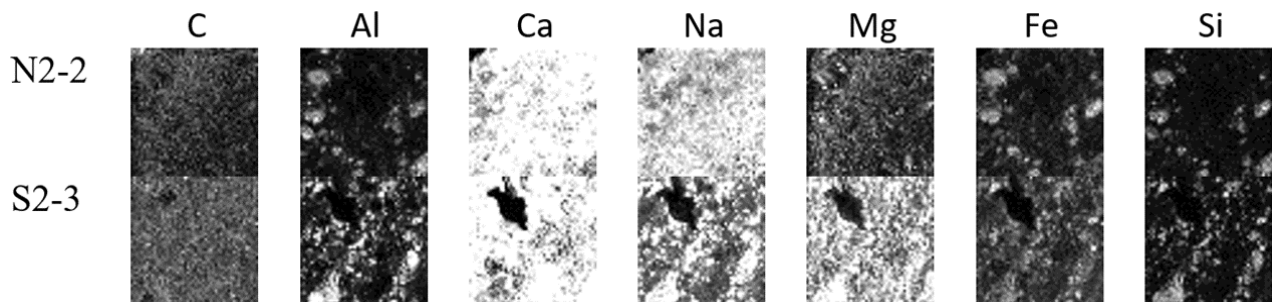


Fig. 38 Elemental distribution in the two samples (Taken from Pagnotta et al. [167]).

Moreover, for the preliminary qualitative characterization of the spatial relations between binders and aggregates the maps of the intensities of the Ca/Mg and Si, Al and Ca were combined.

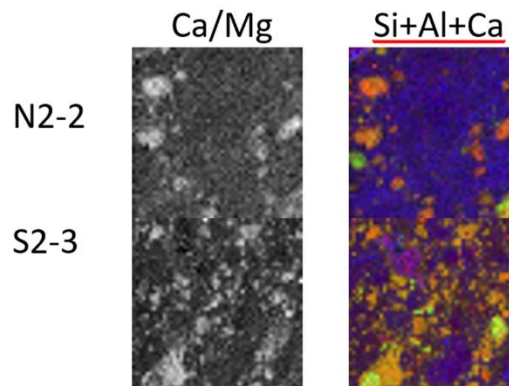


Fig. 39 The Ca/Mg line intensity ratio and the false-color map -distribution of Si –red-, Al –green- and Ca –blue- line intensity- (Taken from Pagnotta et al. [167]).

Looking at the maps in the Fig. 39, it is possible to identify at a glance in the Ca/Mg maps the distribution of aggregates (white areas) and binders (dark areas), while the map in false colors allows to underline their inhomogeneity. This lack of homogeneity may be due to the specific characteristic of the raw material or to the chemical reactions with the environment or between the binder and the aggregate itself. As highlighted by the qualitative analysis, the sample inhomogeneity prevents the use of a single calibration strategy for quantitative analysis, for this reason, a self-organized neural network has been built for automated segmentation of the maps and the averaged spectra for each segment have been processed using the CF-LIBS

method. The SOM network has been optimized with five segments (Fig. 40). This process is the only one that cannot be done automatically but is at the discretion of the operator: a series of tests are carried out starting from a neural network with a low number of neurons (for example 2x1). Then the operator try a number of neurons equal to the number of segments that we expect to find (based on the results of qualitative maps in false colors) and, if the results is not satisfactory, the operator can increase the number of neurons until obtain a number of segments that reflect the false colors maps results.







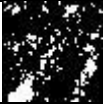
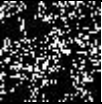

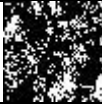
	Seg.1	Seg.2	Seg.3	Seg.4	Seg.5
N2-2					
pixel	238	309	1189	744	20
S2-3					
pixel	163	523	677	682	455

Fig. 40 Elemental maps segmentation realized by SOM with 7 inputs and 5 outputs. The number of pixels occupied by each segment area has been indicated (taken from Pagnotta et al. [1]).

In both the mortar samples, the SOM segmentation reproduced similar patterns, in particular, the segment 3 for sample N2-2 and 5 for sample S2-3 shows the epoxy resin used for consolidation.

The Table 14 shows the percentage of each segment compared to the analyzed area.

Table 14 Percentage of the analyzed areas occupied by segments in each samples.

	Seg.1 %	Seg.2 %	Seg.3 %	Seg.4 %	Seg.5 %
N2-2	9.5	12.4	47.6	29.8	0.8
S2-3	6.5	18	27.1	27.3	20.9

For the sample N2-2, the resin can be easily isolated also without the use of the SOM, while in sample S2-3 is present (6.5%) in different parts of the analyzed area, so a more precise determination of the mortar composition can be carried out only with a proper clusterization, like this one. However, these segments have been removed from the following procedure. As in the case of archaeological ceramics, an average spectrum for each segment has been calculated and processed with the CF-LIBS method. Table 15 shows the selected peak elements. There are several lines for each species to improve the quantitative analysis.

Table 15 Complete list of the elemental peaks used for quantitative analysis by means of CF-LIBS (re-adapted from Pagnotta et al. [167]).

Element	Ion ¹⁰ .	Wavelength (nm)
Al	I	237.31
Fe	II	238.20
Fe	II	239.56
Fe	II	239.92
C	I	247.85
Si	I	250.69
Si	I	251.61
Si	I	251.92
Si	I	252.41
Si	I	252.85
Fe	II	258.58
Fe	II	259.94
Fe	II	260.65
Mg	I	285.21
Si	I	288.15
Al	I	308.21
Al	I	309.27
Ca	II	315.88
Ca	II	317.93
Ti	II	336.12
Ti	II	337.28
Sr	II	346.44
Ca	II	370.60
Ca	II	373.69
Fe	I	385.99
Sr	II	407.77
Sr	II	421.55
Ca	I	422.67
Ca	I	442.54
Ti	I	498.17
Ti	I	499.10
Ti	I	499.95
Ti	I	500.72

The composition of the segments shows a pattern not so different between the two samples. The biggest variations are in carbon and calcium content (Table 16 and Table 17). In the sample N2-2, the aggregate part corresponds to the segment 1 (Seg.1) even if the content in Si is not so high. Probably even the segment 4 (Seg. 4) with a Si content of 9.4% became from the much more fine part of the aggregate. The other segments corresponds to the binder and some reaction between binder (Seg. 3) and aggregate probably in the segment 2 (Seg. 2) that seems to follow the rim of clasts in the Seg. 1. In the sample S2-3, observing the Si contents, the aggregate phase correspond to the segment 2 (Seg. 2) and a much more fine part of it is the segment 3 (Seg. 3). Probably the segment 5 (Seg. 5) correspond to the reaction phase between aggregate and binder (see in Table 17 that the segment seems to follow the rim of clasts in Seg. 2). Segment 4 (Seg. 4) belong to the binder.

¹⁰ I is for neutral line peak element, II is for first ionization stage one.

Table 16 Quantitative analysis of N2-2 sample.











Element	Seg. 1	Seg. 2	Seg. 3	Seg. 4	Seg. 5
					
Al (wt%)	5.8	4.6	1.5	1.0	1.0
C (wt%)	59.4	47.4	56.2	65.4	90.5
Ca (wt%)	6.9	13.4	21.1	15.0	2.2
Fe (wt%)	17.7	25.4	13.4	8.0	4.2
Mg (wt%)	0.5	0.5	0.4	0.3	0.1
Na (wt%)	0.4	0.5	0.5	0.3	0.3
Si (wt%)	7.5	6.1	5.8	9.2	1.6
Sr (wt%)	0.1	0.2	0.3	0.2	0.0

Table 17 Quantitative analysis of S2-3 sample.

Element	Seg. 1	Seg. 2	Seg. 3	Seg. 4	Seg. 5
					
Al (wt%)	0.7	7.2	3.2	1.4	1.4
C (wt%)	93.6	28.4	47.3	67.2	63.1
Ca (wt%)	0.9	6.7	9.0	11.0	12.8
Fe (wt%)	2.8	40.4	32.3	16.6	18.3
Mg (wt%)	0.1	0.6	0.3	0.2	0.3
Na (wt%)	0.1	0.4	0.3	0.2	0.1
Si (wt%)	1.7	14.4	6.6	2.8	3.5
Sr (wt%)	0.0	0.1	0.1	0.1	0.1

Finally, it is possible to transfer the quantitative information back onto the elementary maps to have a real image of the composition of the areas analyzed for each sample.

The LIBS system proved its effectiveness in the analysis of ancient mortars, a highly heterogeneous material. The knowledge developed in the study may have also interesting applications in the analysis and study of modern binding materials and techniques.

3.2 Other geomaterials

In this section, two works on materials that are not strictly related to the cultural heritage materials are presented to show the capability of the instrument to analyze and quantify materials that are composed of several layers. Rocks, for instance, are natural solid aggregate of one or more minerals. The types and abundance of minerals in a rock are determined by the manner in which it was formed. Rocks are classified according to mineral, chemical composition and their formation in: igneous, sedimentary and metamorphic.

3.2.1 μ -LIBS analysis of geostandard

The aim of the work is to test the capability of the μ -LIBS-Scan on a set of geo-standards previously analyzed by XRF at the Earth Sciences Department-University of Pisa [176]. In this way, it is also possible to compare the performances of the tool with those of a standard technique for this kind of measurement [177–183,183–187].

Materials and methods

Pellets of about (13x5mm²) using 3 mg of standard powder (grinded at 20-30 μ m) have been prepared according to the standard methods used for XRF analysis [176]. LIBS technique requires less amount of sample with respect to XRF, due to reduced spot size of the measurement, so it is possible to use of the same amount of powders needed for XRF, but without adding other elements such as KBr. However, in order to preserve as much as possible the pellet, the lamp energy has been reduced from 17.5 joule to 14.5 joule. In this way, 19 geostandards samples ranging from the disthene¹¹ to the granite have been analysed; the certified contents in oxides (see data in Appendix) have been converted in elemental concentration and, are shown in the table below (Table 18).

Table 18 Contents in Si and Na+K and their conversion in SiO₂ (w %) and Na₂O+K₂O (wt%) of the analysed rock standards.

Id	Rock type	Si%	Na+K%	SiO ₂ %	Na ₂ O+K ₂ O%
AC-E	Disthene	64.0	16.7	70.9	11.1
AGV-1	Basalt	52.6	10.7	60.0	7.3
BE-N	Gabbro	32.1	6.3	39.6	4.7
BIR-1	Peridotite	40.0	2.4	47.7	1.8
DR-N	Basalt	46.6	6.9	54.1	4.8
DT-N	Basalt	34.1	0.3	37.2	0.2
GS-N	Basalt	59.7	12.9	66.9	8.5
JA-2	Diorite	50.2	7.3	57.6	5.0
JA-3	Andesite	55.2	6.7	62.4	4.6
JB-2	Andesite	45.0	3.4	52.8	2.4
JB-3	Andesite	43.3	5.0	50.9	3.6
JF-1	Feldspar	59.5	21.0	67.1	13.7
JF-2	Granite	57.5	24.0	65.6	15.7
JG-1a	Feldspar	66.5	11.6	72.9	7.5
JG-2	Granodiorite	71.4	13.0	77.4	8.3
JG-3	Granite	60.9	10.1	67.6	6.7
JGb-1	Granodiorite	36.4	2.0	43.7	1.5
JP-1	Rhyolite	37.6	<0.1	44.3	<0.1
JR-1	Granite	70.3	13.4	76.4	8.6

Starting from a well-known composition of these standards, the capability of the LIBS of obtaining quantitative bulk analysis on geo-standard with a method that can be named micro-drilling-Laser Analysis Method (MD-LAM) has been tested. This process has a double purpose: the first one is to obtain a bulk

¹¹ For the term see <https://www.mindat.org/min-25543.html>. Same term is used in the classical TAS (Total Alkali-Silica diagram) [178].

analysis by accumulating the plasma emission spectra on the same point and then on different points; the second one is to make depth profiles (on the single point). The spectra accumulation in depth provides a better s/n ratio, while the averaging over the different points on the surface gives the range of inhomogeneity of the powder pellets (Fig. 41).

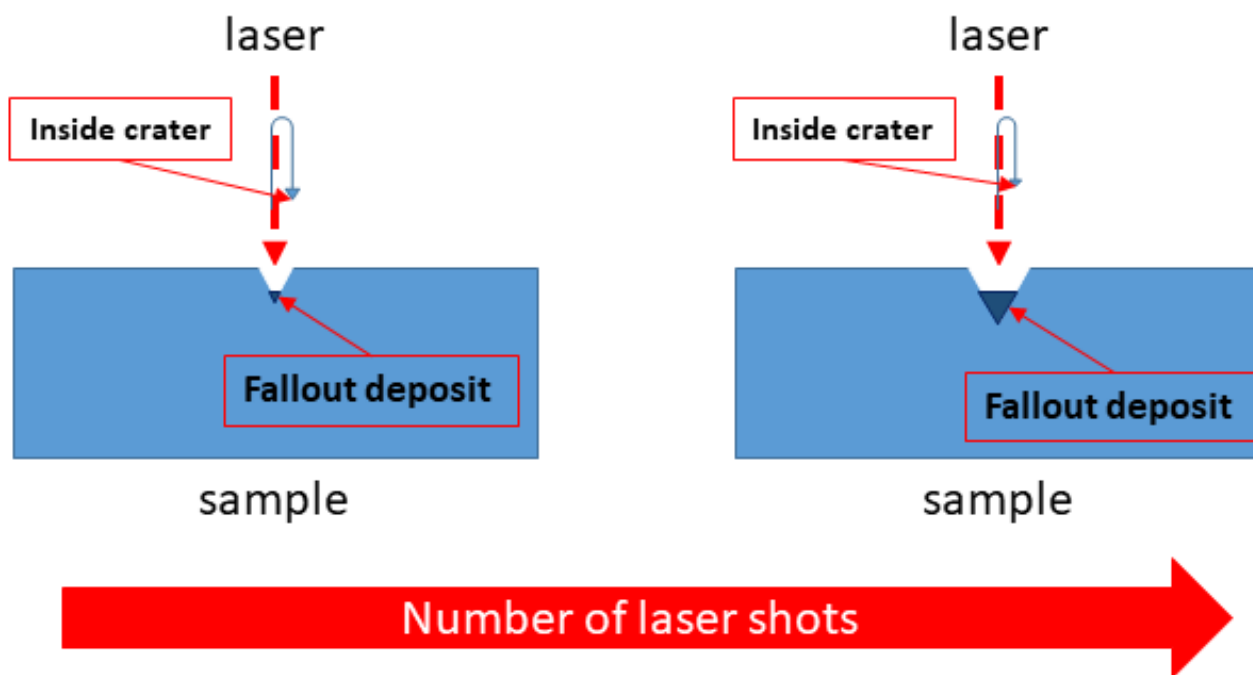


Fig. 41 The schematization of the continuous ablation in a single point of the sample.

At the end of the measurements, the produced crater on each point of the pellets is quite large (about 600 μm in diameter (Fig. 42).



Fig. 42 Spot size after five repetition shots (about 0.61mm).

The selected line for each major elements of interest are reported in the

Table 19.

Table 19 The Element peak lines for each chosen elements.

Element	Wavelength (nm)
NaI	588.98
MgII	280.27
AlI	309.24
SiI	288.16
background	253.40
KI	766.50
CaI	422.67
TiII	337.22
MnII	257.52
FeII	259.88

To calculate the composition, a neural network approach has been used [188–190]; it guarantees a better limit of detection and the time for the analysis is drastically reduced with respect to more standard approach, as, for example, the calibration curve or the CF-LIBS method [3,4,6,92,149–151,191,192]. With the MATLAB® routine, developed for this purpose, the network was built with ten neurons in the hidden layer (using as inputs the maximum peak intensity of the nine elements and background indicated in

Table 19 and a Levenberg-Marquardt algorithm (Fig. 43). The 4x19 averaged spectra was used as input and the fifth one for each samples was chosen as unknown sample for a simultaneous external validation, using the network to predict the relative concentrations. In this way, it is possible to obtain a more detailed information about the accuracy of the network, evaluating it for each element. For the internal evaluation of the validation, It has been used the internal system of the MATLAB® Artificial Neural Network (ANN) tool: it is based on a histogram that shows the Root Square Error in respect of the 0-error value (Fig. 44). I have retrained the net until reach the minimum RSE and the maximum correlation possible.

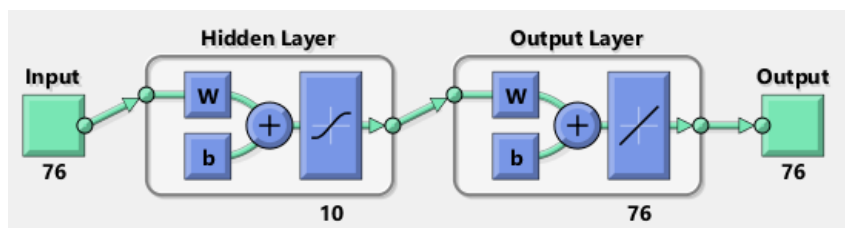


Fig. 43 Structure of a single perceptron with 76 inputs (19x4 spectra) and 76 outputs (reference value taken from reference standard certificate).

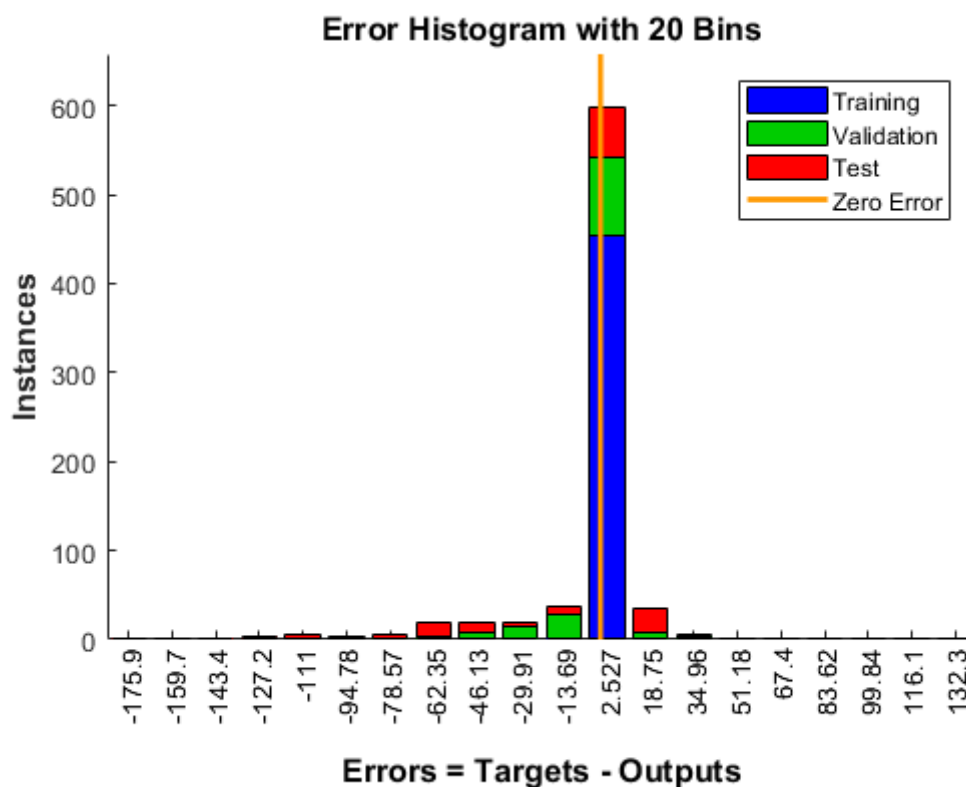


Fig. 44 Error Histogram of the ANN. The most part of the sample are close to the zero-error value.

In the Table 20, the accuracy, calculated for each sample and for each element, using the following formula of Euclidean distance is reported:

$$\sqrt{|C_{N_v} - C_{P_v}|^2}$$

where C_{N_v} is the concentration of the certified value and C_{P_v} is the concentration of the predicted value.

Table 20 Accuracy of the measurements (absolute value for all the elements simultaneously).

		Na %	Mg %	Al %	Si %	K %	Ca %	Ti %
AC-E	Granite	2.4	0.7	1.6	1.8	1.9	2.6	0.9
AGV-1	Andesite	1.5	1.0	2.4	0.7	0.7	0.8	0.3
BE-N	Basalt	0.7	0.6	2.4	0.9	0.7	1.5	0.7
BIR-1	Basalt	0.2	1.2	2.2	0.4	0.5	1.0	0.7
DR-N	Diorite	0.7	0.6	1.7	1.9	0.4	1.8	0.9
DT-N	Disthene	1.1	1.2	4.5	2.1	0.7	1.0	0.3
GS-N	Granite	0.4	0.1	2.3	1.8	1.7	1.2	0.6
JA-2	Andesite	0.7	1.5	2.3	1.4	0.7	0.5	0.5
JA-3	Andesite	0.7	0.9	2.3	2.8	0.8	1.4	0.6
JB-2	Basalt	0.7	1.6	2.3	2.4	0.6	1.1	0.3
JB-3	Basalt	1.3	1.2	2.6	2.1	0.8	0.8	0.4
JF-1	Feldspar	1.1	0.6	2.8	1.2	1.8	0.8	0.5
JF-2	Feldspar	0.9	1.5	0.7	1.6	1.8	0.4	0.2
JG-1a	Granodiorite	1.2	1.2	2.6	3.6	0.3	1.4	0.7
JG-2	Granite	1.4	1.3	2.2	2.2	0.7	0.7	0.5
JG-3	Granodiorite	0.9	1.3	1.5	0.9	1.6	1.4	0.2
JGb-1	Gabbro	0.7	0.6	1.6	1.6	0.4	0.4	0.3
JP-1	Peridotite	1.0	2.8	1.7	1.8	1.3	0.9	0.1
JR-1	Rhyolite	0.4	0.8	1.2	1.6	1.7	0.2	0.6

Although in the Total Alkali-Silica diagram (TAS) the variation in terms of contents in Silicon and Potassium + Sodium (pure elements) present a wide range of value (see technical appendix Fig. 52), the accuracy of the predictions obtained with the ANN method are very interesting, giving quantitative results with absolute errors below 3% (Table 20).

3.2.2 μ -LIBS analysis of weathered limestone

Limestone is a sedimentary rock mainly composed by calcite and/or dolomite [193], it can be used as building material and it is very common in the Italian Cultural Heritage. Due to its chemical composition and the tendency to deteriorate easily due to air pollution, the limestone, used for Italian Cultural Heritage Buildings, is subject to constant monitoring, cleaning and restoration by conservation scientists and restorers.

Materials and methods

For this study, a fragment of weathered limestone from the Svevo Castle of Bari was analysed. The sample was supplied by the NANOTEC institute of the CNR of Bari and the results published in Senesi et al. [168]. The sample shown a stratificated black crust deposit on the surface. In this case, in addition to the previous steps, described for the other applications, thanks to a proper MATLAB® script it was possible to reassemble the elementary maps in order to visualize them in 3D (Fig. 45).

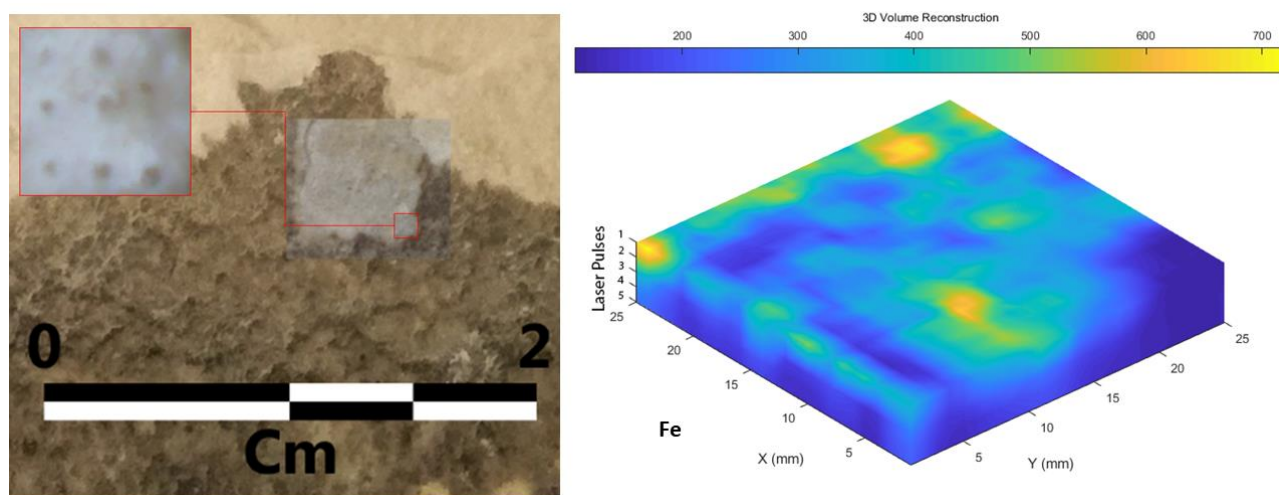


Fig. 45 sample analyzed with 3D map reconstruction of Iron.

The 3D maps can be cut virtually along the plane perpendicular to the ablated surface, allowing to visualize a sort of VECS (Virtual Elemental Cross Section) (Fig. 46). The elemental imaging was performed on the sample rough surface without further preparation, using a grid of analytical spots of about 20 μm diameter, spaced at 200 μm intervals, on a 5 mm² square surface (625 points) and for 5 (double) laser pulses in order to evaluate the change of elemental composition with depth. A spectrum was acquired for each analysed point (3125 spectra in total). The time needed to acquire the 3D map was around 35 min. The 3D compositional map was generated plotting the intensity of the LIBS emission line of the elements of interest at the pixel (x,y) corresponding to the x and y steps of the raster (200 μm), and at a z coordinate representing the depth

of the laser crater, which was estimated by microscopic analysis of the samples to be about 1 μm per laser pulse. The grey scale elemental 'sections' can be combined to form three-chromatic false-color images. In particular (Fig. 46), false color red-green-blue (RGB) maps were constructed assigning the intensity map of Al to the red channel, of Mg to the green channel and Fe to the blue channel, whereas the yellow zone correspond to high simultaneous concentrations of Red + Green, i.e. Al + Mg, magenta zones corresponds to Red + Blue, simultaneous high concentrations of Al and Fe, while the cyan color (Green + Blue) indicates high simultaneous concentrations of Mg and Fe. Finally, the white zones correspond to the co-presence, at high concentrations, of all the elements considered in the map. Although this kind of imaging may help in identifying the compositional variation in the sample, the determination of the mineralogical composition of the black crust remains a difficult task to perform because only three elements can be mapped in a single section, as the number of bands that can be visualized in a color image is limited to three (RGB).

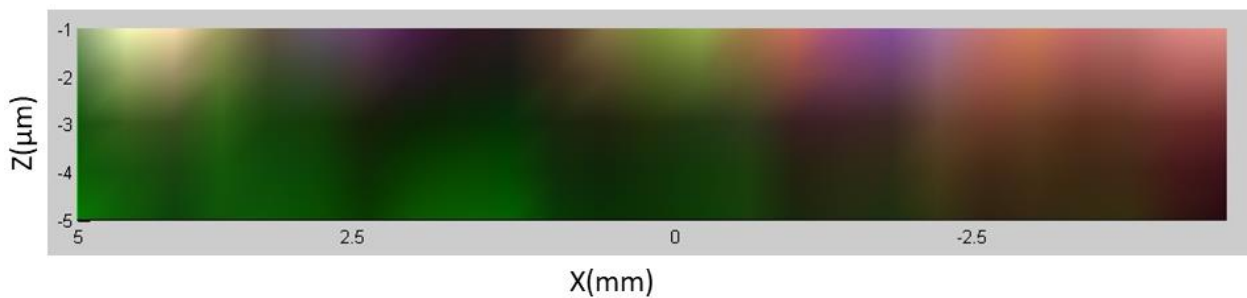


Fig. 46 VECS of the black crust (Red=Al, Mg=Green, Fe=Blue).

3.2.3 Layered rocks

An interesting and challenging type of rock to test the capabilities of the micro-LIBS-scan is the schist, a medium-grade metamorphic rock. The specimen, in fact, shows the characteristic schistose texture made by layers (flat, planar) that include several minerals. In this work, a green shale collected around the lake of Vagli (Tuscany) was studied.

Materials and methods

The map size was of 50x50 steps with 100 μm of lateral resolution (Fig. 47).

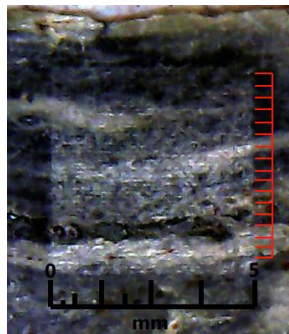


Fig. 47 Photo of the scanned area (5x5mm).

The obtained spectra, one from each point of the scanned area, were processed through the MATLAB® script, (in the Appendix). The main elements identified within the spectra for the CF-LIBS were shown in the

Table 21, while the elements quantified are shown in Table 22.

Table 21 Lists of the elemental peaks selected for the CF-LIBS.

Elemental Peak	Wavelength (nm)
Fe II	259.94
Mg II	280.27
Mg I	285.21
Si I	288.16
Ti II	334.94
Ti II	336.12
Ti II	337.22
Al II	358.60
Mg I	383.22
Mg I	383.82
Fe I	385.63
Fe I	385.99
Si I	390.55
Ca II	393.36
Al I	394.40
Al I	396.15
Ca II	396.84
Ti I	398.17
Ti I	398.97
Ti I	399.86
Mn I	403.07
Fe I	404.58
Fe I	406.35
Fe I	407.17
Ca I	422.67
Mg I	516.73
Mg I	517.26
Mg I	518.36
Fe I	526.95
Fe I	532.80
Na I	588.99
Na I	589.59
Si II	636.94

Table 22 List of principal elements individuated inside the spectra and used for generating the false color PCA map.

Elements	Al	Ca	Fe	K	Mg	Mn	Na	Si	Ti
----------	----	----	----	---	----	----	----	----	----

A first combination of the elemental maps was generated exploiting a false color image based on PCA (Fig. 48).

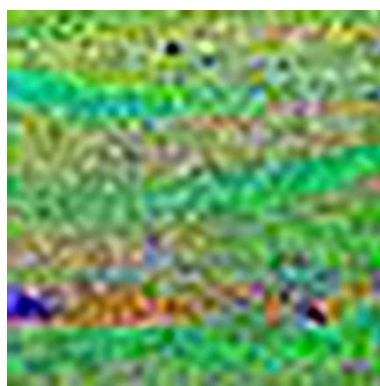


Fig. 48 The false color image of the scanned area. Red=component1; green= component2; blue= component3. The blurry effect is due the resize of the original image (1.20x1.20 cm² to 5x5 cm²).

From the Fig. 48, it is possible to observe that there are at least three distinct zones (greenish, yellowish and orange) and a series of blue areas. In order to calculate the elementary composition a SOM network has been built with four neurons (Fig. 49).

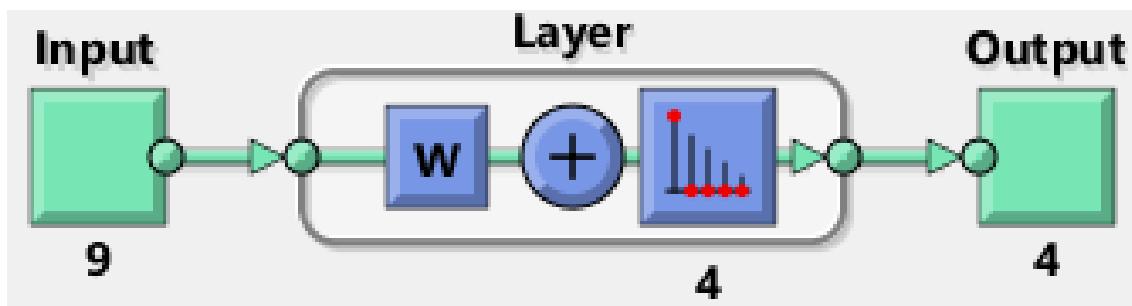


Fig. 49 Structure of the SOM network with 9 inputs (elemental peak intensities) and 4 outputs (segments).

The four segments produced by the SOM confirm the features identified by the PCA image in false colors making the layers and features of the material more clear and visible (Fig. 50).

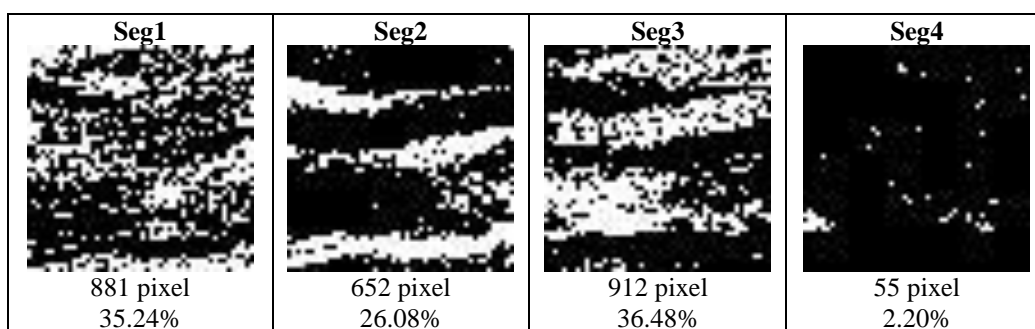

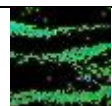

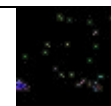


Fig. 50 The four segments obtained from SOM. In white the area occupied by the segment. Below each image, the number of the pixel and the percentage of the sample covered by the segment.

From these binary images, it is easy to extrapolate the spectra belonging to each segment and to mediate them to obtain a spectrum for each segment to be analyzed using a calibration free procedure (Table 23).

Table 23 Mean composition of the four segments.

				
Al	8.9	10.3	10.4	5.3
Ca	0.2	0.3	0.2	0.6
Fe	35.6	21.7	45.0	22.2
K	2.1	2.7	1.6	1.0
Mg	2.2	1.5	2.7	1.5
Mn	1.1	0.4	1.4	1.3
Na	0.5	1.0	0.5	0.6
Si	31.7	31.6	28.3	60.6
Ti	17.8	30.4	9.8	7.0
	Seg1 (wt%)	Seg2 (wt%)	Seg3 (wt%)	Seg4 (wt%)

The analysis reveals the presence of two sequence of layers (Seg2 and Seg3) differing from iron contents and a mixed interfaces layer (Seg1) with a mean composition between Seg2 and Seg3. The Seg4 has a completely different composition showing a very high content of silicon.

Conclusions and Future works

This work arises in the framework between the ALS-Lab of ICCOM-CNR of Pisa and the group GEO/09 of the University of Pisa. I was able to analyze and characterize different types of materials and, with them, understand the limits and the advantages of the LIBS technique and, in particular, the micro-LIBS technique applied to geological materials of interest for cultural heritage.

Clearly, this is an instrument and a technique that can not replace the classical methods of analysis, but could represent an effective tool, thanks to its portability, making possible of being used in the field without or with a minimum sample preparation as a valid preliminary screening tool.

The presented case studies do not complete the panorama of possible applications, but they are an effective testbed for the technique and the instrument.

The use of the LIBS and μ -LIBS technique combined with a method of proper spectra processing with statistical methods has proved to be a robust approach: it has shown an excellent ability to cluster materials in representative groups.

The μ -LIBS-Scan elementary mapping of the materials, in case of inhomogeneous materials, allows for quick measurements without any sample preparation. The instrument does not require gas flows (argon or helium), which are very expensive. A further advantage is the possibility of using standardless quantitative methods that reduce analysis time, once automated, to a few seconds. The coupling with neural networks allows to segment the areas investigated in sections with similar elementary characteristics and then to obtain a quantitative analysis. In case of multilayer analysis the capability of carry out a VECS (Virtual Elemental Cross Section) is a powerful tool for multi-layered materials in order to visualize the depth profile.

To improve the accuracy of the quantitative results, the ANN can supply for the construction of multivariate calibration curves, in a fraction of second.

A precise analysis protocol has been established, able to provide certain map sizes with a well-defined spot and lateral resolution optimized for the analysis of geomaterials in Cultural Heritage. It is summarized in the following Table 24:

Table 24 Standard protocol of analysis for Cultural Heritage materials

X axis (numbers of steps)	50
Y axis (number of steps)	50
Lateral resolution	100 μ m
Pumping lamp energy	13.5 J

The μ -LIBS-Scan allows also to perform standardless compositional analyses, in a fast way, realizing elementary maps in a differentiated way: separating the various components, total rock analysis or with spot measurements (25 microns).

In the following table, the main features that should have a micro-LIBS system to scan for geological applications are reporting, together with the possible improvements (Table 25). For instance, to reduce the spot size it could be recommended to use the second (532 nm) and third harmonic (266 nm) of Nd:YAG laser source. In this way, it is also possible to reduce the continuum, improving the s / n ratio.

Table 25 Scheme of main features of actual and a future system.

	Actual Instrument	Future Instrument
Laser type	Q-Switch double pulse	Q-Switch double pulse
Laser Wavelength(s)	$\lambda=1064$ nm	$\lambda=1064$ nm, 532 nm, 266 nm
Magnification objective	10X (manual focus)	10X, 20X, 40X, 80X (with auto focus)
Plasma Light Collecting System	Ball lens @45°to laser beam	In axis
Spectrometer	190-400nm UV-Vis 0.1 nm resolution. 400-900nm VIS-Ir 0.3 nm resolution	190-400 nm UV-Vis 0.1 nm resolution. 400-900 nm VIS-Ir 0.3 nm resolution
UNI EN 60529	No	IP65

References

- [1] A.W. Miziolek, V. Palleschi, I. Schechter, *Laser induced breakdown spectroscopy*, Cambridge University Press, 2006.
- [2] G. Cristoforetti, A. De Giacomo, M. Dell'Aglio, S. Legnaioli, E. Tognoni, V. Palleschi, N. Omenetto, Local thermodynamic equilibrium in laser-induced breakdown spectroscopy: beyond the McWhirter criterion, *Spectrochim. Acta Part B At. Spectrosc.* 65 (2010) 86–95.
- [3] E. Tognoni, G. Cristoforetti, S. Legnaioli, V. Palleschi, Calibration-free laser-induced breakdown spectroscopy: state of the art, *Spectrochim. Acta Part B At. Spectrosc.* 65 (2010) 1–14.
- [4] E. Tognoni, G. Cristoforetti, S. Legnaioli, V. Palleschi, A. Salvetti, M. Müller, U. Panne, I. Gornushkin, A numerical study of expected accuracy and precision in calibration-free laser-induced breakdown spectroscopy in the assumption of ideal analytical plasma, *Spectrochim. Acta Part B At. Spectrosc.* 62 (2007) 1287–1302.
- [5] M. Corsi, G. Cristoforetti, M. Giuffrida, M. Hidalgo, S. Legnaioli, V. Palleschi, A. Salvetti, E. Tognoni, C. Vallebona, Three-dimensional analysis of laser induced plasmas in single and double pulse configuration, *Spectrochim. Acta Part B At. Spectrosc.* 59 (2004) 723–735.
- [6] R. Fantoni, L. Caneve, F. Colao, L. Fornarini, V. Lazic, V. Spizzichino, Methodologies for laboratory laser induced breakdown spectroscopy semi-quantitative and quantitative analysis—a review, *Spectrochim. Acta Part B At. Spectrosc.* 63 (2008) 1097–1108.
- [7] C. Gautier, P. Fichet, D. Menut, J.-L. Lacour, D. L'Hermite, J. Dubessy, Main parameters influencing the double-pulse laser-induced breakdown spectroscopy in the collinear beam geometry, *Spectrochim. Acta Part B At. Spectrosc.* 60 (2005) 792–804.
- [8] S. Musazzi, U. Perini, *Laser-induced breakdown spectroscopy*, *Laser-Induced Break. Spectrosc. Theory Appl.* Springer Ser. Opt. Sci. Vol. 182. ISBN 978-3-642-45084-6. Springer-Verlag Berlin Heidelberg, 2014. 1 (2014).
- [9] B.E. Naes, S. Umpierrez, S. Ryland, C. Barnett, J.R. Almirall, A comparison of laser ablation inductively coupled plasma mass spectrometry, micro X-ray fluorescence spectroscopy, and laser induced breakdown spectroscopy for the discrimination of automotive glass, *Spectrochim. Acta Part B At. Spectrosc.* 63 (2008) 1145–1150.
- [10] J.A. Crisp, M. Adler, J.R. Matijevic, S.W. Squyres, R.E. Arvidson, D.M. Kass, Mars exploration rover mission, *J. Geophys. Res. Planets.* 108 (2003).
- [11] R. Li, S.W. Squyres, R.E. Arvidson, B.A. Archinal, J. Bell, Y. Cheng, L. Crumpler, D.J. Des Marais, K. Di, T.A. Ely, Initial results of rover localization and topographic mapping for the 2003 Mars Exploration Rover mission, *Photogramm. Eng. Remote Sens.* 71 (2005) 1129–1142.
- [12] S.P. Gorevan, T. Myrick, K. Davis, J.J. Chau, P. Bartlett, S. Mukherjee, R. Anderson, S.W. Squyres, R.E. Arvidson, M.B. Madsen, Rock abrasion tool: Mars exploration rover mission, *J. Geophys. Res. Planets.* 108 (2003).
- [13] R.E. Arvidson, J.F. Bell III, P. Bellutta, N.A. Cabrol, J.G. Catalano, J. Cohen, L.S. Crumpler, D.J. Des Marais, T.A. Estlin, W.H. Farrand, Spirit Mars Rover Mission: Overview and selected results from the northern Home Plate Winter Haven to the side of Scamander crater, *J. Geophys. Res. Planets.* 115 (2010).
- [14] J.P. Grotzinger, J. Crisp, A.R. Vasavada, R.C. Anderson, C.J. Baker, R. Barry, D.F. Blake, P. Conrad, K.S. Edgett, B. Ferdowski, Mars Science Laboratory mission and science investigation, *Space Sci. Rev.* 170 (2012) 5–56.
- [15] R.C. Anderson, L. Jandura, A.B. Okon, D. Sunshine, C. Roumeliotis, L.W. Beegle, J. Hurowitz, B. Kennedy, D. Limonadi, S. McCloskey, Collecting samples in Gale Crater, Mars; an overview of the Mars Science Laboratory sample acquisition, sample processing and handling system, *Space Sci. Rev.* 170 (2012) 57–75.
- [16] A. Steltzner, D. Kipp, A. Chen, D. Burkhart, C. Guernsey, G. Mendek, R. Mitcheltree, R. Powell, T. Rivellini, M. San Martin, Mars Science Laboratory entry, descent, and landing system, in: *Aerosp. Conf. 2006 IEEE*, IEEE, 2006: p. 15–pp.
- [17] A.R. Vasavada, J.P. Grotzinger, R.E. Arvidson, F.J. Calef, J.A. Crisp, S. Gupta, J. Hurowitz, N. Mangold, S. Maurice, M.E. Schmidt, Overview of the Mars Science Laboratory mission: Bradbury landing to Yellowknife Bay and beyond, *J. Geophys. Res. Planets.* 119 (2014) 1134–1161.
- [18] K.S. Series, Mars Science Laboratory Mission, Policy. 2017 (2018).

- [19] S. Maurice, R.C. Wiens, M. Saccoccio, B. Barraclough, O. Gasnault, O. Forni, N. Mangold, D. Baratoux, S. Bender, G. Berger, The ChemCam instrument suite on the Mars Science Laboratory (MSL) rover: Science objectives and mast unit description, *Space Sci. Rev.* 170 (2012) 95–166.
- [20] S. Turkle, W.J. Clancey, S. Helmreich, Y.A. Loukissas, N. Myers, *Simulation and its Discontents*, MIT Press Cambridge, MA, 2009.
- [21] R. Wiens, S. Maurice, N. Bridges, B. Clark, D. Cremers, K. Herkenhoff, L. Kirkland, N. Mangold, G. Manhes, P. Mauchien, ChemCam science objectives for the Mars Science Laboratory (MSL) rover, (2005).
- [22] N.L. Lanza, S.M. Clegg, R.C. Wiens, R.E. McInroy, H.E. Newsom, M.D. Deans, Examining natural rock varnish and weathering rinds with laser-induced breakdown spectroscopy for application to ChemCam on Mars, *Appl. Opt.* 51 (2012) B74–B82.
- [23] T.G. Graff, R. V Morris, S.M. Clegg, R.C. Wiens, R.B. Anderson, Dust removal on Mars using laser-induced breakdown spectroscopy, (2011).
- [24] C. Fabre, S. Maurice, R. Wiens, V. Sautter, C. Team, ChemCam LIBS Instrument: Complete Characterization of the Onboard Calibration Silicate Targets (MSL Rover), in: 41st Lunar Planet. Sci. Conf., Citeseer, 2010: p. 1835.
- [25] P. Mahaffy, Exploration of the habitability of Mars: Development of analytical protocols for measurement of organic carbon on the 2009 Mars Science Laboratory, *Space Sci. Rev.* 135 (2008) 255–268.
- [26] V.I. Moroz, Summary of preliminary results of the Venera 13 and Venera 14 missions, *Venus.* (1983) 45–68.
- [27] Z.A. Arp, D.A. Cremers, R.D. Harris, D.M. Oschwald, G.R. Parker Jr, D.M. Wayne, Feasibility of generating a useful laser-induced breakdown spectroscopy plasma on rocks at high pressure: preliminary study for a Venus mission, *Spectrochim. Acta Part B At. Spectrosc.* 59 (2004) 987–999.
- [28] J.L. Lambert, J. Morookian, T. Roberts, J. Polk, S. Smrekar, S.M. Clegg, R.C. Weins, M.D. Dyar, A. Treiman, Standoff LIBS and Raman spectroscopy under Venus conditions, in: Lunar Planet. Sci. Conf., 2010: p. 2608.
- [29] S.M. Clegg, J.E. Barefield, R.C. Wiens, C.R. Quick, S.K. Sharma, A.K. Misra, M.D. Dyar, M.C. McCanta, L. Elkins-Tanton, Venus Geochemical Analysis by Remote Raman--Laser Induced Breakdown Spectroscopy (Raman-LIBS), in: *Venus Geochemistry Progress, Prospect. New Mission.*, 2009: pp. 12–13.
- [30] S.M. Clegg, J.E. Barefield, S.D. Humphries, R.C. Wiens, D.T. Vaniman, S.K. Sharma, A.K. Misra, M.D. Dyar, S.E. Smrekar, Remote Raman-laser induced breakdown spectroscopy (LIBS) geochemical investigation under Venus atmospheric conditions, Los Alamos National Lab.(LANL), Los Alamos, NM (United States), 2010.
- [31] S.M. Clegg, J.E. Barefield, R.C. Wiens, S.K. Sharma, A.K. Misra, J. Tucker, M.D. Dyar, J. Lambert, S. Smrekar, A. Treiman, Venus geochemical analysis by remote laser-induced breakdown spectroscopy (LIBS), in: Lunar Planet. Sci. Conf., 2010: p. 1631.
- [32] J.L. Gottfried, F.C. De Lucia Jr, C.A. Munson, A.W. Miziolek, Double-pulse standoff laser-induced breakdown spectroscopy for versatile hazardous materials detection, *Spectrochim. Acta Part B At. Spectrosc.* 62 (2007) 1405–1411.
- [33] F. Colao, R. Fantoni, P. Ortiz, M.A. Vazquez, J.M. Martin, R. Ortiz, N. Idris, Quarry identification of historical building materials by means of laser induced breakdown spectroscopy, X-ray fluorescence and chemometric analysis, *Spectrochim. Acta Part B At. Spectrosc.* 65 (2010) 688–694.
- [34] M.A. Gondal, M.M. Nasr, Z. Ahmed, Z.H. Yamani, Determination of trace elements in volcanic rock samples collected from cenozoic lava eruption sites using LIBS, *J. Environ. Sci. Heal. Part A.* 44 (2009) 528–535.
- [35] S. Yoshino, T. Takahashi, B. Thornton, Towards in-situ chemical classification of seafloor deposits: Application of neural networks to underwater laser-induced breakdown spectroscopy, in: *Ocean. 2017-Aberdeen*, IEEE, 2017: pp. 1–5.
- [36] X. Zhu, T. Xu, Q. Lin, L. Liang, G. Niu, H. Lai, M. Xu, X. Wang, H. Li, Y. Duan, Advanced statistical analysis of laser-induced breakdown spectroscopy data to discriminate sedimentary rocks based on Czerny–Turner and Echelle spectrometers, *Spectrochim. Acta Part B At. Spectrosc.* 93 (2014) 8–13.
- [37] J.L. Gottfried, R.S. Harmon, F.C. De Lucia, A.W. Miziolek, Multivariate analysis of laser-induced breakdown spectroscopy chemical signatures for geomaterial classification, *Spectrochim. Acta Part B*

- At. Spectrosc. 64 (2009) 1009–1019.
- [38] R.S. Harmon, R.E. Russo, R.R. Hark, Applications of laser-induced breakdown spectroscopy for geochemical and environmental analysis: A comprehensive review, *Spectrochim. Acta - Part B At. Spectrosc.* 87 (2013). doi:10.1016/j.sab.2013.05.017.
- [39] J. Klus, P. Pořízka, D. Prochazka, P. Mikysek, J. Novotný, K. Novotný, M. Slobodník, J. Kaiser, Application of self-organizing maps to the study of U-Zr-Ti-Nb distribution in sandstone-hosted uranium ores, *Spectrochim. Acta Part B At. Spectrosc.* 131 (2017) 66–73.
- [40] S.-L. Lui, A. Koujelev, Accurate identification of geological samples using artificial neural network processing of laser-induced breakdown spectroscopy data, *J. Anal. At. Spectrom.* 26 (2011) 2419–2427.
- [41] N.J. McMillan, R.S. Harmon, F.C. De Lucia, A.M. Miziolek, Laser-induced breakdown spectroscopy analysis of minerals: carbonates and silicates, *Spectrochim. Acta Part B At. Spectrosc.* 62 (2007) 1528–1536.
- [42] P. Pořízka, A. Demidov, J. Kaiser, J. Keivanian, I. Gornushkin, U. Panne, J. Riedel, Laser-induced breakdown spectroscopy for in situ qualitative and quantitative analysis of mineral ores, in: *Spectrochim. Acta - Part B At. Spectrosc.*, 2014. doi:10.1016/j.sab.2014.08.027.
- [43] C.P.M. Roux, J. Rakovský, O. Musset, F. Monna, J.F. Buoncristiani, P. Pellenard, C. Thomazo, In situ Laser Induced Breakdown Spectroscopy as a tool to discriminate volcanic rocks and magmatic series, Iceland, *Spectrochim. Acta - Part B At. Spectrosc.* 103–104 (2015). doi:10.1016/j.sab.2014.11.013.
- [44] G.S. Senesi, Laser-Induced Breakdown Spectroscopy (LIBS) applied to terrestrial and extraterrestrial analogue geomaterials with emphasis to minerals and rocks, *Earth-Science Rev.* 139 (2014). doi:10.1016/j.earscirev.2014.09.008.
- [45] G.S. Senesi, D. Manzini, O. De Pascale, Application of a laser-induced breakdown spectroscopy handheld instrument to the diagnostic analysis of stone monuments, *Appl. Geochemistry.* (2018).
- [46] E.C. Ferreira, D.M.B.P. Milori, E.J. Ferreira, R.M. Da Silva, L. Martin-Neto, Artificial neural network for Cu quantitative determination in soil using a portable laser induced breakdown spectroscopy system, *Spectrochim. Acta Part B At. Spectrosc.* 63 (2008) 1216–1220.
- [47] K.Y. Yamamoto, D.A. Cremers, M.J. Ferris, L.E. Foster, Detection of metals in the environment using a portable laser-induced breakdown spectroscopy instrument, *Appl. Spectrosc.* 50 (1996) 222–233.
- [48] J. Cuñat, F.J. Fortes, L.M. Cabalín, F. Carrasco, M.D. Simón, J.J. Laserna, Man-portable laser-induced breakdown spectroscopy system for in situ characterization of karstic formations, *Appl. Spectrosc.* 62 (2008) 1250–1255.
- [49] B.T. Manard, E.M. Wylie, S.P. Willson, Analysis of Rare Earth Elements in Uranium Using Handheld Laser-Induced Breakdown Spectroscopy (HH LIBS), *Appl. Spectrosc.* (2018) 0003702818775431.
- [50] L. Gómez-Nubla, J. Aramendia, S.F.-O. de Vallejuelo, J.M. Madariaga, Analytical methodology to elemental quantification of weathered terrestrial analogues to meteorites using a portable Laser-Induced Breakdown Spectroscopy (LIBS) instrument and Partial Least Squares (PLS) as multivariate calibration technique, *Microchem. J.* 137 (2018) 392–401.
- [51] G.S. Senesi, P. Manzari, A. Consiglio, O. De Pascale, Identification and classification of meteorites using a handheld LIBS instrument coupled with a fuzzy logic-based method, *J. Anal. At. Spectrom.* 33 (2018) 1664–1675.
- [52] R.S. Harmon, J. Remus, N.J. McMillan, C. McManus, L. Collins, J.L. Gottfried Jr, F.C. DeLucia, A.W. Miziolek, LIBS analysis of geomaterials: geochemical fingerprinting for the rapid analysis and discrimination of minerals, *Appl. Geochemistry.* 24 (2009) 1125–1141.
- [53] D.C. Alvey, K. Morton, R.S. Harmon, J.L. Gottfried, J.J. Remus, L.M. Collins, M.A. Wise, Laser-induced breakdown spectroscopy-based geochemical fingerprinting for the rapid analysis and discrimination of minerals: the example of garnet, *Appl. Opt.* 49 (2010) C168–C180.
- [54] B.S. Kamber, Geochemical fingerprinting: 40 years of analytical development and real world applications, *Appl. Geochemistry.* 24 (2009) 1074–1086.
- [55] B. Mason, *Principles of geochemistry*, LWW, 1952.
- [56] G. Faure, *Principles and applications of geochemistry: a comprehensive textbook for geology students*, Prentice Hall, 1998.
- [57] Z. Sharp, *Principles of stable isotope geochemistry*, (2017).

- [58] B. Mason, C.B. Moore, *Principles of geochemistry*, (1985).
- [59] K.C. Misra, *Introduction to geochemistry: principles and applications*, John Wiley & Sons, 2012.
- [60] S.M. Clegg, E. Sklute, M.D. Dyar, J.E. Barefield, R.C. Wiens, Multivariate analysis of remote laser-induced breakdown spectroscopy spectra using partial least squares, principal component analysis, and related techniques, *Spectrochim. Acta Part B At. Spectrosc.* 64 (2009) 79–88.
- [61] S. Qiao, Y. Ding, D. Tian, L. Yao, G. Yang, A review of laser-induced breakdown spectroscopy for analysis of geological materials, *Appl. Spectrosc. Rev.* 50 (2015) 1–26.
- [62] L. Sheng, T. Zhang, G. Niu, K. Wang, H. Tang, Y. Duan, H. Li, Classification of iron ores by laser-induced breakdown spectroscopy (LIBS) combined with random forest (RF), *J. Anal. At. Spectrom.* 30 (2015). doi:10.1039/C4JA00352G.
- [63] L. Breiman, Random forest, *Mach. Learn.* 45 (2001) 5–32.
- [64] C.-W. Hsu, C.-C. Chang, C.-J. Lin, *A practical guide to support vector classification*, (2003).
- [65] S.R. Gunn, Support vector machines for classification and regression, *ISIS Tech. Rep.* 14 (1998) 5–16.
- [66] D.A. Cremers, F. Yueh, J.P. Singh, H. Zhang, Laser-induced breakdown spectroscopy, elemental analysis, *Encycl. Anal. Chem. Appl. Theory Instrum.* (2006).
- [67] A. Ciucci, M. Corsi, V. Palleschi, S. Rastelli, A. Salvetti, E. Tognoni, New procedure for quantitative elemental analysis by laser-induced plasma spectroscopy, *Appl. Spectrosc.* 53 (1999). doi:10.1366/0003702991947612.
- [68] S. Kaski, H. Häkkinen, J. Korppi-Tommola, Sulfide mineral identification using laser-induced plasma spectroscopy, *Miner. Eng.* 16 (2003) 1239–1243.
- [69] K.J. Grant, G.L. Paul, J.A. O’Neill, Quantitative elemental analysis of iron ore by laser-induced breakdown spectroscopy, *Appl. Spectrosc.* 45 (1991) 701–705.
- [70] R.J. Lasheras, C. Bello-Gálvez, J.M. Anzano, Quantitative analysis of oxide materials by laser-induced breakdown spectroscopy with argon as an internal standard, *Spectrochim. Acta Part B At. Spectrosc.* 82 (2013) 65–70.
- [71] F. Colao, R. Fantoni, V. Lazic, A. Paolini, F. Fabbri, G.G. Ori, L. Marinangeli, A. Baliva, Investigation of LIBS feasibility for in situ planetary exploration: an analysis on Martian rock analogues, *Planet. Space Sci.* 52 (2004) 117–123.
- [72] J. Hermann, C. Boulmer-Leborgne, D. Hong, Diagnostics of the early phase of an ultraviolet laser induced plasma by spectral line analysis considering self-absorption, *J. Appl. Phys.* 83 (1998) 691–696.
- [73] D. Bulajic, M. Corsi, G. Cristoforetti, S. Legnaioli, V. Palleschi, A. Salvetti, E. Tognoni, A procedure for correcting self-absorption in calibration free-laser induced breakdown spectroscopy, *Spectrochim. Acta Part B At. Spectrosc.* 57 (2002) 339–353.
- [74] V. Lazic, R. Barbini, F. Colao, R. Fantoni, A. Palucci, Self-absorption model in quantitative laser induced breakdown spectroscopy measurements on soils and sediments, *Spectrochim. Acta Part B At. Spectrosc.* 56 (2001) 807–820.
- [75] E. Grifoni, S. Legnaioli, G. Lorenzetti, S. Pagnotta, F. Poggialini, V. Palleschi, From Calibration-Free to Fundamental Parameters Analysis: A comparison of three recently proposed approaches, *Spectrochim. Acta - Part B At. Spectrosc.* 124 (2016). doi:10.1016/j.sab.2016.08.022.
- [76] N.J. McMillan, C.E. McManus, R.S. Harmon, F.C. De Lucia, A.W. Miziolek, Laser-induced breakdown spectroscopy analysis of complex silicate minerals—beryl, *Anal. Bioanal. Chem.* 385 (2006) 263–271.
- [77] C.E. McManus, N.J. McMillan, R.S. Harmon, R.C. Whitmore, F.C. De Lucia Jr, A.W. Miziolek, Use of laser induced breakdown spectroscopy in the determination of gem provenance: beryls, *Appl. Opt.* 47 (2008) G72–G79.
- [78] N.J. McMillan, C. Montoya, W.H. Chesner, Correlation of limestone beds using laser-induced breakdown spectroscopy and chemometric analysis, *Appl. Opt.* 51 (2012) B213–B222.
- [79] A. Koujelev, M. Sabsabi, V. Motto-Ros, S. Laville, S.L. Lui, Laser-induced breakdown spectroscopy with artificial neural network processing for material identification, *Planet. Space Sci.* 58 (2010) 682–690.
- [80] V. Motto-Ros, A.S. Koujelev, G.R. Osinski, A.E. Dudelzak, Quantitative multi-elemental laser-induced breakdown spectroscopy using artificial neural networks, *J. Eur. Opt. Soc. Publ.* 3 (2008).
- [81] L. Guo, Y. Guo, Z. Hao, Y. Tang, S. Ma, Q. Zeng, S.-S. Tang, X. Li, Y.-F. Lu, X. Zeng, Accuracy improvement of iron ore analysis using laser-induced breakdown spectroscopy with a hybrid sparse

- partial least squares and least-squares support vector machine model, *J. Anal. At. Spectrom.* (2018).
- [82] J.A. Bolger, Semi-quantitative laser-induced breakdown spectroscopy for analysis of mineral drill core, *Appl. Spectrosc.* 54 (2000) 181–189.
- [83] J.M. Tucker, M.D. Dyar, M.W. Schaefer, S.M. Clegg, R.C. Wiens, Optimization of laser-induced breakdown spectroscopy for rapid geochemical analysis, *Chem. Geol.* 277 (2010) 137–148.
- [84] R.B. Anderson, R. V Morris, S.M. Clegg, J.F. Bell, R.C. Wiens, S.D. Humphries, S.A. Mertzman, T.G. Graff, R. McInroy, The influence of multivariate analysis methods and target grain size on the accuracy of remote quantitative chemical analysis of rocks using laser induced breakdown spectroscopy, *Icarus.* 215 (2011) 608–627.
- [85] M.D. Dyar, M.L. Carmosino, E.A. Breves, M. V Ozanne, S.M. Clegg, R.C. Wiens, Comparison of partial least squares and lasso regression techniques as applied to laser-induced breakdown spectroscopy of geological samples, *Spectrochim. Acta Part B At. Spectrosc.* 70 (2012) 51–67.
- [86] B. Sallé, J.-L. Lacour, P. Mauchien, P. Fichet, S. Maurice, G. Manhes, Comparative study of different methodologies for quantitative rock analysis by laser-induced breakdown spectroscopy in a simulated Martian atmosphere, *Spectrochim. Acta Part B At. Spectrosc.* 61 (2006) 301–313.
- [87] F. Colao, R. Fantoni, V. Lazic, A. Morone, A. Santagata, A. Giardini, LIBS used as a diagnostic tool during the laser cleaning of ancient marble from Mediterranean areas, *Appl. Phys. A.* 79 (2004) 213–219.
- [88] F. Colao, R. Fantoni, V. Lazic, L. Caneve, A. Giardini, V. Spizzichino, LIBS as a diagnostic tool during the laser cleaning of copper based alloys: experimental results, *J. Anal. At. Spectrom.* 19 (2004) 502–504.
- [89] B. Sallé, P. Mauchien, S. Maurice, Laser-Induced Breakdown Spectroscopy in open-path configuration for the analysis of distant objects, *Spectrochim. Acta Part B At. Spectrosc.* 62 (2007) 739–768. doi:10.1016/j.sab.2007.07.001.
- [90] B. Sallé, D.A. Cremers, S. Maurice, R.C. Wiens, P. Fichet, Evaluation of a compact spectrograph for in-situ and stand-off laser-induced breakdown spectroscopy analyses of geological samples on Mars missions, *Spectrochim. Acta Part B At. Spectrosc.* 60 (2005) 805–815.
- [91] J.-B. Sirven, B. Salle, P. Mauchien, J.-L. Lacour, S. Maurice, G. Manhes, Feasibility study of rock identification at the surface of Mars by remote laser-induced breakdown spectroscopy and three chemometric methods, *J. Anal. At. Spectrom.* 22 (2007) 1471–1480.
- [92] C.M. Davies, H.H. Telle, D.J. Montgomery, R.E. Corbett, Quantitative analysis using remote laser-induced breakdown spectroscopy (LIBS), *Spectrochim. Acta Part B At. Spectrosc.* 50 (1995) 1059–1075.
- [93] S.G. Pavlov, E.K. Jessberger, H.-W. Hübers, S. Schröder, I. Rauschenbach, S. Florek, J. Neumann, H. Henkel, S. Klinkner, Miniaturized laser-induced plasma spectrometry for planetary in situ analysis—The case for Jupiter’s moon Europa, *Adv. Sp. Res.* 48 (2011) 764–778.
- [94] J. Thompson, R.C. Wiens, D.A. Cremers, J. Barefield, C. Wetteland, The suitability of Laser Induced Breakdown Spectroscopy for determining the compositions of extraterrestrial material, in: *Lunar Planet. Sci. Conf.*, 2004.
- [95] J. Kwak, C. Lenth, C. Salb, E.-J. Ko, K.-W. Kim, K. Park, Quantitative analysis of arsenic in mine tailing soils using double pulse-laser induced breakdown spectroscopy, *Spectrochim. Acta Part B At. Spectrosc.* 64 (2009) 1105–1110.
- [96] M.A. Gondal, T. Hussain, Z.H. Yamani, Z. Ahmed, Determination of toxic metals in petroleum, cultivated land and ore samples using laser-induced breakdown spectroscopy, *Bull. Environ. Contam. Toxicol.* 78 (2007) 270–274.
- [97] D.L. Death, A.P. Cunningham, L.J. Pollard, Multi-element analysis of iron ore pellets by laser-induced breakdown spectroscopy and principal components regression, *Spectrochim. Acta Part B At. Spectrosc.* 63 (2008) 763–769.
- [98] R.S. Harmon, K.M. Shughrue, J.J. Remus, M.A. Wise, L.J. East, R.R. Hark, Can the provenance of the conflict minerals columbite and tantalite be ascertained by laser-induced breakdown spectroscopy?, *Anal. Bioanal. Chem.* 400 (2011) 3377–3382.
- [99] R.R. Hark, J.J. Remus, L.J. East, R.S. Harmon, M.A. Wise, B.M. Tansi, K.M. Shughrue, K.S. Dunsin, C. Liu, Geographical analysis of “conflict minerals” utilizing laser-induced breakdown spectroscopy, *Spectrochim. Acta Part B At. Spectrosc.* 74 (2012) 131–136.
- [100] F. Melcher, M.A. Sitnikova, T. Graupner, N. Martin, T. Oberthür, F. Henjes-Kunst, E. Gäbler, A. Gerdes, H. Brätz, D.W. Davis, Fingerprinting of conflict minerals: columbite-tantalite (“coltan”) ores,

SGA News. 23 (2008) 7–14.

- [101] F. Melcher, T. Graupner, F. Henjes-Kunst, T. Oberthür, M. Sitnikova, E. Gäbler, A. Gerdes, H. Brätz, D. Davis, S. Dewaele, Analytical fingerprint of columbite-tantalite (coltan) mineralization in pegmatites: focus on Africa, in: *Proceedings, Ninth Int. Congr. Appl. Mineral.*, 2008: pp. 615–624.
- [102] D. Montague, Stolen goods: Coltan and conflict in the Democratic Republic of Congo, *Sais Rev.* 22 (2002) 103–118.
- [103] J.M. Vadillo, I. Vadillo, F. Carrasco, J.J. Laserna, Spatial distribution profiles of magnesium and strontium in speleothems using laser-induced breakdown spectrometry, *Fresenius. J. Anal. Chem.* 361 (1998) 119–123.
- [104] J. Cunat, S. Palanco, F. Carrasco, M.D. Simon, J.J. Laserna, Portable instrument and analytical method using laser-induced breakdown spectrometry for in situ characterization of speleothems in karstic caves, *J. Anal. At. Spectrom.* 20 (2005) 295–300.
- [105] Q.L. Ma, V. Motto-Ros, W.Q. Lei, M. Boueri, L.J. Zheng, H.P. Zeng, M. Bar-Matthews, A. Ayalon, G. Panczer, J. Yu, Multi-elemental mapping of a speleothem using laser-induced breakdown spectroscopy, *Spectrochim. Acta Part B At. Spectrosc.* 65 (2010) 707–714.
- [106] G. Galbács, I. Kevei-Bárány, E. Szőke, N. Jedlinszki, I.B. Gornushkin, M.Z. Galbács, A study of stalagmite samples from Baradla Cave (Hungary) by laser induced plasma spectrometry with automatic signal correction, *Microchem. J.* 99 (2011) 406–414.
- [107] F.J. Fortes, I. Vadillo, H. Stoll, M. Jiménez-Sánchez, A. Moreno, J.J. Laserna, Spatial distribution of paleoclimatic proxies in stalagmite slabs using laser-induced breakdown spectroscopy, *J. Anal. At. Spectrom.* 27 (2012) 868–873.
- [108] C.T. Halperin, R.L. Bishop, Chemical analysis of Late Classic Maya polychrome pottery paints and pastes from Central Petén, Guatemala, *J. Archaeol. Sci.* 69 (2016) 118–129.
- [109] M.T. Boulanger, D. V Hill, Petrographic analysis of Contact Period Native American pottery from Fort Hill (27CH85), Hinsdale, NH, USA, *Archaeol. Anthropol. Sci.* 7 (2015) 517–532.
- [110] A. Jones, Archaeometry and materiality: materials-based analysis in theory and practice, *Archaeometry.* 46 (2004) 327–338.
- [111] G. Barone, L. Bartoli, C.M. Belfiore, V. Crupi, F. Longo, D. Majolino, P. Mazzoleni, V. Venuti, Comparison between TOF-ND and XRD quantitative phase analysis of ancient potteries, *J. Anal. At. Spectrom.* 26 (2011) 1060–1067.
- [112] K.L. Rasmussen, G.A. De La Fuente, A.D. Bond, K.K. Mathiesen, S.D. Vera, Pottery firing temperatures: a new method for determining the firing temperature of ceramics and burnt clay, *J. Archaeol. Sci.* 39 (2012) 1705–1716. doi:10.1016/j.jas.2012.01.008.
- [113] C. Capelli, R. Cabella, M. Piazza, E. Starnini, Archaeometric analyses of Early and Middle Neolithic pottery from the Pian del Ciliegio rock shelter (Finale Ligure, NW Italy), *ArchéoSciences.* (2008) 115–124.
- [114] P.M. Rice, *Pottery Analysis: A Sourcebook.*, 1987. doi:10.2307/2804120.
- [115] A.J. Sakalis, N.A. Kazakis, N. Merousis, N.C. Tsirliganis, Study of Neolithic pottery from Polyplatanos (Imathia) using micro X-ray fluorescence spectroscopy, stereoscopic microscopy and multivariate statistical analysis, *J. Cult. Herit.* 14 (2013). doi:10.1016/j.culher.2012.11.005.
- [116] M.L. Teoh, S.B. McClure, E. Podrug, Macroscopic, petrographic and XRD analysis of Middle Neolithic figulina pottery from central Dalmatia, *J. Archaeol. Sci.* 50 (2014). doi:10.1016/j.jas.2014.07.007.
- [117] J. Zhu, Y. Zhang, T. Wang, C.H. Zhao, J.C. Yu, M.D. Glascock, C.S. Wang, Determining the firing temperature of low-fired ancient pottery: An example from the donghulin site, Beijing, China, *Archaeometry.* 56 (2014). doi:10.1111/arc.12033.
- [118] G. Ricci, L. Caneve, D. Pedron, N. Holesch, E. Zendri, A multi-spectroscopic study for the characterization and definition of production techniques of German ceramic sherds, *Microchem. J.* 126 (2016). doi:10.1016/j.microc.2015.12.009.
- [119] P.S. Quinn, *Ceramic petrography: the interpretation of archaeological pottery & related artefacts in thin section*, Archaeopress, 2013.
- [120] G.A. De La Fuente, J.R. Ferguson, M.D. Glascock, Chemical and Petrographic Analysis of Pre-Hispanic Pottery from the Southern Abaucán Valley, Catamarca, Argentina, *Archaeometry.* 57 (2015) 1–17.
- [121] H. Bennett, G.J. Oliver, *XRF analysis of ceramics, minerals and allied materials*, (1992).
- [122] I. Liritzis, N. Zacharias, Portable XRF of archaeological artifacts: current research, potentials and

- limitations, in: X-Ray Fluoresc. Spectrom. Geoarchaeology, Springer, 2011: pp. 109–142.
- [123] R.J. Speakman, N.C. Little, D. Creel, M.R. Miller, J.G. Iñáñez, Sourcing ceramics with portable XRF spectrometers? A comparison with INAA using Mimbres pottery from the American Southwest, *J. Archaeol. Sci.* 38 (2011) 3483–3496.
- [124] L.M. Mallory-Greenough, J.D. Greenough, J.V. Owen, New data for old pots: trace-element characterization of ancient Egyptian pottery using ICP-MS, *J. Archaeol. Sci.* 25 (1998) 85–97.
- [125] M.S. Tite, Ceramic production, provenance and use—a review, *Archaeometry*. 50 (2008) 216–231.
- [126] R. Padilla, P. Van Espen, P.P.G. Torres, The suitability of XRF analysis for compositional classification of archaeological ceramic fabric: A comparison with a previous NAA study, *Anal. Chim. Acta.* 558 (2006) 283–289.
- [127] S. Karacic, M.T. Boulanger, M.D. Glascock, Geochemical Analysis of the Hittite-Period Pottery from Tarsus-Gözlükule, Turkey, *Archaeometry*. (2016).
- [128] G. Barone, P. Mazzoleni, A. Aquilia, G. Barbera, The Hellenistic and Roman Syracuse (Sicily) fine pottery production explored by chemical and petrographic analysis, *Archaeometry*. 56 (2014) 70–87.
- [129] G. Dal Sasso, L. Maritan, S. Salvatori, C. Mazzoli, G. Artioli, Discriminating pottery production by image analysis: a case study of Mesolithic and Neolithic pottery from Al Khiday (Khartoum, Sudan), *J. Archaeol. Sci.* 46 (2014) 125–143.
- [130] N.A. Kazakis, A.J. Sakalis, D. Tsiafakis, N.C. Tsirliganis, ISLAND OF ANDROS POTTERY IN ARGILLOS? ARCHAEOLOGICAL STUDY USING μ -XRF AND MULTIVARIATE STATISTICAL ANALYSIS, *Mediterr. Archaeol. Archaeom.* 15 (2015) 73–86.
- [131] M.N. Miller, Ceramic Technology, Production, and Exchange as Seen through Macroscopic Analysis of Pottery Fragments from the Early Horizon Center Caylán, Nepeña Valley, Peru, (2016).
- [132] R. Ravisankar, A. Naseerutheen, A. Rajalakshmi, G.R. Annamalai, A. Chandrasekaran, Application of thermogravimetry–differential thermal analysis (TG–DTA) technique to study the ancient potteries from Vellore dist, Tamilnadu, India, *Spectrochim. Acta Part A Mol. Biomol. Spectrosc.* 129 (2014) 201–208.
- [133] I.T. Memmi, Pottery production and distribution: the contribution of mineralogical and petrographical methodologies in Italy. State of the art and future developments, *Period. Di Mineral.* 73 (2004) 239–257.
- [134] Y. Yoon, T. Kim, M. Yang, K. Lee, G. Lee, Quantitative analysis of pottery glaze by laser induced breakdown spectroscopy, *Microchem. J.* 68 (2001) 251–256. doi:10.1016/S0026-265X(00)00155-7.
- [135] F. Colao, R. Fantoni, V. Lazic, V. Spizzichino, Laser-induced breakdown spectroscopy for semi-quantitative and quantitative analyses of artworks - Application on multi-layered ceramics and copper based alloys, *Spectrochim. Acta - Part B At. Spectrosc.* 57 (2002) 1219–1234. doi:10.1016/S0584-8547(02)00054-X.
- [136] K. Melessanaki, M. Mateo, S.C. Ferrence, P.P. Betancourt, D. Anglos, The application of LIBS for the analysis of archaeological ceramic and metal artifacts, *Appl. Surf. Sci.* 197 (2002) 156–163.
- [137] J.M. Anzano, M.A. Villoria, I.B. Gornushkin, B.W. Smith, J.D. Winefordner, Laser-induced plasma spectroscopy for characterization of archaeological material, *Can. J. Anal. Sci. Spectrosc.* 47 (2002) 134–140. <https://www.scopus.com/inward/record.uri?eid=2-s2.0-0036942472&partnerID=40&md5=eb3d189cf1fff6f4d181c6db872261b8>.
- [138] V. Lazic, F. Colao, R. Fantoni, A. Palucci, V. Spizzichino, I. Borgia, B.G. Brunetti, A. Sgamellotti, Characterisation of lustre and pigment composition in ancient pottery by laser induced fluorescence and breakdown spectroscopy, *J. Cult. Herit.* 4 (2003) 303–308. <https://www.scopus.com/inward/record.uri?eid=2-s2.0-0037252362&partnerID=40&md5=b2a16caefc2e6f528f09e75c746b815f>.
- [139] E. Xenogiannopoulou, C. Andreouli, C. Stournaras, Application of LIBS technique for the compositional analysis of an attic black pottery, *J. Nano Res.* 8 (2009) 61–70. doi:10.4028/www.scientific.net/JNanoR.8.61.
- [140] A. Khedr, O. Abdel-Kareem, S.H. Elnabi, M.A. Harith, Compositional analysis of ceramic glaze by laser induced breakdown spectroscopy and energy dispersive x-ray, in: AIP Conf. Proc., 2011: pp. 87–92. doi:10.1063/1.3631815.
- [141] B. Genc Oztoprak, M.A. Sinmaz, F. Tülek, Composition analysis of medieval ceramics by laser-induced breakdown spectroscopy (LIBS), *Appl. Phys. A Mater. Sci. Process.* 122 (2016). doi:10.1007/s00339-016-0085-9.
- [142] A. Erdem, A. Çilingiroğlu, A. Giakoumaki, M. Castanys, E. Kartsonaki, C. Fotakis, D. Anglos,

- Characterization of Iron age pottery from eastern Turkey by laser- induced breakdown spectroscopy (LIBS), *J. Archaeol. Sci.* 35 (2008) 2486–2494. doi:10.1016/j.jas.2008.03.019.
- [143] K. Melessanaki, S.C. Ferrence, P.P. Betancourt, D. Anglos, Application of LIBS in the analysis of archaeological objects, in: C.A. Righini G.C. (Ed.), *Proc. SPIE - Int. Soc. Opt. Eng.*, 2003: pp. 79–80. doi:10.1117/12.524915.
- [144] A.J. López, G. Nicolás, M.P. Mateo, V. Piñón, M.J. Tobar, A. Ramil, Compositional analysis of Hispanic Terra Sigillata by laser-induced breakdown spectroscopy, *Spectrochim. Acta - Part B At. Spectrosc.* 60 (2005) 1149–1154. doi:10.1016/j.sab.2005.05.009.
- [145] X. Wang, V. Motto-Ros, G. Panczer, D. De Ligny, J. Yu, J.-M. Benoit, J.-L. Dussossoy, S. Peugeot, Mapping of rare earth elements in nuclear waste glass–ceramic using micro laser-induced breakdown spectroscopy, *Spectrochim. Acta Part B At. Spectrosc.* 87 (2013) 139–146.
- [146] S.S. Rai, N.K. Rai, A.K. Rai, U.C. Chattopadhyaya, Rare earth elements analysis in archaeological pottery by laser induced breakdown spectroscopy, *Spectrosc. Lett.* 49 (2016) 57–62.
- [147] R.-J. Lasheras, J. Anzano, C. Bello-Gálvez, M. Escudero, J. Cáceres, Quantitative Analysis of Roman Archeological Ceramics by Laser-Induced Breakdown Spectroscopy, *Anal. Lett.* 50 (2017) 1325–1334. doi:10.1080/00032719.2016.1217000.
- [148] A. Bertolini, G. Carelli, F. Francesconi, M. Francesconi, L. Marchesini, P. Marsili, F. Sorrentino, G. Cristoforetti, S. Legnaioli, V. Palleschi, L. Pardini, A. Salvetti, Modi: A new mobile instrument for in situ double-pulse LIBS analysis, in: *Anal. Bioanal. Chem.*, 2006: pp. 240–247. doi:10.1007/s00216-006-0413-6.
- [149] M. Corsi, G. Cristoforetti, M. Hidalgo, S. Legnaioli, V. Palleschi, A. Salvetti, E. Tognoni, C. Vallebona, Double pulse, calibration-free laser-induced breakdown spectroscopy: a new technique for in situ standard-less analysis of polluted soils, *Appl. Geochemistry.* 21 (2006) 748–755.
- [150] E. Tognoni, V. Palleschi, M. Corsi, G. Cristoforetti, Quantitative micro-analysis by laser-induced breakdown spectroscopy: a review of the experimental approaches, *Spectrochim. Acta Part B At. Spectrosc.* 57 (2002) 1115–1130.
- [151] P. Yaroshchuk, D. Body, R.J.S. Morrison, B.L. Chadwick, A semi-quantitative standard-less analysis method for laser-induced breakdown spectroscopy, *Spectrochim. Acta Part B At. Spectrosc.* 61 (2006) 200–209.
- [152] O. V Borisov, X. Mao, R.E. Russo, Effects of crater development on fractionation and signal intensity during laser ablation inductively coupled plasma mass spectrometry, *Spectrochim. Acta Part B At. Spectrosc.* 55 (2000) 1693–1704.
- [153] B. Busser, S. Moncayo, J.-L. Coll, L. Sancey, V. Motto-Ros, Elemental imaging using laser-induced breakdown spectroscopy: A new and promising approach for biological and medical applications, *Coord. Chem. Rev.* 358 (2018) 70–79. doi:10.1016/j.ccr.2017.12.006.
- [154] S. Moncayo, L. Duponchel, G. Panczer, F. Trichard, B. Bousquet, F. Pelascini, V. Motto-Ros, Exploration of megapixel hyperspectral LIBS images using Principal Component Analysis, *J. Anal. At. Spectrom.* (2018).
- [155] C.J.R. Sheppard, Depth of field in optical microscopy, *J. Microsc.* 149 (1988) 73–75.
- [156] V.I. Babushok, F.C. DeLucia Jr, J.L. Gottfried, C.A. Munson, A.W. Miziolek, Double pulse laser ablation and plasma: Laser induced breakdown spectroscopy signal enhancement, *Spectrochim. Acta Part B At. Spectrosc.* 61 (2006) 999–1014.
- [157] R. Grassi, E. Grifoni, S. Gufoni, S. Legnaioli, G. Lorenzetti, N. Macro, L. Menichetti, S. Pagnotta, F. Poggialini, C. Schiavo, V. Palleschi, Three-dimensional compositional mapping using double-pulse micro-laser-induced breakdown spectroscopy technique, *Spectrochim. Acta - Part B At. Spectrosc.* 127 (2017). doi:10.1016/j.sab.2016.11.004.
- [158] M. Ringnér, What is principal component analysis?, *Nat. Biotechnol.* 26 (2008) 303.
- [159] B. Moore, Principal component analysis in linear systems: Controllability, observability, and model reduction, *IEEE Trans. Automat. Contr.* 26 (1981) 17–32.
- [160] L. Hyvärinen, Principal component analysis, in: *Math. Model. Ind. Process.*, Springer, 1970: pp. 82–104.
- [161] C. Chatfield, A.J. Collins, Principal component analysis, in: *Introd. to Multivar. Anal.*, Springer, 1980: pp. 57–81.
- [162] I. Jolliffe, Principal component analysis, in: *Int. Encycl. Stat. Sci.*, Springer, 2011: pp. 1094–1096.
- [163] M. Richardson, Principal component analysis, URL [Http//People. Maths. Ox. Ac. Uk/Richardsonm/SignalProcPCA. Pdf](http://People.Maths.Ox.Ac.Uk/Richardsonm/SignalProcPCA.Pdf) (Last Access 3.5. 2013). Aleš Hladník Dr., Ass. Prof., Chair

- Inf. Graph. Arts Technol. Fac. Nat. Sci. Eng. Univ. Ljubljana, Slov. A. 6 (2009) 16.
- [164] S. Wold, K. Esbensen, P. Geladi, Principal component analysis, *Chemom. Intell. Lab. Syst.* 2 (1987) 37–52.
- [165] P.G. Kotula, M.R. Keenan, J.R. Michael, Automated analysis of SEM X-ray spectral images: A powerful new microanalysis tool, *Microsc. Microanal.* 9 (2003) 1–17.
- [166] S. Baronti, A. Casini, F. Lotti, S. Porcinai, Multispectral imaging system for the mapping of pigments in works of art by use of principal-component analysis, *Appl. Opt.* 37 (1998) 1299–1309.
- [167] S. Pagnotta, M. Lezzerini, B. Campanella, G. Gallelo, E. Grifoni, S. Legnaioli, G. Lorenzetti, F. Poggialini, S. Raneri, A. Safi, V. Palleschi, Fast quantitative elemental mapping of highly inhomogeneous materials by micro-Laser-Induced Breakdown Spectroscopy, *Spectrochim. Acta - Part B At. Spectrosc.* 146 (2018). doi:10.1016/j.sab.2018.04.018.
- [168] G.S. Senesi, B. Campanella, E. Grifoni, S. Legnaioli, G. Lorenzetti, S. Pagnotta, F. Poggialini, V. Palleschi, O. De Pascale, Elemental and mineralogical imaging of a weathered limestone rock by double-pulse micro-Laser-Induced Breakdown Spectroscopy, *Spectrochim. Acta - Part B At. Spectrosc.* 143 (2018). doi:10.1016/j.sab.2018.02.018.
- [169] S. Pagnotta, M. Lezzerini, L. Ripoll-Seguer, M. Hidalgo, E. Grifoni, S. Legnaioli, G. Lorenzetti, F. Poggialini, V. Palleschi, Micro-Laser-Induced Breakdown Spectroscopy (Micro-LIBS) Study on Ancient Roman Mortars, *Appl. Spectrosc.* 71 (2017) 721–727.
- [170] M. Lezzerini, E. Grifoni, S. Legnaioli, G. Lorenzetti, S. Pagnotta, V. Palleschi, Application of double-pulse micro-LIBS 3D compositional mapping to the analysis of ceramics, in: *IMEKO Int. Conf. Metrol. Archeol. Cult. Heritage, MetroArcheo 2016*, 2016.
- [171] G. Pagnotta, S., Arias, C., Radi, G., Lezzerini, M., Grifoni, E., Legnaioli, L., Lorenzetti, G., Palleschi, Classificazione di Ceramiche Archeologiche utilizzando algoritmi neurali applicati a spettri di plasmii indotti da laser (liBs), *APLAR* 5. 5 (2016) 1–11.
- [172] D.A. Spielman, Spectral graph theory and its applications, in: *Found. Comput. Sci. 2007. FOCS'07. 48th Annu. IEEE Symp., IEEE, 2007*: pp. 29–38.
- [173] V.D. Blondel, J.L. Guillaume, R. Lambiotte, E. Lefebvre, Fast unfolding of communities in large networks, *J. Stat. Mech. Theory Exp.* 2008 (2008). doi:10.1088/1742-5468/2008/10/P10008.
- [174] R. Lambiotte, J.-C. Delvenne, M. Barahona, Laplacian Dynamics and Multiscale Modular Structure in Networks, (2008) 1–29. doi:10.1109/TNSE.2015.2391998.
- [175] M.E.J. Newman, Modularity and community structure in networks, *Proc. Natl. Acad. Sci.* 103 (2006) 8577–8582.
- [176] M. Lezzerini, M. Tamponi, M. Bertoli, Calibration of XRF data on silicate rocks using chemicals as in-house standards, *Atti Soc Tosc Sci Nat, Mem, Ser. A.* 121 (2014) 65–70.
- [177] R.W. Le Maitre, A proposal by the IUGS Subcommittee on the Systematics of Igneous Rocks for a chemical classification of volcanic rocks based on the total alkali silica (TAS) diagram: (on behalf of the IUGS Subcommittee on the Systematics of Igneous Rocks), *Aust. J. Earth Sci.* 31 (1984) 243–255.
- [178] B. Zanettin, Classificazione chimica delle rocce vulcaniche mediante il diagramma TAS (Total Alkali · Silica), *Rend. Soc. Ital. Di Mineral. e Petrol.* 41 (1986).
- [179] I. ROELANDTS, G. MICHEL, Sequential Inductively Coupled Plasma Determination Of Some Rare-Earth Elements in Five French Geostandards, *Geostand. Geoanalytical Res.* 10 (1986) 135–154.
- [180] D. Johnson, P. Hooper, R. Conrey, XRF Method XRF Analysis of Rocks and Minerals for Major and Trace Elements on a Single Low Dilution Li-Tetraborate Fused Bead, *Adv. X-Ray Anal.* 41 (1999) 843–867.
- [181] M.A. Vendemiatto, J. Enzweiler, Routine Control of Accuracy in Silicate Rock Analysis by X-Ray Fluorescence Spectrometry, *Geostand. Geoanalytical Res.* 25 (2001) 283–291.
- [182] S.M. Eggins, Laser ablation ICP-MS analysis of geological materials prepared as lithium borate glasses, *Geostand. Geoanalytical Res.* 27 (2003) 147–162.
- [183] Z. Yu, M.D. Norman, P. Robinson, Major and Trace Element Analysis of Silicate Rocks by XRF and Laser Ablation ICP-MS Using Lithium Borate Fused Glasses: Matrix Effects, Instrument Response and Results for International Reference Materials, *Geostand. Geoanalytical Res.* 27 (2003) 67–89.
- [184] A.O. Brunfelt, E. Steinnes, Neutron activation analysis for trace element determination in geostandards, *Geostand. Geoanalytical Res.* 2 (1978) 3–7.
- [185] K. Govindaraju, G. Mevelle, Geostandards and geochemical analysis, *Spectrochim. Acta Part B At. Spectrosc.* 38 (1983) 1447–1456.

- [186] D.E. Jacob, High sensitivity analysis of trace element-poor geological reference glasses by laser ablation-inductively coupled plasma-mass spectrometry (LA-ICP-MS), *Geostand. Geoanalytical Res.* 30 (2006) 221–235.
- [187] R. Tanaka, Y. Orihashi, XRF analysis of major and trace elements for silicate rocks using low dilution ratio fused glass, *HUEPS Tech. Rep.* 2 (1997) 1–20.
- [188] E. D’Andrea, S. Pagnotta, E. Grifoni, G. Lorenzetti, S. Legnaioli, V. Palleschi, B. Lazznerini, An artificial neural network approach to laser-induced breakdown spectroscopy quantitative analysis, *Spectrochim. Acta - Part B At. Spectrosc.* 99 (2014) 52–58. doi:10.1016/j.sab.2014.06.012.
- [189] E. D’Andrea, S. Pagnotta, E. Grifoni, S. Legnaioli, G. Lorenzetti, V. Palleschi, B. Lazznerini, A hybrid calibration-free/artificial neural networks approach to the quantitative analysis of LIBS spectra, *Appl. Phys. B Lasers Opt.* 118 (2015) 353–360. doi:10.1007/s00340-014-5990-z.
- [190] E. D’Andrea, B. Lazznerini, V. Palleschi, S. Pagnotta, Determining the composition of bronze alloys by means of high-dimensional feature selection and Artificial Neural Networks, in: *Conf. Rec. - IEEE Instrum. Meas. Technol. Conf.*, 2015: pp. 2049–2054. doi:10.1109/I2MTC.2015.7151598.
- [191] G.H. Cavalcanti, D. V Teixeira, S. Legnaioli, G. Lorenzetti, L. Pardini, V. Palleschi, One-point calibration for calibration-free laser-induced breakdown spectroscopy quantitative analysis, *Spectrochim. Acta Part B At. Spectrosc.* 87 (2013) 51–56.
- [192] T. Takahashi, B. Thornton, Quantitative methods for compensation of matrix effects and self-absorption in LIBS signals of solids, *Spectrochim. Acta Part B At. Spectrosc.* (2017).
- [193] M. Allaby, M. Allaby, *Oxford Dictionary of Earth Science*, (2008).

Technical appendix

This technical appendix mainly shows the MATLAB® code useful for obtaining and analyzing compositional maps and other data tables not shown in the previous text.. I realize this appendix for anyone who wants to try to work with this kind of stuffs that I found really interesting and stimulating. The possibilities offered by software such as MATLAB® are infinite.

MATLAB® scripts

First step is to load the spectrum files that you want to analyze. This operation requires a series of string code, useful to load the entire spectra set for each samples and to allocate it in a vector matrix to be previously declared as **poly1** (every time we need a new vector it is necessary to declare it in advance giving it the name that we want). The “for cycle” (for, if, else, end) allow to load each spectrum in the directory that start with name **filename** and is followed by numbers from **0001** to **4999** (that are the name of sequential spectra given by our spectrometer- each spectrometer save data in different way).

```
clear %clear all the memory and workspace%
sample='samplename'
poly1=[]

%the follow "for cycle" allow to create a matrix containing the spectra you want
to analyze(poly1).
for i=(1:2:4999)
    q=strcat('000',num2str(i));
    z=length(q);
    if z > 8 z1=q(z-4:z)
    else z1=q(z-3:z)
    end
s=strcat('C:\Users\folder1\filename', z1, '.jnd'); %%Load from the pc the
spectrum files (ASCII)- specify the exact position and filename%%

ss=load(s);
poly1=[poly1 ss(:,2)];
end
```

Now the vector matrix **poly1** contains all the spectra of the sample “samplename” ordered in row (spectrum of the single point) and columns (full spectrum wavelength). Once we have the data, we can start to select inside them the part of the spectrum (columns value) that we want analyze. The simplest way to operate is to extract the single elemental map indicating the coordinates of this value in the **poly1** (sequential number from start of spectrum to the end of it that correspond a precise wavelength that we can recognize with LIBS++ software or other spectra visualization software). If I want to extract the iron map from **poly1** I must

declare a new empty vector and populate it with all the values referring to the position of the iron peak that interests me. I must create a new matrix vector with giving it the square shape (I have to remember how many side steps I set in the scan).

```
fe=[]%declaration of existence of a new vector matrix%
fe=poly1(2123,:); %%Iron. the number 2123 correspond to the position of the iron
peak that i want to map%%
rsfe=reshape(fe,[50,50]); %reshape the data of fe linear vector in a 50x50
matrix map%
```

In this case, I set 50x50 steps maps because in my analysis I have scanned an area of 50x50 step.

Once we have extracted the set of compositional maps we want to study. We can begin to create elaborations for qualitative analysis. We have different possibilities. We can start with elemental intensity distribution ratio between Ca and Fe. In this case, the point serves to divide each point of a map with each point of the other.

```
fe1=poly1(2123,:); %Iron LIBS intensity taken at position 2123%
ca1=poly1(1816,:); %Calcium LIBS intensity at position 1816%
rsfe1=reshape(fe1./ Ca1,[50,50]); %%Fe/Ca ratio%%
```

In the same way, we can perform every kind of operation directly on, and with, the compositional maps.

Regarding the possibility of carrying out a PCA directly on the maps, the speech begins to be more complicated. We need to reconstruct a long linear vector by sequencing all the maps. To do this you can operate on the already created matrices (compositional maps) present in our workspace or start from images (in color or in gray tones that we have already created and saved previously). In my opinion, it is more useful and interesting to show how to read a map already saved (image .bmp or jpg), how to re-transform it into a linear vector and create a matrix placing them one after the other.

```
Im_1=double(imread('C:\imagefolder\mapname.bmp')); %load the map saved in .bmp
format%
nm=size(Im_1) %indexing the image%
nm2=nm(1)*nm(2); %linearization of the image in a linear vector%
```

Now we can build a new matrix that contains our images (transformed into linear vectors) in consecutive sequence.

```
%Load the previous linear vector created from saved images and place them in a
matrix vector%
mixedsig=[reshape(Im_1,1,nm2);reshape(Im_2,1,nm2);reshape(Im_3,1,nm2)];
```

Now we have a vector matrix that we can begin to process through a PCA. I emphasize that each linear vector that makes up this matrix corresponds to an elemental map. MATLAB® has an integrated function called **princomp** (in the versions subsequent to 2017 it will be replaced by **PCA**) which performs the analysis of the main components automatically on the matrix we built. Let us assume that the first three main components are able to explain the total variation in the intensity within our maps and we build a PCA with only three components to which we assign respectively the **Red**, **Green** and **Blue** channel of a color image.

We recompose the three images and obtain a false-RGB image.

```
[pc,score,latent,tsquare] = princomp(mixedsig'); %PCA performed with only 3
components%

x1=score(:,1);
x2=score(:,2);
x3=score(:,3);

R=(x1-min(x1))./(max(x1)-min(x1));
G=(x2-min(x2))./(max(x2)-min(x2));
B=(x3-min(x3))./(max(x3)-min(x3));

IM_R=reshape(R,nm);
IM_G=reshape(G,nm);
IM_B=reshape(B,nm);

IM_R=IM_R/max(max(IM_R));
IM_G=IM_G/max(max(IM_G));
IM_B=IM_B/max(max(IM_B));

im = cat(3,IM_R,IM_G,IM_B);

imwrite(im,'C:\filefolder\filename.jpg','JPG');
```

In the next step, we can use a Kohonen SOM neural network to segment the maps of the analyzed areas. This procedure allows us to divide the areas into smaller portions that possess the same properties of the spectrum.

```
% Create a Self-Organizing Map with 2x2 neuron. You can change this grid
changing "dimension1 and 2 number" and adding new segment to the follow script
dimension1 = 2;
dimension2 = 2;
net = selforgmap([dimension1 dimension2]);
net.trainParam.epochs = 10000;

% Train the Network
[net,tr] = train(net,inputs);

% View the Network
```

```

view(net)

% Extract weight of the SOM %%
wb=getwb(net)

% Test the Network
outputs = net(inputs);

segn_1=reshape(outputs(1,:),nm);
segn_2=reshape(outputs(2,:),nm);
segn_3=reshape(outputs(3,:),nm);
segn_4=reshape(outputs(4,:),nm);
%Linearizzation of image matrix obtained by SOM segmentation
seg1=reshape(segn_1,[1,2500]);
seg2=reshape(segn_2,[1,2500]);
seg3=reshape(segn_3,[1,2500]);
seg4=reshape(segn_4,[1,2500]);
%Transform linear vector in matrix similar to "poly" matrix.
segmento1= repmat(seg1,3532,1)
segmento2= repmat(seg2,3532,1)
segmento3= repmat(seg3,3532,1)
segmento4= repmat(seg4,3532,1)

%multiply "segmento" matrix by "poly" matrix in order to obtain a matrix wich
columnar value are the spectrum of the selected segment
sg1=segmento1.*poly1
sg2=segmento2.*poly1
sg3=segmento3.*poly1
sg4=segmento4.*poly1

>Delete the 0 column indexed by vector "seg", giving a vector matrix containing
onli the selected and non-zero spectra
idx1=find(seg1==0)
sg1(:,idx1)=[]

idx2=find(seg2==0)
sg2(:,idx2)=[]

idx3=find(seg3==0)
sg3(:,idx3)=[]

idx4=find(seg4==0)
sg4(:,idx4)=[]

%Column vector obtained by averaging the single spectra in the same segment%
mean1=mean(sg1')'
mean2=mean(sg2')'
mean3=mean(sg3')'
mean4=mean(sg4')'

%--salva gli spettri medi in files CSV che possono essere trattati con origin--
%%
csvwrite('C:\filefolder\Map5sg1.csv',mean1)
csvwrite('C:\filefolder\Map5sg2.csv',mean2)
csvwrite('C:\filefolder\Map5sg3.csv',mean3)
csvwrite('C:\filefolder\Map5sg4.csv',mean4)

```

In this script, I also inserted some command strings to extract the weights of the network, in case it was necessary to study the weight of each input within the segments obtained. Furthermore, if necessary, you can also normalize the images before making the SOM.

```
hnorm = dsp.Normalizer('Method','2-norm'); %normalize a vector with 2-norm
method%
x = mixedsig;
inputs = step(hnorm, x); %returns a normalized outputs for y
```

In order to effectively implement the idea, a MATLAB® program was written starting from the previously created elementary maps/segments (prototypes or center of the clusters. Starting from these maps, useful indices have been extracted to trace the spectra belonging to the same spectral map/segment within the spectral database. Having done this it was relatively easy to select the spectra of each segment and to mediate them to obtain a single spectrum to be analyzed with a supervised CF-LIBS procedure. The following code starts with a new transformation of the map/segment in a linear vector that contains binary information (the zero-value, means no spectrum and 1 means that spectrum in that position belong to the SOM segment). The follow idea is very simple: using these vectors as index to extract only the spectra that belong to the correspondent SOM segment.

```
% Vector linearization of all the segment/map obtained by SOM
seg1=reshape(segn_1, [1,2500]);
seg2=reshape(segn_2, [1,2500]);
seg3=reshape(segn_3, [1,2500]);
seg4=reshape(segn_4, [1,2500]);
```

Now we have four long vector composed by binary index of the presence absence of a spectrum in the segment-map. I construct another four matrix vector with all the 2500 spectra placed in a columnar form with dimension of 3532x2500 each ones where first dimension correspond to the points of each single spectrum and the second dimension corresponds to the single pixel of the map.

```
%transform the linear vector in matrix similar matrice poly (spettri
%caricati)
segmento1=repmat(seg1, 3532, 1)
segmento2=repmat(seg2, 3532, 1)
segmento3=repmat(seg3, 3532, 1)
segmento4=repmat(seg4, 3532, 1)
```

These new matrix (segmento1, segmento2, segmento3 and segmento4) contains zero value (black pixels) in the column where the associated spectrum does not belongs to the map-segment, and ones-value (white pixels) where the associated spectrum belongs to the map-segments (Fig. 51). The previous code permit to construct a matrix of indexes (for each map segment) that we can multiply for the matrix of spectrum (in my case poly1) in order to obtain a new matrices that contain values (the spectra) only in the column correspondent to the white pixels.

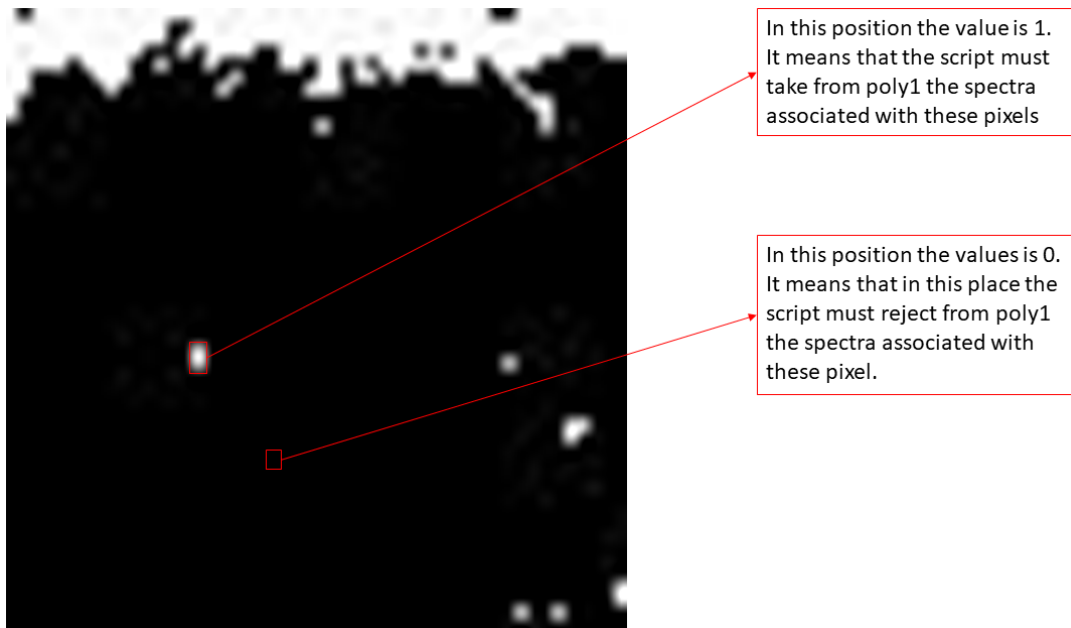


Fig. 51 Schematic simplification of the place where the matrix are ones value and where they are 0

The multiplication between matrices is a very simple operation and precisely where the value in poly multiplies zero the result will be zero, where it multiplies a ones-value the result will be the value itself.

```
%% multiplies the "segment" matrix for the poly matrix obtaining a new
matrix %that in the column has the spectra relative to the zone selected by
the %segmentation. Thus, we obtain a matrix of spectra
sg1=segmento1.*poly1
sg2=segmento2.*poly1
sg3=segmento3.*poly1
sg4=segmento4.*poly1
```

Now that we have obtained a matrix of spectra, where those corresponding to the white pixels in the segment-map are non-zero values while those that correspond to black pixels are zero values. We have to clean up this matrix by automatically eliminating all zero values. The simplest way I had in mind was to use index vectors (seg1, seg2, seg3 and seg4) to indicate to the program which columns among the 2,500 present (in this case) had to be eliminated.

```
%Eliminate the zero column values as indexed in the seg1...seg4 vector giving
as %results a matrix containing only the non-zero columns that represents
the %selected spectra associated with the SOM segment.
```

```
idx1=find(seg1==0)
sg1(:,idx1)=[]
```

```
idx2=find(seg2==0)
sg2(:,idx2)=[]
```

```
idx3=find(seg3==0)
sg3(:,idx3)=[]
```

```
idx4=find(seg4==0)
sg4(:,idx4)=[]
```

The resulting matrix consists of the spectra belonging to the single segment. The software automatically averages between these spectra, thus returning a medium spectrum that can be analyzed using CF_LIBS.

```
%Averaging of the segment spectra.
```

```
mean1=mean(sg1')'
mean2=mean(sg2')'
mean3=mean(sg3')'
mean4=mean(sg4')'
```

Once these average spectra have been obtained, we only possess the values of Y without any relative reference on the respective wavelengths (X) to which they refer. In this regard, working on an arbitrary spectrum taken with my spectrometer, I extracted the wavelengths from this and from them I created a reference file (calling it ref). I load my reference files (that each can get from any spectrum taken, under equal conditions, with its own spectrometer) and create a new matrix: in the first column the values of ref will go and in the second column the values of the spectrum will go medium (mean1, mean2 etc.). Finally, save each matrix in a .dat files (comma separated).

```
%%Saves .dat files using ref as wavelenght reference.
```

```
ref=load ('C:\foldername\refspectrnm.dat')
aseg1=[ref,mean1];
aseg2=[ref,mean2];
aseg3=[ref,mean3];
aseg4=[ref,mean4];
dlmwrite('C:\foldername\aseg1.dat',aseg1)
dlmwrite('C:\foldername\aseg1.dat',aseg2)
dlmwrite('C:\foldername\aseg1.dat',aseg3)
dlmwrite('C:\foldername\aseg1.dat',aseg4)
```

Data sheets

In this section, I inserted all the tables of data that, because of the legibility of the same and the text to which they refer, it was preferable to insert separately from the text.

Table 26 Raw compositional map data from Cap3: quantitative maps each element for each segment of N2-2 Sample. The grayscale map are flattened on the highest value and this cause sharp rims. For better visualizzation you must expand the histogram in a photo editing software.




































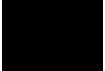



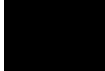
N2-2	Seg.1	Seg.2	Seg.3	Seg.4	Seg.5
Al (wt%)					
C (wt%)					
Ca (wt%)					
Fe (wt%)					
Mg (wt%)					
Na (wt%)					
Si (wt%)					
Sr (wt%)					

Table 27 Raw compositional map data from Cap3: quantitative maps each element for each segment of N2-2 Sample. The grayscale map are flattened on the highest value and this cause sharp rims. For better visualization you must expand the histogram in a photo editing software.

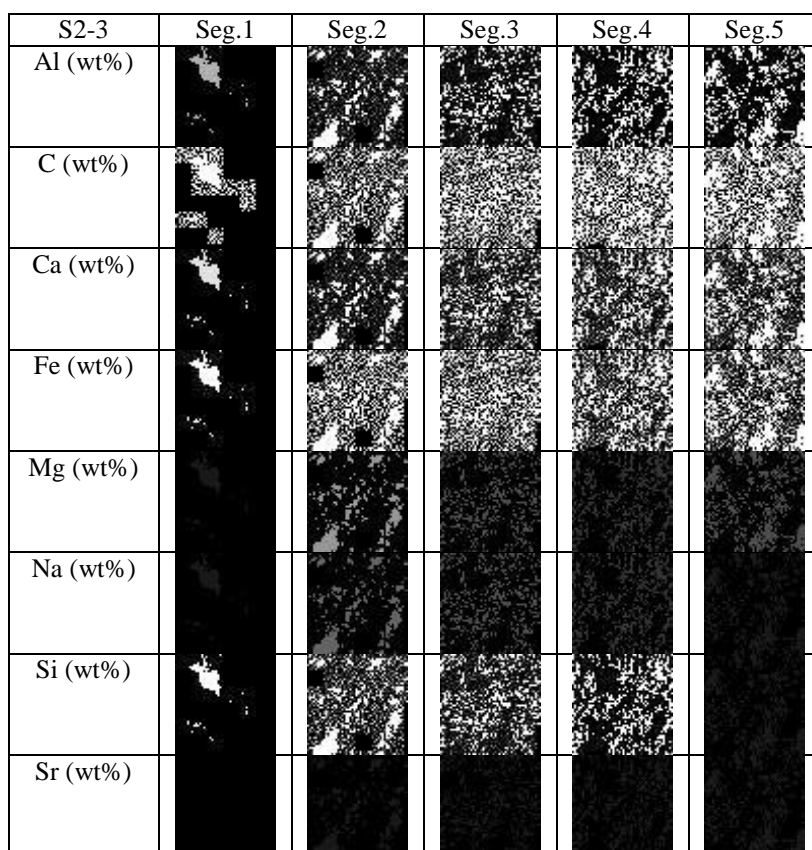


Table 28 Certified value for the analyzed geostandards. Lab=Laboratory; Id.=Identification of the standard. All the value are reconverted in w% from the certified oxide.

Lab.	Id.	Rock Type	Na	Mg	Al	Si	P	K	Ca	Ti	Mn	Fe
CNRS	AC-E	Granite	9.48	0.04	15.13	63.96	0.01	7.25	0.47	0.13	0.09	3.44
USGS	AGV-1	Andesite	6.08	1.77	17.37	52.61	0.41	4.64	6.76	1.2	0.13	9.03
CNRS	BE-N	Basalt	4.26	14.24	9.57	32.04	0.82	2.07	17.8	2.81	0.28	16.12
USGS	BIR-1	Basalt	2.34	10.47	14.57	40.02	0.04	0.04	16.97	1.03	0.24	14.29
CNRS	DR-N	Diorite	4.2	5	17.49	46.58	0.21	2.66	9.5	1.23	0.32	12.8
CNRS	DT-N	Disthene	0.06	0.05	62.79	34.14	0.08	0.2	0.06	1.68	0.01	0.93
CNRS	GS-N	Granite	5.45	2.69	15.06	59.66	0.24	7.46	3.47	0.79	0.08	5.1
GSI	JA-2	Andesite	4.39	8.86	15.51	50.25	0.13	2.86	8.86	0.77	0.16	8.2
GSI	JA-3	Andesite	4.48	4.18	15.63	55.2	0.09	2.22	8.52	0.77	0.16	8.75
GSI	JB-2	Basalt	2.74	5.08	14.04	44.95	0.08	0.63	12.78	1.29	0.28	18.14
GSI	JB-3	Basalt	3.81	5.69	16.21	43.25	0.23	1.17	12.78	1.58	0.22	15.06
GSI	JF-1	Feldspar	5.04	0.01	18.19	59.51	0.01	15.97	1.26	0.01	0	0
GSI	JF-2	Feldspar	3.46	0	18.4	57.49	0	20.53	0.12	0	0	0
GSI	JG-1a	Granodiorite	5.01	0.82	14.83	66.49	0.07	6.56	3	0.3	0.09	2.83
GSI	JG-2	Granite	5.25	0.05	13.03	71.39	0	7.78	1.13	0.05	0.02	1.3
GSI	JG-3	Granodiorite	5.83	2.09	15.94	60.85	0.1	4.24	5.21	0.56	0.11	5.07
GSI	JGb-1	Gabbro	1.64	8.47	16.76	36.4	0.04	0.36	15.35	1.74	0.24	19.01
GSI	JP-1	Peridotite	0.03	50.05	0.61	37.56	0	0.01	0.74	0	0.17	10.83
GSI	JR-1	Rhyolite	6.1	0.11	13.62	70.33	0.02	7.31	0.9	0.12	0.15	1.34

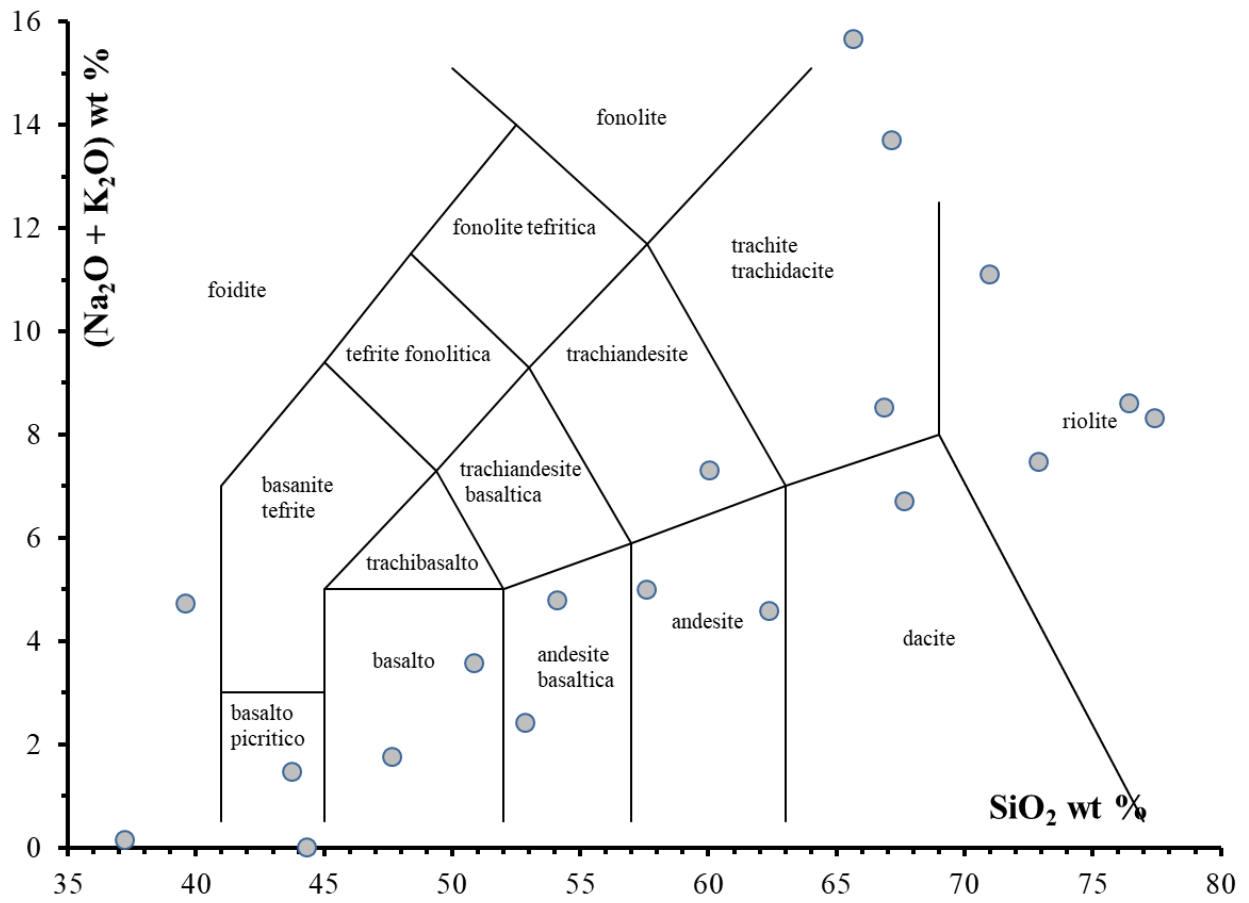


Fig. 52 TAS diagram of the certified geostandards

Table 29 Predicted value (pure elements) on geostandards CAP4

JR-1	JP-1	JG-1	JG-2	JG-3	JG-1a	JF-2	JF-1	JB-3	JB-2	JA-3	JA-2	GS-N	DT-N	DR-N	BIR-N	BE-N	AGV-I	AC-E
Ryolite	Peridotite	Gabbro	Granodiorite	Granodiorite	Granodiorite	Feldspar	Feldspar	Basalt	Basalt	Andesite	Andesite	Granite	Dishtene	Diorite	Basalt	Basalt	Andesite	Granite
6.0	0	1.9	5.4	5.4	5.7	3.9	4.5	3.0	3.0	4.3	4.2	5.5	0.7	4.0	2.4	4.0	4.9	6.6
0.2	0.6	0.3	0.2	0.2	0.4	0.6	0.2	0.6	0.6	0.4	0.4	0.4	1.0	0.2	0.5	0.3	0.7	0.9
8.7	0.8	0.3	5.5	5.5	6.5	22.2	14.3	0.8	0.8	2.6	2.6	6.1	0	2.6	0	2.3	4.9	5.4
1.3	1.1	0.6	0.4	0.4	1.2	2.0	1.6	0.3	0.3	0.3	0.7	0.5	0.5	0.8	0.1	1.1	0.8	0.3
71.6	35.9	37.7	60.4	60.4	60.1	56.3	60.2	42.0	42.0	51.3	51.3	61.2	31.8	44.8	40.1	32.4	52.3	62.3
1.2	3.3	1.4	0.7	0.7	3.1	3.4	0.7	1.1	1.1	2.0	0.9	0.9	4.0	0.9	0.9	0.8	1.7	2.4
0	54.0	8.6	3.0	3.0	1.6	1.1	0.2	6.4	6.4	4.6	7.7	2.7	0.8	5.2	9.8	14.1	2.3	0.3
0.7	4.1	1.0	0.6	0.6	0.6	1.0	0.5	0.9	0.9	0.4	1.1	0.5	2.0	1.2	0.6	1.3	0.4	0.9
14.4	0	18.0	17.0	17.0	18.3	18.1	22.2	16.6	16.6	18.2	18.2	17.7	72.7	19.0	16.9	12.4	20.3	16.5
0.7	1.4	1.0	0.9	0.9	0.5	6.5	1.7	0.8	0.8	1.3	1.4	0.8	3.7	0.5	1.2	1.4	1.7	3.8
0.9	0.3	15.3	4.3	4.3	4.0	0.2	1.0	13.4	13.4	9.5	8.7	4.1	0.5	11.1	16.4	16.7	6.5	4.0
0.3	1.6	0.8	0.9	0.9	0.2	0.7	0.4	0.4	0.4	0.9	0.5	0.4	0.6	0.6	0.9	0.1	0.7	0.7
0.0	0.0	1.7	0.5	0.5	0.5	0.0	0.1	1.3	1.3	1.0	0.9	0.6	1.6	1.6	1.3	2.6	1.2	0.6
0.2	0.0	0.2	0.2	0.2	0.1	0.1	0.2	0.2	0.2	0.2	0.2	0.1	0.1	0.2	0.2	0.1	0.2	0.2
0.1	0.1	0.2	0.1	0.1	0.1	0.0	0.0	0.2	0.2	0.2	0.2	0.1	0.1	0.2	0.3	0.3	0.1	0.1
0.0	0.1	0.0	0.0	0.0	0.0	0.0	0.0	0.0	0.0	0.0	0.0	0.0	0.1	0.1	0.1	0.0	0.0	0.0
0.6	11.0	18.2	5.3	5.3	5.1	0.4	0.3	16.4	17.9	10.3	8.1	3.6	0.3	13.3	15.1	15.8	9.4	5.7
0.4	1.0	0.9	0.5	0.5	1.3	2.2	0.4	1.5	1.5	0.8	0.9	0.5	0.6	1.1	0.6	0.5	0.4	1.3
0.9	0.3	15.3	4.3	4.3	4.0	0.2	1.0	13.4	13.4	9.5	8.7	4.1	0.5	11.1	16.4	16.7	6.5	4.0
0.3	1.6	0.8	0.9	0.9	0.2	0.7	0.4	0.4	0.4	0.9	0.5	0.4	0.6	0.6	0.9	0.1	0.7	0.7

Other schemes and data

Table 30 Lists of HH-LIBS system in commerce with reference website.

	Manufacturer	Model	Website
1	Bruker	EOS 500	https://www.bruker.com/products/x-ray-diffraction-and-elemental-analysis/libs/eos-500/overview.html
2	SciAps	Z200	https://www.sciaps.com/libs-handheld-laser-analyzers/z-series/
3	SciAps	Z200 C+	https://www.sciaps.com/libs-handheld-laser-analyzers/z-series/
4	SciAps	Z300	https://www.sciaps.com/libs-handheld-laser-analyzers/z-series/
5	SciAps	Z50	https://www.sciaps.com/libs-handheld-laser-analyzers/z-series/
	SciAps	Z500	https://www.sciaps.com/libs-handheld-laser-analyzers/z-series/
6	Rigaku	KT-100S™ KATANA	https://www.rigaku.com/en/press/katana/rd100
7	Hitachi	Vulcan Smart	https://hha.hitachi-hightech.com/en/product-range/products/handheld-xrf-libs-analysers/handheld-libs-analysers
8	TSI	CHEMLITE™	http://www.tsi.com/ChemLite-Portable-LIBS-Metal-Analyzer/
9	Oxford Instruments	mPulse	https://www.bergeng.com/product/MPULSE.html
10	BwTek	NanoLIBS-Q	http://bwtek.com/products/nanolibs-q/

Table 31 Micro-LIBS on the market.

	Producer	Model	Website
1	Leica	DM6 M ¹²	https://www.leica-microsystems.com/products/light-microscopes/upright-microscopes/details/product/libs-module
2	Marwan technology	MicroLIBS	http://www.marwan-technology.com/prodotti/strumentazione-analitica/strumentazione-libs/microlibs/

¹² This is a module for the Leica DM6 and consist of a single pulse laser and spectrometer attached to the microscope

Abbreviations

1. AES= Atomic Emission Spectroscopy
2. ANN= Artificial Neural Network
3. BMP= Bitmap (file extension)
4. CF-LIBS= Calibration-Free Laser-Induced Breakdown Spectroscopy
5. C-Sigma= Calibration Sigma method
6. COLTAN= Columbite-Tantalite (abbr., Common name)
7. DLL= Dynamic-Link Library
8. DOF= Depth of focus
9. EMP= Electro Magnetic Pulse Analysis
10. EMSLIBS= Euro-Mediterranean Symposium on Laser-Induced Breakdown Spectroscopy
11. HH-LIBS= Hand Held Laser-Induced Breakdown Spectroscopy
12. iCCD= Intensified Charge Coupled Device
13. ICP= Ion Coupled Plasma analysis
14. ICP-AES= Ion Coupled Plasma-Atomic Emission Spectroscopy
15. ICP-MS= Ion Coupled Plasma-Mass Spectrometry Analysis
16. INAA=Instrumental Neutron Activation Analysis
17. IR= Infrared
18. J= Joule
19. JCH= Journal of Cultural Heritage
20. JOGMEC= Japan Oil, Gas and Metals National Corporation
21. JPG= Joint Portable Graphic (file extension)
22. K= Kelvin (unit of temperature)
23. KBr= Potassium bromide
24. LA-ICP-MS=Laser Ablation-Ion Coupled Plasma-Mass Spectrometry Analysis
25. LIBS= Laser-Induced Breakdown Spectroscopy
26. LOO= Leave One Out
27. LS-SVM= Least Square Support Vector machine algorithm
28. LTE= Local Thermal Equilibrium (Condition of)
29. MAA= Mediterranean Archaeology and Archaeometry
30. MD= Mean Deviation

31. MD-LAM= Micro-Drilling Laser Analysis Method
32. mJ= milli-Joule
33. MODi= Mobile Dual-Pulse Instrument
34. MV-MC= Maximum Variance modification to Maximum Correlation
35. Nd:YAG= Yttrium-Aluminum crystal doped with neodymium ($\text{Nd:Y}_3\text{Al}_5\text{O}_{12}$)
36. NIST= National Institute of Standards and Technology
37. OPC= One Point Calibration
38. OREAS= Ore Research and Exploration of Australia
39. PCA= Principal Component Analysis
40. PLS-DA= Partial Least Square with Discriminant Analysis Approach
41. RF= Random Forest Algorithm
42. RGB= Red, Green, Blue (channel of a digital image)
43. RMSE= Relative Mean Square Error
44. RMSEP= Root Mean Square Error
45. RSD= Relative Standard Deviation
46. SEM= Scanning Electron Microscope
47. SEM-EDX= Scanning Electron Microscope-Energy Dispersion X-Ray micro-probe
48. SIMCA= Soft Independent Modeling by Class Analogy
49. s/n= Signal to noise (ratio)
50. SOM= Kohonen Self-Organizing Maps (ANN algorithm)
51. SPLS= Sparse Partial Least Square
52. SVM= Support Vector Machine
53. TFe= Total (amount of) Iron
54. TPA= Time Used per Analysis
55. UI= User Interface
56. UV= Ultra Violet
57. VECS=Virtual Elemental Cross-Section
58. VIS= Visible
59. XRF= X-Ray Fluorescence Spectroscopy

Figure Captions

Fig. 1 A simple scheme of the Laser Induced Breakdown Spectroscopy (LIBS) apparatus.....	3
Fig. 2 A scheme to resume the mechanism of double pulse.....	4
Fig. 3 The main configurations used for Double Pulse LIBS.....	5
Fig. 4 Double pulse stand-off system scheme (based on the model developed by U.S. Army Research Laboratory [32]). In this scheme laser 1 hides the laser 2. In this system, there are two laser in order to realize the double pulse technique.	7
Fig. 5 The internal analytical chamber. The sealing door, placed for security reasons, is useful for retain the atmosphere when the chamber is flushed with inert gas.....	16
Fig. 6 The insert gas nozzle in the Backpanel of Modi.....	16
Fig. 7 External arm of the Modi system. A complex mirroring system whit five junctions guides the laser outside the instrument. An optical fiber placed at 45° respect of the surface of the sample collects the plasma light.....	17
Fig. 8 Craters made by laser in the analytical chamber. From left to right: after 25, 50 and 100 laser shots.....	18
Fig. 9 Depth of craters (µm) versus number of laser pulses. We can estimate that the depth of craters follow approximatively an exponential curve.....	19
Fig. 10 Photo of the microscope mounted on the micro-LIBS system.....	20
Fig. 11 A front and side view of the motorized stage.....	21
Fig. 12 The Dinolite™ Cam mounted in the tri-ocular eyepieces.....	21
Fig. 13 Scheme of the focal point.....	22
Fig. 14 User Interface (UI) of the micro-libs-scanner.....	23
Fig. 15 Diagram of operation for control system.....	24
Fig. 16 UI of the laser control software.....	24
Fig. 17 Double Pulse LIBS spectrum of a brass sample (2 mJ per pulse, 1 µs between pulses). The crater is not circular due a little divergence of the two beams. Figure is taken from Grassi et al. [157] and re-elaborated.....	26
Fig. 18 Single Pulse LIBS spectrum of a brass sample (10 mJ pulse). We can see a very low intensity of the entire spectrum. On the main peak (around 525 nm) the intensity is lower of about 3000 counts. Figure is taken from Grassi et al. [157] and re-elaborated.....	26
Fig. 19 Principal UI of LIBS++ Software.....	28
Fig. 20 Different approaches to elaborate data to create the maps.....	29
Fig. 21 A scheme of the realization of false color maps, useful for identifying the distribution of the main elements. ...	29
Fig. 22 Workflow for generating the elemental maps.....	30
Fig. 23 Data flow and processing for obtain a false color PCA map.....	31
Fig. 24 Data flow and processing trough SOM algorithm for obtaining segmentation of elemental maps.....	32
Fig. 25 The analyzed samples from Settefonti a Prata d'Ansidonia archaeological site (AQ-Italy). The sample 7FFig.2 is not in the table.....	35
Fig. 26 Thin section of the samples analyzed. First row, from left to right: 7FFig2, 7FFig3, 7FFig8, 7FFig1. Second row, from left to right: 7FFN36, 7FFN35, 7FFN7. Third row, from left to right: 7FFR22, 7FFR25, 7FFR1. The last pic is 7FGr17.....	36
Fig. 27 Graph showing the clusters obtained applying a modularity class algorithm.....	38
Fig. 28 The analysed samples.....	39
Fig. 29 LIBS spectrum of a potsherd.....	40
Fig. 30 A representation of a Hyperspectral cube.....	41
Fig. 31 False-RGB using elemental maps of Si, Al and Ca compared to real photo of scanned surfaces.....	42
Fig. 32 Segmentation of the analyzed areas on samples using Self Organized Maps.....	43
Fig. 33 POFN1 Quantitative analysis on segmented elemental map.....	44
Fig. 34 POFN2 Quantitative analysis on segmented elemental map.....	44
Fig. 35 POFN3 Quantitative analysis on segmented elemental map.....	45
Fig. 36 POFN4 Quantitative analysis on segmented elemental map.....	45
Fig. 37 Micro-photos of the two analyzed samples (Taken from Pagnotta et al. [167]).....	46
Fig. 38 Elemental distribution in the two samples (Taken from Pagnotta et al. [167]).....	47
Fig. 39 The Ca/Mg line intensity ratio and the false-color map -distribution of Si –red-, Al –green- and Ca –blue- line intensity- (Taken from Pagnotta et al. [167]).....	47
Fig. 40 Elemental maps segmentation realized by SOM with 7 inputs and 5 outputs. The number of pixels occupied by each segment area has been indicated (taken from Pagnotta et al. [1]).	48
Fig. 41 The schematization of the continous ablation in a single point of the sample.....	53
Fig. 42 Spot size after five repetition shots (about 0.61mm).....	53
Fig. 43 Structure of a single perceptron with 76 inputs (19x4 spectra) and 76 outputs (reference value taken from reference standard certificate).....	54
Fig. 44 Eerror Histogram of the ANN. The most part of the sample are close to the zero-error value.....	55

Fig. 45 sample analyzed with 3D map reconstruction of Iron.	57
Fig. 46 VECS of the black crust (Red=Al, Mg=Green, Fe=Blue).	58
Fig. 47 Photo of the scanned area (5x5mm).	59
Fig. 48 The false color image of the scanned area. Red=component1; green= component2; blue= component3. The blurry effect is due the resize of the original image (1.20x1.20 cm ² to 5x5 cm ²).	60
Fig. 49 Structure of the SOM network with 9 inputs (elemental peak intensities) and 4 outputs (segments).	61
Fig. 50 The four segments obtained from SOM. In white the area occupied by the segment. Below each image, the number of the pixel and the percentage of the sample covered by the segment.	61
Fig. 51 Schematic simplification of the place where the matrix are ones value and where they are 0	80
Fig. 52 TAS diagram of the certified geostandards	84

Table captions

Table 1 The LIBS techniques compared with other classical methods for geochemical analysis (adapted from Musazzi & Perini [8] p. 314 and from Naes et al. [9]). EMP=Electro Magnetic Pulse Analysis; pXRF= X-Ray Fluorescence; INAA=Instrumental Neutron Activation Analysis; LA-ICP-MS=Laser Ablation-Ion Coupled Plasma with Mass Spectrometry; RSD= Relative Standard Deviation; TPA= Time used Per Analysis.	6
Table 2 List of commercial Hand Held LIBS on the market.	7
Table 3 Survey of works dealing with LIBS classification of geological materials as reported by Quiao et al [61] (p.10 Table 2).MV-MC=Maximum variance modification to Maximum Correlation; PCA=Principal Component Analysis; PLS-DA=Partial Least Square-Discriminant Analysis; SIMCA=Soft Independent Modeling by Class Analogy; ANN=Artificial Neural Network; SVM=Support Vector Machines; SPLS= Sparse Partial Least Square; LS-SVM= Least Square-Support Vector Machines; TFe= Total Iron.....	10
Table 4 Works dealing with LIBS quantitative analysis as reported in Quiao et al [61] (p.11 Table 3 modified by adding recent works and correcting some results). ANN=Artificial Neural Network; PLS= Partial Least Square; CF-LIBS= Calibration Free Laser-Induced Breakdown Spectroscopy.....	11
Table 5 System characteristics of the Micro-Scan.....	22
Table 6 Table of the energies measured for the Modi laser. First pulse (F1), second pulse (F2) and F1+F2. Notice that the F1+F2 value is not the sum of the F1 and F2, but a completely independent measure performed directly on the double pulse.	25
Table 7 Clusterization of potsherds based on archaeological classification.	35
Table 8 Thin section analysis of samples. Q=Quartz; K=K-Feldspar; Pl=Plagioclase; Ph=Phyllosilicate; C=Carbonate; Cal= Calcite; Gg=Grog*; Fs= Fossils. *Grog is a technical term that indicates the use of shredded ceramics in the raw materials.....	36
Table 9 Modularity class applied to the graph of the samples.	37
Table 10 Summary table of analyzed samples.	40
Table 11 Wavelength of the characteristic elements studied.	40
Table 12 Percentage of the scanned area occupied by each segment.	43
Table 13 Selected elements and central wavelength (Taken from Pagnotta et al. [167]).	47
Table 14 Percentage of the analyzed areas occupied by segments in each samples.	48
Table 15 Complete list of the elemental peaks used for quantitative analysis by means of CF-LIBS (re-adapted from Pagnotta et al. [167]).....	49
Table 16 Quantitative analysis of N2-2 sample.	50
Table 17 Quantitative analysis of S2-3 sample.....	50
Table 18 Contents in Si and Na+K and their conversion in SiO ₂ (w %) and Na ₂ O+K ₂ O (wt%) of the analysed rock standards.	52
Table 19 The Element peak lines for each chosen elements.	54
Table 20 Accuracy of the measurements (absolute value for all the elements simultaneously).	56
Table 21 Lists of the elemental peaks selected for the CF-LIBS.	60
Table 22 List of principal elements individuated inside the spectra and used for generating the false color PCA map...	60
Table 23 Mean composition of the four segments.	61
Table 24 Standard protocol of analysis for Cultural Heritage materials.....	63
Table 25 Scheme of main features of actual and a future system.	64
Table 26 Raw compositional map data from Cap3: quantitative maps each element for each segment of N2-2 Sample. The grayscale map are flattened on the highest value and this cause sharp rims. For better visualizzazione you must expand the histogram in a photo editing software.	82
Table 27 Raw compositional map data from Cap3: quantitative maps each element for each segment of N2-2 Sample. The grayscale map are flattened on the highest value and this cause sharp rims. For better visualizzazione you must expand the histogram in a photo editing software.	83
Table 28 Certified value for the analyzed geostandards. Lab=Laboratory; Id.=Identification of the standard. All the value are reconverted in w% from the certified oxide.	83
Table 29 Predicted value (pure elements) on geostandards CAP4	85
Table 30 Lists of HH-LIBS system in commerce with reference website.	86
Table 31 Micro-LIBS on the market.....	86



UNIVERSITÀ
DEGLI STUDI
FIRENZE